

E. Wolf, Progress in Optics 43
© 2002 Elsevier Science B.V.
All rights reserved

Chapter 2

Variational methods in nonlinear fiber optics and related fields

by

Boris A. Malomed

*Department of Interdisciplinary Studies, Faculty of Engineering,
Tel Aviv University, Tel Aviv 69978, Israel*

Contents

	Page
§ 1. Introduction	71
§ 2. Dynamics of solitons in a single-mode nonlinear optical fiber or waveguide	85
§ 3. Variational approximation for the inverse scattering transform	121
§ 4. Internal dynamics of vector (two-component) solitons	125
§ 5. Spatially nonuniform fibers and dispersion management	138
§ 6. Solitons in dual-core optical fibers	162
§ 7. Bragg-grating (gap) solitons	172
§ 8. Stable beams in a layered focusing–defocusing Kerr medium	180
§ 9. Conclusion	184
Acronyms adopted in the text	184
Acknowledgements	185
References	186

§ 1. Introduction

1.1. *The nonlinear Schrödinger equation and simplest optical solitons*

The mathematical basis of nonlinear optics is Maxwell's system of equations governing propagation of electromagnetic waves in a material medium, combined with relations accounting for the nonlinear response of the medium to the electromagnetic field (Newell and Moloney [1992]). In most cases, application of well-known asymptotic methods makes it possible to derive simplified partial differential equations (PDEs) governing the spatial and/or temporal evolution of essential field modes in the medium.

A typical and most important example of the thus derived asymptotic PDE is the nonlinear Schrödinger (NLS) equation, which governs the propagation of an electromagnetic wave in a glass fiber, or the spatial evolution of the electromagnetic field in a planar waveguide. In the case of a *single-mode* fiber, i.e., one permitting the propagation of a single electromagnetic-wave mode, the electric component of the field with a fixed polarization is taken in the form

$$\mathcal{E}(z, t) = u(z, \tau) V_0(r) \exp(ik_0 z - i\omega_0 t), \quad (1)$$

where z , r and t are, respectively, the propagation distance along the fiber, the radial coordinate in the transverse plane, and time; the frequency ω_0 and wavenumber k_0 of the *carrier wave* obey a linear dispersion relation for the fiber, $k = k(\omega)$, and $V_0(r)$ describes the transverse structure of the propagating mode [the physical field is given by the real part of the complex expression (1)]. The dispersion relation determines the carrier's group velocity $V_{\text{gr}} \equiv 1/k'$, dispersion coefficient $D \equiv -k''$, and "reduced time" $\tau \equiv t - z/V_{\text{gr}}$, where the prime stands for the derivative $d/d\omega$ taken at $\omega = \omega_0$. Both $D > 0$ and $D < 0$ are possible, being referred to as, respectively, anomalous and normal dispersion.

The NLS equation for the slowly varying amplitude $u(z, \tau)$ of the modulated wave (1), derived from the Maxwell equations in the absence of dissipation, is (Agrawal [1995])

$$iu_z + \frac{1}{2}Du_{\tau\tau} + \gamma|u|^2u = 0. \quad (2)$$

Here, the nonlinearity coefficient is

$$\gamma \equiv \frac{n_2 \omega_0}{c A_{\text{eff}}}, \quad (3)$$

where n_2 , c and A_{eff} are, respectively, the Kerr coefficient, the light velocity in vacuum, and the fiber's effective cross-sectional area. Usually, γ is scaled out of eq. (2) by means of an obvious transformation. The dispersion coefficient D can also be scaled out, provided that it is constant. However, in many important applications which will be considered in detail below in § 5, D is a function of the propagation coordinate z . The dispersion D can readily be made variable (modulated), as it is contributed to by the material dispersion of the silica glass and the geometric dispersion of the fiber waveguide. These two contributions may nearly cancel each other near the *zero-dispersion point*, so relatively small variations in the fiber's cross-section area, while only slightly affecting γ , can strongly change the small residual dispersion coefficient. Thus, a continuous variation of the cross-section in the process of drawing the fiber from glass melt gives rise to *dispersion-decreasing fibers* (see § 5.1). Uniform fibers can be fabricated with different constant values of D , making it possible to build a long *dispersion-compensated* optical link by periodically alternating pieces with anomalous and normal dispersion. This is a basis for the *dispersion-management* (DM) technique, which finds important applications in transmitting signals through fiber-optic links in linear (Lin, Kogelnik and Cohen [1980]) and nonlinear regimes, see § 5.4.

The same NLS equation finds another well-known application to nonlinear optics, describing the spatial distribution of the stationary electromagnetic field in a planar waveguide (film). In that case, the electric field with fixed polarization is taken as

$$\mathcal{E}(z, x, t) = u(z, x) V_0(y) \exp(ik_0 z - i\omega_0 t) \quad (4)$$

(cf. eq. 1), where x and y are transverse (relative to the propagation distance z) coordinates, directed, respectively, along the film and perpendicular to it, and the function $V_0(y)$ accounts for the transverse structure of the propagating mode. Note that, unlike the case of propagation in a fiber, the slowly varying amplitude u from eq. (4) is a function of the transverse coordinate x , rather than the temporal variable τ . The NLS equation governing the spatial evolution of $u(z, x)$ in the lossless waveguide can be derived, after rescalings, in the form (see details in the book by Hasegawa and Kodama [1995])

$$iu_z + \frac{1}{2}u_{xx} + |u|^2 u = U(x)u, \quad (5)$$

where, as in eq. (2), the cubic term is generated by the Kerr effect (a nonlinear correction to the effective refractive index in the material medium), while the

second-derivative term, unlike that in eq. (1), accounts for the spatial diffraction of the field, rather than temporal dispersion. The term on the right-hand side (rhs) of eq. (5) takes into regard possible modulation of the waveguide in the transverse direction, which gives rise to an effective real potential $U(x)$. Note that the positive sign in front of the nonlinear term in eq. (5) assumes that the Kerr nonlinearity is *self-focusing* (corresponding to a positive nonlinear correction to the effective refractive index), which is the case in most optical media, including silica glass. In the opposite case of a self-defocusing Kerr nonlinearity, which occurs in semiconductor waveguides (see, e.g., the paper by Michaelis, Peschel and Lederer [1997] and references therein), eq. (5) takes the form $iu_z + \frac{1}{2}u_{xx} - |u|^2u = U(x)u$.

The NLS equation with constant coefficients is one of the basic equations of modern mathematical physics. This equation finds numerous applications, not only in optics, but also in plasma physics, hydrodynamics, etc. Its most fundamental property is exact integrability by means of the *inverse scattering transform* (IST), which is based on a representation of the constant-coefficient NLS equation as a compatibility condition for two systems of auxiliary linear equations (see books by Zakharov, Manakov, Novikov and Pitaevskii [1980], Ablowitz and Segur [1981] and Newell [1985], and some details in § 3 below). The exact integrability makes it possible to produce a vast class of exact solutions to the NLS equation, the simplest and most fundamental one being a *soliton* (solitary wave),

$$u_{\text{sol}} = \frac{\eta}{\sqrt{\gamma}} \operatorname{sech} \left(\frac{\eta}{\sqrt{D}} (\tau - \tau_0) \right) \exp \left(\frac{1}{2} i \eta^2 z + i \phi_0 \right), \quad (6)$$

where η is an arbitrary amplitude of the soliton, which also determines its temporal width $\sim \sqrt{D}/\eta$ and propagation constant (wavenumber shift) $\frac{1}{2}\eta^2$, and τ_0 and ϕ_0 are arbitrary real constants.

The NLS equation (2) is invariant with respect to the Galilean transformations, which allows one to generate a family of *walking* solitons (this term was introduced by Torner, Mazilu and Mihalache [1996]) out of the “quiescent” one (6):

$$u_{\text{sol}} = \frac{\eta}{\sqrt{\gamma}} \operatorname{sech} \left(\frac{\eta}{\sqrt{D}} (\tau - cz - \tau_0) \right) \exp \left[\frac{1}{2} i \left(\eta^2 - \frac{c^2}{D} \right) z + i \frac{c}{D} \tau + i \phi_0 \right], \quad (7)$$

where c is a real walk parameter. Physically, c represents a shift of the central frequency in the soliton’s Fourier transform, which gives rise to a velocity shift via the fiber’s dispersion.

As concerns the propagation of a soliton in an optical fiber, the most important length scale is the *soliton period* z_0 : it is the propagation distance over which the soliton's phase changes by $\frac{1}{2}\pi$ (Agrawal [1995]), so that

$$z_0 = \frac{\pi}{2\eta^2}. \quad (8)$$

As will be explained in different sections of this review, an essential transformation of a strongly perturbed soliton requires a propagation distance $z \gtrsim z_0$.

The soliton solution (7) is characterized by its *area*, *energy* and *momentum*,

$$S \equiv \int_{-\infty}^{+\infty} |u(\tau)| \, d\tau = \pi \sqrt{\frac{D}{\gamma}}, \quad (9)$$

$$E \equiv \frac{1}{2} \int_{-\infty}^{+\infty} |u(\tau)|^2 \, d\tau = \frac{\sqrt{D}}{\gamma} \eta, \quad (10)$$

$$P \equiv i \int_{-\infty}^{+\infty} uu_\tau^* \, d\tau = \frac{1}{\sqrt{D}\gamma} c\eta \quad (11)$$

(the factor $\frac{1}{2}$ in the definition of E is introduced in order to simplify notation below). The energy and momentum, which are defined for an arbitrary field configuration by means of the integral expressions in eqs. (10) and (11), are dynamical invariants (integrals of motion) of eq. (2), while the area is *not* a dynamical invariant. Due to the fact that the NLS equation is exactly integrable by means of IST, the energy and momentum are but the two first items in an infinite set of dynamical invariants conserved by the NLS equation. The third invariant is the Hamiltonian of the NLS equation,

$$H = \frac{1}{2} \int_{-\infty}^{+\infty} (D|u_\tau|^2 - \gamma|u|^4) \, d\tau, \quad (12)$$

while higher-order invariants do not have a straightforward physical interpretation (Zakharov, Manakov, Novikov and Pitaevskii [1980]).

Solitons in various optical media have attracted a great deal of attention, first of all, as objects for fundamental research. In glass fibers, *temporal solitons*, predicted by eq. (2), were first observed by Mollenauer, Stolen and Gordon [1980], and the first observations of *spatial solitons* in planar waveguides of various types, predicted by eq. (5), were reported by Maneuf and Reynaud [1988] and Aitchison, Weiner, Silberberg, Oliver, Jackel, Leaird, Vogel and Smith [1990]. Besides being a physical object of fundamental interest, solitons in fibers

also have a great potential for application to optical communications, as a basis for the so-called return-to-zero format of data transmission, in which a soliton carries a single bit of information. Detailed descriptions of this topic can be found in books by Agrawal [1997] and Iannone, Matera, Mecozzi and Settembre [1998].

1.2. Introduction of variational methods

1.2.1. Models without losses

In a real physical situation, it is necessary to deal with perturbed (deformed) pulses whose area is different from that given by eq. (9). In other words, for real pulses the initial relation between their amplitude and width may strongly deviate from that for the ideal soliton, even if the functional form of the pulse is still close to sech. The evolution of such a perturbed soliton is a problem of great practical importance. Formally, it can be solved exactly by means of IST, but the exact solution is really usable only at an asymptotic stage of the evolution (at $z \rightarrow \infty$), which makes it necessary to develop an approximation that yields a sufficiently accurate explicit result for all values of z .

The corresponding *variational approximation* (VA) for solitons in optical fibers was introduced in the cornerstone paper by Anderson [1983], following the pattern of VA for solitons in other physical media (chiefly, plasmas), which had been developed earlier by Bondeson, Lisak and Anderson [1979]. The VA technique for optical solitons was further developed in an important paper by Anderson, Lisak and Reichel [1988a]. These works became the basis for the rapid development of analytical methods in nonlinear optics based on VA.

The approximation begins with postulating an *ansatz*, i.e., a trial analytical form of the field configuration sought for (in most cases, the configuration is a solitary wave). In the case of the NLS equation (2), a commonly adopted ansatz approximating a perturbed soliton is

$$u_{\text{ansatz}}(z, \tau) = A \operatorname{sech}\left(\frac{\tau}{a}\right) \exp(i\phi + ib\tau^2). \quad (13)$$

The functional form of the ansatz is fixed as concerns its τ -dependence, while it contains several free parameters, for instance the real amplitude A , width a , phase ϕ , and the so-called *chirp* b in the case of the ansatz (13). The free parameters are allowed to be functions of the evolutionary variable, which is z in the case of eq. (2).

Equations governing the evolution of these parameters in z can be derived in a natural way, provided that the underlying equation(s) (e.g., eq. 2) can be

derived by means of the standard variational procedure, equating to zero the variational derivative $\delta S/\delta u^*$ of the corresponding *action functional* $S\{u, u^*\}$ (the asterisk stands for complex conjugation). The variational representation is usually available for conservative models [including those with an explicit coordinate dependence, e.g., the above-mentioned case when the dispersion coefficient D in eq. (2) is a function of z]. Only in some special cases do dissipative models also admit a natural variational representation, see below.

The action is represented in the form $S = \int L dz$, where z is realized as the evolutionary variable, and L is a *Lagrangian*, which is represented in its own integral form,

$$L = \int \mathcal{L} d\tau d\mathbf{r}, \quad (14)$$

where \mathcal{L} is a *Lagrangian density*, that must be real, and \mathbf{r} is the vector set of transverse coordinates (implying the possibility to consider spatiotemporal evolution of fields in two- and three-dimensional dispersive nonlinear media). If the transverse coordinates are present, the ansatz must be a definite function of both τ and \mathbf{r} .

For the NLS equation (2), the Lagrangian density is

$$\mathcal{L} = \frac{1}{2}i(u^* u_z - uu_z^*) - \frac{1}{2}D|u_\tau|^2 + \frac{1}{2}\gamma|u|^4, \quad (15)$$

and $d\mathbf{r}$ is dropped in eq. (14). Generally, in the case of a system of NLS-like equations for complex variables $u_n(z, \tau, \mathbf{r})$, the density is

$$\mathcal{L} = \mathcal{L}(u_n, u_n^*, (u_n)_z, (u_n^*)_z, (u_n)_\tau, (u_n^*)_\tau, \nabla u_n, \nabla u_n^*),$$

where ∇ is the gradient with respect to the transverse coordinates. In this case, the equations following from the variational principle, $\delta S/\delta u_n^* = 0$, take the form

$$\frac{\partial}{\partial z} \frac{\partial \mathcal{L}}{\partial [(u_n^*)_z]} + \frac{\partial}{\partial \tau} \frac{\partial \mathcal{L}}{\partial [(u_n^*)_\tau]} + \nabla \cdot \left[\frac{\partial \mathcal{L}}{\partial (\nabla u_n^*)} \right] - \frac{\partial \mathcal{L}}{\partial u_n^*} = 0. \quad (16)$$

The Lagrangian representation of the nonlinear wave equations is related to their Hamiltonian representation, which, for a broad class of equations of the NLS type, is

$$(u_n)_z = -i \frac{\delta H}{\delta u_n^*}, \quad (17)$$

where the functional $H\{u, u^*\}$ is the Hamiltonian. In particular, for the NLS equation (2) proper, it is given by the expression (12).

In order to apply VA to a given problem, one should insert the adopted ansatz into the expression (14) and calculate the integral in an analytical form. The necessity to perform the integration analytically imposes conditions on the choice of the ansatz: on one hand, it must not be too primitive, in order to have a chance to accurately approximate basic features of the pulse, and, on the other hand, it must not be too complex, otherwise VA will be intractable.

If the ansatz contains a set of free parameters $p_j(z)$ [for instance, $p_1 \equiv A$, $p_2 \equiv a$, $p_3 \equiv b$, $p_4 \equiv \phi$ in the case of the ansatz (13)], the calculation of the integral (14) after the substitution of the ansatz yields an *effective Lagrangian*, L_{eff} , which is a function of p_j and their derivatives $dp_j/dz \equiv p'_j$ (the derivatives appear because of the presence of the z -derivatives in the Lagrangian density). For example, the effective Lagrangian obtained by substitution of the ansatz (13) into the NLS Lagrangian corresponding to the density (15) can be easily calculated analytically:

$$L_{\text{eff}}^{(\text{NLS})} = -2A^2 a \phi' - \frac{\pi^2}{6} A^2 a^3 b' - \frac{1}{3} \frac{DA^2}{a} - \frac{\pi^2}{3} DA^2 a^3 b^2 + \frac{2}{3} \gamma A^4 a. \quad (18)$$

It is noteworthy that only the z -derivatives of the phase parameters ϕ and b appear in this expression, and ϕ itself does not appear at all.

The effective Lagrangian gives rise to a set of variational equations for the variables $p_j(z)$,

$$\frac{d}{dz} \frac{\partial L_{\text{eff}}}{\partial (p'_j)} - \frac{\partial L_{\text{eff}}}{\partial p_j} = 0, \quad (19)$$

which can then be solved by means of analytical or numerical methods. In particular, the system of variational equations generated by the effective Lagrangian (18) for the NLS soliton will be considered in detail in § 2.

First of all, one should find *fixed points* (FPs) of the ordinary differential equation (ODE) system (19), $dp_j/dz = 0$, which correspond to a stationary soliton of the underlying model. Next, stability of the fixed points against small perturbations can be analyzed, linearizing eqs. (19) near the FP solutions, which should predict whether the soliton is expected to be dynamically stable. Full dynamical solutions to eqs. (19) (rather than linearization around the fixed points), that correspond to a strong perturbation of the solitons, may also be of interest from the viewpoint of the underlying model.

Thus, the essence of VA is approximating an unknown field configuration by an appropriate ansatz, whose free parameters evolve in z according to the system of ODEs (19). It is necessary to stress that there is no direct formal

relation between the underlying PDEs (for instance, the NLS equation) and the system of variational equations (19). Thus, VA is always based, to a large extent, on physical intuition rather than on rigorous mathematical arguments, and the relevance of the application of a particular variational ansatz to a given problem can only be checked *a posteriori* by comparison of the results with direct numerical simulations of the underlying PDEs. Comparison with direct simulations is especially necessary if one is dealing with the stability problem: while the shape of a static soliton may be readily mimicked by a reasonably chosen ansatz, the approximation can miss a specific perturbation mode leading to an instability of the soliton; moreover, VA can sometimes introduce a *false instability* that the soliton in fact does not have, see § 7.1 below.

Despite its drawbacks, VA turns out to be a very efficient technique, as it is, as a matter of fact, the only consistent approximation producing analytical or semi-analytical results for complex dynamical models. As for the necessity to verify the validity of the results against direct simulations, this does not devalue VA, since it is frequently sufficient to perform the comparison at a few different values of the problem's control parameters. If the comparison at several benchmark points corroborates the applicability of VA, then its (semi-)analytical predictions are reliable enough to describe solitons in broad parametric regions.

1.2.2. Generalization to models with losses and gain or drive

1.2.2.1. *Models with intrinsic gain.* A physically important and relatively simple generalization of the NLS equation is that which includes losses and amplification. In the general case, it can be written in the form

$$iu_z + \frac{1}{2}Du_{\tau\tau} + \gamma|u|^2u = i\alpha(z)u, \quad (20)$$

where the coefficient $\alpha(z)$ includes a constant negative part $-\alpha_0$ accounting for fiber losses, and an array of δ -functions accounting for the action of strongly localized amplifiers. Thus, in the typical case,

$$\alpha(z) = -\alpha_0 + g \sum_n \delta(z - z_{an}), \quad (21)$$

where $g > 0$ is the gain provided by an individual amplifier, and z_a is the amplification spacing. In the general case, with an arbitrary density $\alpha(z)$ of the

distributed losses and gain, the term on the right-hand side of eq. (20) can be eliminated by means of a transformation

$$u(z, \tau) = \exp\left(\int_0^z \alpha(z) dz\right) \cdot v(z, \tau), \quad (22)$$

which converts eq. (20) into the NLS equation (2) for the field $v(z, \tau)$ with a variable nonlinear coefficient,

$$iv_z + \frac{1}{2}Dv_{\tau\tau} + \gamma \exp\left(2 \int_0^z \alpha(z) dz\right) \cdot |u|^2 u = 0 \quad (23)$$

(Bullough, Fordy and Manakov [1982]). An advantage of this transformed equation is that, unlike the underlying equation (20), it admits a variational representation with the same structure of the Lagrangian density as in eq. (15), γ being replaced by

$$\gamma(z) \equiv \gamma \exp\left(2 \int_0^z \alpha(z) dz\right). \quad (24)$$

Then, *ansätze*¹ of the usual type, e.g., eq. (13), may be used to approximate the field $v(z, \tau)$.

1.2.2.2. Models with an external drive. Another type of models describe systems in which dissipation is compensated not by the intrinsic gain, but rather by an external drive. The first model of this type was introduced by Kaup and Newell [1978]:

$$iu_t + \frac{1}{2}u_{xx} + |u|^2 u = -i\alpha u + \epsilon \exp(-i\omega t), \quad (25)$$

where $\alpha > 0$ is a dissipation constant, and ϵ and ω are the amplitude and frequency of the AC drive applied to the system (this equation is written in “non-optical” notation, as it is less relevant to optics than to other applications). By means of an obvious transformation,

$$u(x, t) \equiv v(x, t) \exp(-i\omega t), \quad (26)$$

eq. (25) can be cast into a more convenient time-independent form,

$$iv_t + \frac{1}{2}v_{xx} + (\omega + |v|^2) v = -i\alpha v + \epsilon. \quad (27)$$

Finally, the dissipative term may be removed from eq. (27) by means of the same transformation (22) as above, leading to an equation representable in the

¹ The word *ansätze* is plural for *ansatz* (which is a synonym for a trial wave form in the variational approximation).

Lagrangian form, which opens the way to apply VA to it. In particular, driving and stabilization of a *cnoidal wave*, i.e., as a matter of fact, a periodic array of NLS solitons, was considered, following this way, by Friedland [1998].

Another possibility is to drive solitons *parametrically*, as described by the following version of the perturbed NLS equation (see, e.g., a paper by Barashenkov, Bogdan and Korobov [1991], where VA was used),

$$iu_t + \frac{1}{2}u_{xx} + |u|^2u = -i\alpha u + \epsilon u^* \exp(-2i\omega t), \quad (28)$$

the asterisk standing for the complex conjugation. The same transformation (26) as above casts eq. (28) into a time-independent form,

$$iu_t + \frac{1}{2}u_{xx} + (\omega + |u|^2)u = -i\alpha u + \epsilon u^*. \quad (29)$$

Note that the last term on the rhs of eq. (29) can be derived from an extra term in the Lagrangian density, $\Delta\mathcal{L} = \frac{1}{2}\epsilon [u^2 + (u^*)^2]$. Therefore, subsequent application of the transformation (22) makes it possible to present eq. (29) in a fully Lagrangian form.

1.3. Comparison with other approximations

Application of VA to optical solitons was not the first instance where this technique was used. Earlier, it was applied by Whitham [1974] to the cnoidal waves in the Korteweg–de Vries (KdV) equation (recall that these waves are periodic arrays of solitons). An exact solution for cnoidal waves in the KdV equation is known in terms of elliptic functions. However, an approximation is necessary when considering a case where parameters of the cnoidal wave are initially subjected to a long-wave modulation. In that case, the ansatz is based on the exact solution, whose arbitrary constant parameters are allowed to be slowly varying functions of the coordinate and time. Upon substituting the ansatz into the corresponding Lagrangian, one can explicitly perform the integration over the rapid variables, arriving at an effective Lagrangian for the slowly varying parameters. Then, the effective Lagrangian yields a system of so-called Whitham's equations (which are also PDEs, but essentially simpler than the underlying KdV equation) governing the slow evolution. The Whitham equations can be used for analysis of various dynamical processes involving the cnoidal waves, e.g., decay of an initial configuration in the form of a step (see chapter 4 in the book by Zakharov, Manakov, Novikov and Pitaevskii [1980]).

As concerns solitary waves proper in models different from those occurring in optics, VA was applied in a systematic way by Gorshkov, Ostrovsky and Pelinovsky [1974] and Gorshkov and Ostrovsky [1981]. Models studied in those works were similar to the KdV equation (but nonintegrable). A typical problem was interaction between far-separated solitons. Using the Lagrangian representation of the underlying model, an effective potential of the interaction between solitons was derived.

Mathematical models for solitons in plasmas are sometimes similar to those in nonlinear optics. In a systematic way, the application of VA to plasma solitons was developed by Bondeson, Lisak and Anderson [1979]. In that work, a generalization of VA allowing to incorporate effects produced by dissipative terms, that cannot be directly derived from the Lagrangian representation, was put forward too.

It should be stressed that when one is dealing with slightly perturbed solitons (for instance, in the case of interactions between far-separated ones), the use of VA is quite legitimate but not necessary. Instead, one may use direct perturbative methods. The most powerful among such methods is based on IST, provided that the underlying PDE is a perturbed version of an integrable equation. This is indeed the case for many problems in nonlinear optics, when the model is described by a perturbed NLS equation. The IST-based perturbation theory was first elaborated by Kaup [1976] (see also a paper by Kaup and Newell [1978]) and, independently, by Karpman, Maslov, and Solov'ev (see an early review by Karpman [1979] and a later important paper by Karpman and Solov'ev [1981], in which the interaction between NLS solitons was treated as a perturbation). Many results obtained by means of the perturbation theory based on IST were collected in a review by Kivshar and Malomed [1989a]. Second-order perturbation effects for the solitons in optical fibers may be taken into regard to improve the accuracy of this technique; this was systematically investigated by Kaup [1991].

As a matter of fact, VA belongs to a class of nonrigorous approximate methods whose objective is to reduce complex dynamics described by PDEs to a relatively simple system of a few ODEs. All these methods aim to “project” the full dynamics onto a finite-mode space, or, in other words, truncate a system with infinitely many degrees of freedom to a finite-dimensional one. This general procedure is often called *Galerkin truncation* (its mathematically rigorous description can be found in a book by Blanchard and Brüning [1992]). It applies not only to conservative systems which admit the Lagrangian representation, but also to dissipative and mixed conservative–dissipative ones. In some cases – typically, slightly above a threshold of an instability that gives rise to formation

of nontrivial patterns – the truncation of dissipative or mixed systems can be performed in a consistent way, using a corresponding small parameter (*overcriticality*). Examples are the derivation, by Malomed and Nepomnyashchy [1990] in the 1D case, and by Zaks, Nepomnyashchy and Malomed [1996] in the 2D case, of a finite-dimensional dynamical system to approximate the pattern formation in the complex cubic Ginzburg–Landau equation with periodic boundary conditions just above the threshold of the modulational instability of a finite-amplitude spatially uniform state. However, in most cases no small parameter is available, and the Galerkin truncation is, as a matter of fact, based solely on intuition.

A specific version of the truncation is the method of *integral momenta*, when the underlying PDE is replaced by several relations obtained, after substituting an adopted ansatz for the approximate solution, by multiplication of the equation by certain *weight functions* and integration of the resultant expression over the temporal and/or transverse spatial variables. The momenta method in its various forms has been used widely in various problems of nonlinear optics, e.g., by Caglioti, Trillo, Wabnitz, Crossignani and DiPorto [1990], Romagnoli, Trillo and Wabnitz [1992] and Maimistov [1993] for the study of soliton dynamics in dual-core fibers, by Akhmediev and Soto-Crespo [1994] for the description of soliton dynamics in a bimodal birefringent fiber, and by Turitsyn, Schaefer and Mezentsev [1998] and Bélanger and Paré [1999] in the study of pulse propagation in dispersion-managed fiber links. A similar method was employed by Barashenkov, Smirnov and Alexeeva [1998] and Barashenkov and Zemlyanaya [1999] to consider bound states of solitons in the driven NLS equations (25) and (28).

The VA technique does not have a rigorous justification either. Nevertheless, it is essentially less arbitrary than other truncation-based approximations, as it is based on the variational principle, which is known to be the most fundamental one unifying various physical models. In this connection, it is relevant to mention that VA for *linear* physical systems (unlike nonlinear ones which are the subject of the present review) has been developed long ago under the name of the *Rayleigh–Ritz optimization procedure*, reviewed by Gerjuoy, Rau and Spruch [1983], that has well-known applications, e.g., to finding stationary wave functions in quantum mechanics (Landau and Lifshitz [1977]). It is relevant to mention that essentially the same method was used by Barashenkov, Bogdan and Korobov [1991] to analyze the stability, in terms of the corresponding eigenmodes, of a soliton in the parametrically driven NLS equation (28), and by Barashenkov, Gocheva, Makhankov and Puzynin [1989] in their consideration of the stability of dark solitons. A rigorous

mathematical account of the Rayleigh–Ritz procedure is given in the book by Blanchard and Brüning [1992].

1.4. *Objective of this review*

There is a huge number of papers using VA in various problems of nonlinear optics and in other areas of “nonlinear physics”. The present review, being limited in size, is necessarily limited in scope too. It does not aim to give a comprehensive review of all applications of VA to optics, nor does it give references to all relevant publications. Instead, the objective is to collect most important examples of the application of variational methods to solitons in optical fibers, and a few examples concerning solitons in other optical media (chiefly, in planar waveguides), which can be used as paradigms for many other applications. The review is focused on solitons (this term is realized in a loose mathematical sense, i.e., it does not imply integrability of the underlying models), as they are the most natural objects for the application of variational methods, and the absolute majority of results have been obtained for solitons. Fibers are selected as the main medium to be considered in this review, as in this field variational methods have been developed better than in any other, and fibers are most important for applications. In § 2, the consideration will start with the most fundamental case of a single soliton in a uniform nonlinear optical fiber. Then, at the end of § 2 and in subsequent sections, more complex models will be introduced and considered, increasing the number of solitons, or the number of equations, or considering nonuniform optical media. In several cases, which are fundamentally important for applications, the presentation is not limited solely to results which can be obtained by means of VA, but a more comprehensive account of the problem as a whole is given; examples are bound states of solitons (§ 2.3.2), and generation of solitons of different types by a pulse passing a point where the local dispersion changes sign from normal to anomalous (§ 5.2).

Three large topics belonging to the field of nonlinear optics are not included in this review. These are systems with quadratic ($\chi^{(2)}$) nonlinearities (second-harmonic-generating media), spatiotemporal solitons (“light bullets”), and discrete systems. The first topic has recently been reviewed in a systematic way by Etrich, Lederer, Malomed, T. Peschel and U. Peschel [2000]. That review includes, *inter alia*, a thorough account of the application of VA to $\chi^{(2)}$ systems. Additionally, variational methods for $\chi^{(2)}$ models were the main subject of another (more special) recent review by Malomed [2000].

In particular, as concerns “light bullets”, a large part of the theoretical analysis, and the only experimental observations of the spatiotemporal solitons reported thus far (by Liu, Qian and Wise [1999b] and Liu, Beckwitt and Wise [2000]), pertain to $\chi^{(2)}$ media. The theoretical description of $\chi^{(2)}$ spatiotemporal solitons relies heavily upon VA (Malomed, Drummond, He, Berntson, Anderson and Lisak [1997]), and this was included in the above-mentioned recent reviews.

Variational techniques prove to be very useful also for consideration of multidimensional solitons in media with different nonlinearities, such as cubic–quintic (Quiroga-Teixeiro and Michinel [1997], Desyatnikov, Maimistov and Malomed [2000]). In fact, a review of spatiotemporal solitons seems to be necessary, but it cannot be given in the present article due to length limitations.

As for discrete systems, this is a large field which calls for a separate review. Variational methods are frequently used in this field too (see, e.g., a paper by Malomed and Weinstein [1996]), but their technical implementation is quite different from what is considered in the present article.

Lastly, it is necessary to mention that variational techniques, similar to those developed in nonlinear optics, find applications to the description of soliton-like objects in other physical systems. An important example is the Bose–Einstein condensate, i.e., a cloud of ultracold atoms obeying the Bose quantum statistics and held together in a trap. The corresponding model is based on the *Gross–Pitaevskii* equation, which, as a matter of fact, is the three-dimensional NLS equation with an external potential representing the trap. The cubic term in the Gross–Pitaevskii equation has, in most cases, a sign corresponding to repulsive interaction between atoms in the condensate, although it may sometimes be attractive, then making the condensate prone to collapse. VA for the Bose–Einstein condensates with both repulsive and attractive interactions was developed by Dodd [1996], Pérez-García, Michinel, Cirac, Lewenstein and Zoller [1997], and Pérez-García, Konotop and García-Ripoll [2000].

Another noteworthy example of the application of an “optical-like” VA to non-optical systems is the description of intrinsic vibrations of an (effectively) one-dimensional soliton in the *Zakharov system*, which is a fundamental model of the interaction between electron (Langmuir) and ion-acoustic waves in plasmas. As was demonstrated by Malomed, Anderson, Lisak, Quiroga-Teixeiro and Stenflo [1997], VA reduces the internal dynamics of this soliton to a Hamiltonian system with two degrees of freedom, which, in particular, may give rise to dynamical chaos.

§ 2. Dynamics of solitons in a single-mode nonlinear optical fiber or waveguide

2.1. A soliton in an optical fiber

2.1.1. Anderson approximation for a nonstationary NLS soliton

The application of VA to nonlinear optics was initiated by Anderson [1983] when he considered the evolution of a strongly perturbed NLS soliton governed by eq. (2). In that pioneering work, a Gaussian ansatz for the soliton was used. While this type of approximation is very useful in the case of *dispersion management* (see § 5), the most appropriate ansatz for a soliton in a uniform optical fiber is the hyperbolic-secant-based one (13). In fact, the variational equations derived by Anderson [1983] on the basis of the Gaussian ansatz are very close to those which will be displayed below for the ansatz (13).

The effective Lagrangian for this ansatz is given by the expression (18). The corresponding system of variational equations (19) was first derived by Anderson, Lisak and Reichel [1988a]. After some transformations, the equations can be conveniently cast into the following form, which is also valid in the important case when the dispersion coefficient D in eq. (2) is a function of z (Malomed [1993]):

$$\frac{d}{dz} (A^2 a) = 0, \quad (30)$$

$$b = \frac{1}{2Da} \frac{da}{dz}, \quad (31)$$

$$\frac{d}{dz} \left(\frac{1}{D} \frac{da}{dz} \right) = -\frac{\partial U_{\text{eff}}(a)}{\partial a}, \quad (32)$$

$$U_{\text{eff}}(a) \equiv \frac{2}{\pi^2} \left(\frac{D}{a^2} - 2\gamma \frac{E}{a} \right), \quad E \equiv A^2 a, \quad (33)$$

and a separate equation for the phase ϕ ,

$$\frac{d\phi}{dz} = \frac{\pi^2}{12} a^2 \left(\frac{db}{dz} + 2Db^2 \right) + \frac{1}{6} Da^{-2} - \frac{2}{3} \gamma A^2. \quad (34)$$

First of all, eq. (30) implies the existence of the dynamical invariant $E \equiv A^2 a$. The conservation of this quantity is a straightforward manifestation of the conservation of the energy (10) in the NLS equation. Indeed, the substitution of the ansatz (13) into the definition of the energy yields $A^2 a$.

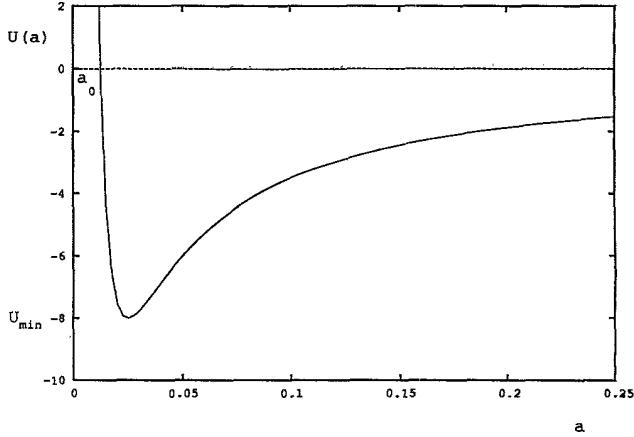


Fig. 1. Shape of the effective potential (33) for $D = 1$, $E = 4\pi^2$ (the large value of E serves to emphasize the characteristic shape of the potential).

An essential remark concerning the formal properties of VA is that one may replace the combination A^2a everywhere in the effective Lagrangian (18) by *constant* E , which is not subject to the variation, and then perform the variation (after this, the phase-evolution equation (34) is derived by the variation in E). The resultant equations have exactly the same form as above. This feature makes it possible to simplify the derivation of the variational equations.

Equation (31) shows that the intrinsic chirp of the soliton is generated by its deformation (change of width). This equation also explains why the chirp must be included into any self-consistent ansatz: otherwise, intrinsic evolution of the soliton, the study of which is the basic objective of VA, cannot be described.

Equations (32) and (33) demonstrate that the evolution of the soliton's width can be represented, in closed form, as the motion of a Newtonian particle with mass D^{-1} and coordinate $a(z)$ in a potential well $U_{\text{eff}}(a)$, the shape of which is shown in fig. 1, while the propagation distance z plays the role of time. In fact, as stressed by Abdullaev and Caputo [1998], the effective potential $U_{\text{eff}}(a)$ is exactly the same as in the classical Kepler problem (see a book by Landau and Lifshitz [1975]). Note that when the dispersion coefficient D is a function of z , both the particle's mass and the potential depend explicitly on "time".

There is an equilibrium position

$$a_{\text{eq}} = \frac{D}{\gamma E} \quad (35)$$

at the bottom of the potential well (33) (if $D = \text{const.}$). Comparison with expression (6) shows that the ansatz (13) with $a = a_{\text{eq}}$ coincides exactly with the

unperturbed soliton solution, i.e., VA correctly reproduces the exact stationary soliton. The Hamiltonian corresponding to eq. (32) is $H = (1/2D)(da/dz)^2 + U_{\text{eff}}(a)$, and, as demonstrated by Anderson, Lisak and Reichel [1988b], it can be obtained in exactly this form by the substitution of ansatz (13) into the Hamiltonian (12) of the underlying NLS equation. If $D = \text{const.}$, the Hamiltonian is a dynamical invariant of eq. (32). Dynamical trajectories with $H < 0$ and $H > 0$ correspond to the motion of a particle which, respectively, is trapped in the potential well or escapes to infinity.

Oscillations of the trapped particle correspond to internal vibrations of a soliton-like pulse which is initially chirped and/or has a relation between its amplitude and width different from that for the exact soliton solution. Near the equilibrium position (35), oscillations with a small amplitude $a_1^{(0)}$ have the form

$$a(z) = a_{\text{eq}} + a_1^{(0)} \sin(K_0 z + \delta), \quad K_0 = 2 \frac{(\gamma E)^2}{\pi D}. \quad (36)$$

Here, δ is an arbitrary constant, and the spatial period of the small oscillations, $z_{\text{osc}} \equiv 2\pi/K_0 = \pi^2 D / (\gamma E)^2$, is not much different from the *soliton period* (8) of the unperturbed soliton, which, in the notation used in eq. (36), is $z_0 = \pi D / (\gamma E)^2$ (in fact, $4z_0$ is more appropriate for the comparison with z_{osc} , as z_0 proper corresponds, by definition, to the change of the soliton's internal phase by $\frac{1}{2}\pi$, rather than 2π).

Exact results for eq. (32) are available too. In particular, an expression for the spatial frequency K of anharmonic oscillations of the trapped particle can be found in papers by Afanasjev, Malomed, Chu and Islam [1998] and Abdullaev and Caputo [1998]. It takes a compact form in terms of the Hamiltonian H ,

$$K = \pi^2 \frac{\sqrt{D}|H|^{3/2}}{\sqrt{2\gamma E}}, \quad (37)$$

and attains the maximum value K_0 given by eq. (36) at $H = -2(\gamma E/\pi)^2 D^{-1}$, that corresponds to the bottom of the potential well. Exact solutions to the effective equation of motion (32) with the potential (33) can be represented in a parametric form, using known results for the above-mentioned Kepler problem (Abdullaev and Caputo [1998]). Setting $D = \gamma = 1$, the exact solutions describing oscillations of the particle trapped in the potential well are

$$a = \frac{2E}{\pi^2 |H|} (1 - e_0 \cos \xi), \quad Kz = \xi - e_0 \sin \xi, \quad (38)$$

where K is the frequency (37), $e_0 \equiv \sqrt{1 - \pi^2 |H| / 2E^2}$ plays the role of the eccentricity in the Kepler problem, and ξ is an auxiliary dynamical variable (the parameter).

Persistent internal vibrations of a perturbed NLS soliton can be easily observed in direct simulations of eq. (2); see, e.g., detailed numerical results in the paper by Kath and Smyth [1995]. In fact, the explanation of the soliton's vibrations as oscillations of the trapped particle in terms of the ansatz was the first result of VA explaining a nontrivial dynamical behavior of the perturbed soliton; note that, while this result is obtained by means of VA in quite a simple way, it is not straightforward to predict the vibrations of perturbed solitons by means of the rigorous IST formalism.

The regime of motion with $H > 0$, corresponding to $a(z) \rightarrow \infty$, implies unlimited spreading out of the pulse, i.e., as a matter of fact, its decay into radiation. Thus, VA can indirectly predict transformation of the pulse into radiation, although the ansatz does not take into regard radiation degrees of freedom. The *separatrix* $H = 0$ is a border between the pulses that are predicted to self-trap into soliton-like states and those which decay completely.

For an initial unchirped pulse (13) with $b = 0$ and arbitrary values of the amplitude A_0 and width a_0 , the soliton content can be found in an exact form, in terms of IST, from a solution to the corresponding ZS equations (Satsuma and Yajima [1974]). An important *exact* result is that the pulse produces a soliton, in the limit $z \rightarrow \infty$, provided that

$$A_0 a_0 > \frac{1}{2} \sqrt{D/\gamma}. \quad (39)$$

On the other hand, the condition $H < 0$, which is necessary for the formation of a soliton-like pulse in terms of VA, yields, for the same initial configuration,

$$A_0 a_0 > \sqrt{D/2\gamma}. \quad (40)$$

Comparing this to the exact result (39), one concludes that VA *underestimates* the soliton's stability, in terms of the soliton-formation threshold, by a factor $\sqrt{2}$. An empirical modification of the variational technique, which can remedy this shortcoming, was proposed by Anderson, Lisak and Reichel [1988a].

2.1.2. Solitons in extended versions of the NLS equation

It is well known that, even if an optical fiber has no losses, the NLS equation for very narrow solitons (roughly speaking, with temporal width < 1 ps and, accordingly, with high power) should be modified against its classical integrable version (2). Additional terms take into regard the *third-order dispersion* (TOD)

with a corresponding coefficient \tilde{D} and, sometimes, a higher-order (quintic) correction to the Kerr nonlinearity, with a coefficient $\tilde{\gamma}$:

$$iu_z + \frac{1}{2}Du_{\tau\tau} + \gamma|u|^2u = i\tilde{D}u_{\tau\tau\tau} + \tilde{\gamma}|u|^4u. \quad (41)$$

If only the quintic term is added, the corresponding *cubic–quintic* (CQ) NLS equation can be rescaled into a normalized form,

$$iu_z + \frac{1}{2}u_{\tau\tau} + |u|^2u - |u|^4u = 0. \quad (42)$$

Equation (42) is not integrable, but it has an exact single-soliton solution (Kh.I. Pushkarov, Pushkarov and Tomov [1979]; see also D.I. Pushkarov and Tanev [1996]),

$$u = e^{ikz} \cdot \frac{2\sqrt{k}}{\sqrt{1 + \sqrt{1 - \frac{16}{3}k} \cosh(2\sqrt{2k}\tau)}}, \quad (43)$$

where k is the propagation constant, taking values $0 < k < \frac{3}{16}$.

As the quintic term in eq. (42) corresponds to an extra term $-\frac{1}{3}|u|^6$ in the Lagrangian density for the NLS equation, VA can be developed to describe internal vibrations of a perturbed soliton in the CQ equation, as was done by Kumar, Sarkar and Ghatak [1986] [they also took into regard a dissipative term, eliminating it by means of the transformation (22)] and De Angelis [1994] on the basis of a Gaussian ansatz. In this connection, it is relevant to mention that, for the NLS equation with a general nonlinear term $|u|^q u$, where q is an arbitrary positive number, Cooper, Shepard, Lucheroni and Sodano [1993] developed VA based on a *super-Gaussian* ansatz, assuming

$$u(z, \tau) = A(z) \exp \left[(-1 + ib(z)) \left| \frac{\tau}{W(z)} \right|^{2n} \right], \quad (44)$$

where $W(z)$ and $b(z)$ are real width and chirp variables, $A(z)$ is a complex amplitude, and n is an appropriately chosen positive constant. This ansatz makes it possible to analyze not only regular dynamics of a perturbed soliton, but also *spatiotemporal collapse* of the pulse, i.e., formation of a singularity after a finite propagation distance, which takes place (in the one-dimensional case) if $q \geq 4$, see a review by Bergé [1998] (VA for describing the collapse of three-dimensional pulses in the usual cubic NLS equation was elaborated by Desaix, Anderson and Lisak [1991]). A general super-Gaussian ansatz was also

used by Dimitrevski, Reimhult, Svensson, Öhgren, Anderson, Berntson, Lisak and Quiroga-Teixeiro [1998] to analyze dynamics of axisymmetric beams in a bulk medium with the CQ nonlinearity (which, in fact, amounts to considering the CQ NLS equation with two transverse coordinates). Lastly, it is relevant to mention that various forms of VA were also applied to construct *spinning* solitons, i.e., solitons with internal vorticity, in the two-dimensional (Wright, Lawrence, Torruellas and Stegeman [1996], Quiroga-Teixeiro and Michinel [1997]) and three-dimensional (Desyatnikov, Maimistov and Malomed [2000]) NLS equations with the CQ nonlinearity.

The TOD term in eq. (41) can also be derived from an extra term in the Lagrangian density, viz., $(i/2)\tilde{D}(uu_{\tau\tau}^* - u^*u_{\tau\tau})$, hence VA applies to this version of the NLS equation too. It is necessary to stress that, strictly speaking, the NLS equation with this additional term has no soliton solution, as any solitary pulse gradually decays into radiation, due to the form of the equation's linear spectrum (Wai, Chen and Lee [1990]). Nevertheless, if the TOD coefficient is small enough, the rate of radiative decay is exponentially small, and it then makes sense to consider evolution of a soliton in this equation. A VA-based approach to the problem was developed by Desaix, Anderson and Lisak [1990].

As the NLS equation upon addition of the TOD term loses its invariance with respect to a sign change of τ , an appropriate ansatz should not be even in τ . In the above-mentioned paper, the ansatz was taken as

$$u(z, \tau) = A(z) \operatorname{sech}(\tau - T(z)) \times \exp[-i(\tau - T(z))\Omega(z) - iM(z)\tanh(\tau - T(z)) + ib(z)(\tau - T(z))^2], \quad (45)$$

where the amplitude $A(z)$ is complex, and all the other variational parameters are real, cf. eq. (13). Consideration of evolution equations for the variational parameters has demonstrated that the soliton shifts itself, in the frequency domain, deeper into the anomalous-dispersion region, so that the relative size of the TOD term becomes small, and the soliton becomes close to its ordinary NLS counterpart. This result is, generally, confirmed by numerical simulations reported by Wai, Menyuk, Chen and Lee [1987], although the simulations also demonstrate that a relatively small wave packet separates from the initial pulse and then drifts in the opposite direction, deeper into the normal-dispersion region, where it completely decays into radiation.

2.1.3. Radiative losses and damping of internal vibrations of a soliton

The most essential limitation of VA is the fact that a simple ansatz, like that given by eq. (13), completely ignores radiation degrees of freedom of the field.

In fact, as known from both the exact solution produced by IST and from numerical simulations, a perturbed soliton, while vibrating in accord with the VA prediction, is also emitting small-amplitude radiation waves, which gives rise to gradual decrease of the vibration amplitude. The exact result of IST is that, at $z \rightarrow \infty$, the pulse will shed a finite fraction of its energy as radiation, and will eventually assume the form of an exact soliton with a reduced value of the energy.

A modification of the ansatz (13) that accounts for the radiation background around the soliton was proposed by Kath and Smyth [1995]:

$$u_{\text{ansatz}}(z, \tau) = [A \operatorname{sech}(\tau/a) + ig] \exp(i\phi + ib\tau^2), \quad (46)$$

where $g(z)$ is a real amplitude of the radiation background that is assumed to be uniform (τ -independent) across the soliton; it was also assumed that $|g| \ll A$, i.e., the background's amplitude is much smaller than that of the soliton. Of course, the substitution of the modified ansatz (46) into the Lagrangian density (15) and subsequent integration in the expression (14) for the full Lagrangian will give rise to a divergence as the term $\sim g$ does not vanish as $|\tau| \rightarrow \infty$. Therefore, the integration was confined to a finite interval $|\tau| < l$; in particular, the net energy of the wave field is then $A^2 a + \frac{1}{2} g^2 l$. To select the parameter l , the condition was adopted that the (spatial) frequency of the small oscillations of the amplitude of the slightly perturbed soliton matches the frequency in eq. (36), which yields $l = 3\pi^2/8a_{\text{eq}}$, where a_{eq} is the equilibrium width (35), and it is implied that $D = \gamma = 1$ in eq. (2).

The variational equations derived by means of the ansatz (46) were further amended by adding, to an equation accounting for the energy conservation, an extra term that directly took into regard radiation losses, as calculated from a linearized equation for the radiation wave far from the soliton's body. The modified variational equations [which turn out to be much more complicated than the system of eqs. (30) through (34) produced by the Anderson approximation] were then solved numerically, showing not only persistent internal vibrations of a perturbed NLS soliton, but also gradual damping of the vibrations due to the emission of radiation. Comparison with direct numerical simulations of eq. (2) has demonstrated that this modified version of VA yields very good accuracy in the description of the soliton's dynamics.

Direct comparison of the VA predictions for the internal vibrations of the NLS solitons with direct simulations of eq. (2) was also a subject of a work by Kuznetsov, Mikhailov and Shimokhin [1995]. In this paper, it was claimed that VA is essentially wrong, as the frequency of the small vibrations revealed

by extremely long simulations was quite different from the expression given by eq. (36). However, this conclusion was a result of an apparent misunderstanding: in fact, the numerical results presented in that work pertained to a very late stage of the evolution, when the emission of radiation by the vibrating pulse has actually ended, and the observed (extremely small) oscillations of the soliton's amplitude were not vibrations of the perturbed pulse, but simply beatings between the stationary soliton and a very small low-frequency component of the radiation wave which had not yet separated from the soliton. Of course, the beating frequency is different from that of the vibrations of a pulse consisting of the soliton and trapped radiation.

2.1.4. The soliton-compression problem and modified variational ansätze

The Anderson approximation, based on the simple ansatz (13) or its Gaussian counterpart used in the first paper by Anderson [1983], can be better adjusted to specific problems without adding radiative degrees of freedom. A particular problem important for applications is compression of pulses based on the so-called soliton effect, i.e., passing a stationary (fundamental) soliton to a fiber with a smaller value of the dispersion coefficient, where the pulse will be a higher-order soliton and will start to self-compress, developing internal chirp (an allied problem is the investigation of conditions for wavebreaking-free propagation of nonsoliton pulses in an optical fiber, which was earlier considered by Anderson, Desaix, Karlsson, Lisak and Quiroga-Teixeiro [1993]). For a given ratio $N^2 \equiv D_1/D_2$ of the dispersion coefficients D_1 in the fiber in which the soliton was formed as a fundamental one and D_2 in the compressing fiber (or, in terms of the soliton effect, for a given order N of the initial N -soliton), and for given energy of the soliton, the most important characteristic of the process is the optimum compression length L of the second fiber at which the narrowest chirp-free pulse is expected to come out. To minimize the number of arbitrary parameters, one can take eq. (2) with $D = \gamma \equiv 1$, and consider compression of the initial N -soliton pulse in which the width is set to be 1,

$$u_0 = N \operatorname{sech} \tau, \quad (47)$$

so that $E \equiv N^2$. Then, the optimum compression length should be found as a function of the single free dimensionless parameter E .

This problem was considered in detail by Afanasjev, Malomed, Chu and Islam [1998], who compared, against direct numerical results, predictions provided by the traditional ansatz (13) and by a modified one,

$$u = A \operatorname{sech}(\tau/a) \exp[i\phi + ib \tanh^2(\tau/a)], \quad (48)$$

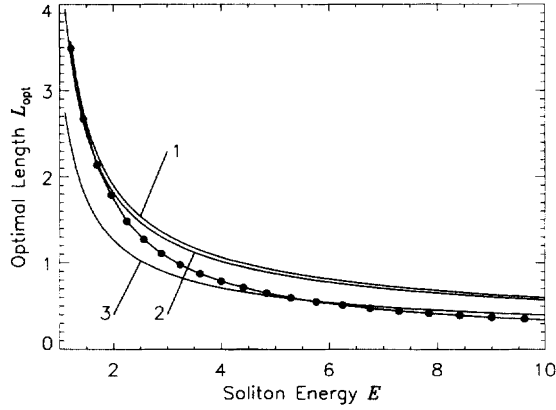


Fig. 2. Optimum compression length for the initial N -soliton pulse (47) in a fiber governed by eq. (2) with $D = \gamma = 1$ vs. energy E : (1) prediction based on the traditional ansatz (13); (2,3) predictions produced by the modified *ansätze* (51) and (48); dots represent results of direct simulations, connected by an interpolating curve.

where b is the chirp parameter. The introduction of this ansatz was suggested by direct simulations, which demonstrated that the intrinsic phase structure of the compressed pulse was very different from the parabolic function assumed by eq. (13). Instead, the phase distribution is parabolic near the soliton's center, and saturates at a constant value far from the soliton's center, which is mimicked by the modified ansatz (48).

VA based on the usual ansatz (13) predicts compression of the initial N -soliton pulse (decreasing $a(z)$) up to the turning point $z = \pi/K$, where K is the spatial frequency of the soliton's vibrations given by eq. (37) with $H = (2/\pi^2)(1 - 2E)$. Thus, $z = \pi/K$ is the optimum compression length as predicted by the usual ansatz. An explicit formula for the predicted optimum compression length is

$$L = \frac{1}{2}\pi^2 E \sqrt{2E - 1}. \quad (49)$$

It has no meaning for $E < 1$, as in this case the deformed soliton will be initially expanding, rather than compressing. VA also predicts the degree of compression,

$$\alpha \equiv \frac{a(z=0)}{a(z=L)} = 2E - 1. \quad (50)$$

In fig. 2, the dependence $L(E)$ as given by eq. (49) (curve 1) is displayed vs. the dependence obtained by direct simulations of the NLS equation with the initial conditions (47). The numerical results are represented by dots connected by an

interpolating curve. The two curves are quite close at $E \leq 2$, which corresponds to small compression degrees, but for larger E the actual optimum compression length is essentially smaller than the predicted value. For the case of relatively small compression rates, a very detailed comparison between direct numerical simulations of the N -soliton compression and the corresponding predictions of the usual version of VA, based on the ansatz (13), has been given by Quiroga-Teixeiro, Anderson, Berntson and Lisak [1995].

To improve VA in the case of large compression rates, the modified ansatz (48) was tried, along with the following one:

$$u = A[\operatorname{sech}(\tau/a)]^{1+ib} e^{i\phi} \quad (51)$$

with a real chirp parameter b and the phase $b \ln(\operatorname{sech}(\tau/a))$ which is growing linearly at $|\tau| \gg a$, i.e., it is sort of intermediate between the phases in eqs. (13) and (48). Note that this ansatz follows the pattern of the initial pulse configuration $u_0 = A[\operatorname{sech}(\tau/a)]^{1+ib}$, which is the most general one for which the ZS equations can be solved in an exact form (Maimistov and Sklyarov [1987], Grünbaum [1989]).

The ansatz (51) gives rise to the effective Lagrangian (cf. eq. 18)

$$L_{\text{eff}} = -\frac{Eb}{a} a' - \frac{1}{3} \frac{Eb^2}{a^2} - \frac{1}{3} \frac{E}{a^2} + \frac{2}{3} \frac{E^2}{a}, \quad (52)$$

and a set of evolutionary equations that reduces to

$$b = -\frac{3}{2} a \frac{da}{dz}, \quad a'' = \frac{4}{9} \left(\frac{1}{a^3} - \frac{E}{a^2} \right). \quad (53)$$

Comparison with eqs. (32) and (33) shows that, although the expression for the chirp parameter is different from eq. (31), the evolution equation for the soliton's width keeps the same form of the Newton equation of motion for a particle with a coordinate $a(z)$ in the Kepler-problem potential (33), the only difference being a change of the particle's mass from 1 to $m_{\text{eff}}^{(1)} = 9/\pi^2 \approx 0.912$ (recall we now set $D = \gamma \equiv 1$). In terms of the plot $L(E)$, this difference amounts to a simple rescaling: the original curve 1 in fig. 2 should be uniformly stretched in the horizontal direction by the factor $(m_{\text{eff}}^{(1)})^{-1/2} \approx 1.047$, which gives rise to curve 2. This minor change renders the theoretical prediction slightly closer to the numerical data at $E \leq 2$, but it does not remedy the major discrepancy at larger values of E .

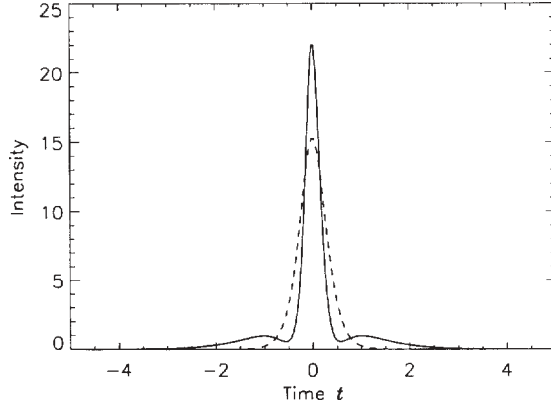


Fig. 3. Intensity distribution $|u|^2$ in a pulse with energy $E = 5.5$ at point $z = 0.5$, close to the optimum compression point, as predicted by the modified variational ansatz (48) (dashed curve) and as per direct simulations (solid curve).

The effective Lagrangian for the modified ansatz (48) is

$$L_{\text{eff}} = \frac{2Eb}{3}a' - \frac{32Eb^2}{105} \frac{1}{a^2} - \frac{1}{3} \frac{E}{a^2} + \frac{2}{3} \frac{E^2}{a}, \quad (54)$$

producing the evolution equations (cf. eqs. 53, 53)

$$b = \frac{35}{32}a a', \quad a'' = \frac{32}{35} \left(\frac{1}{a^3} - \frac{E}{a^2} \right). \quad (55)$$

Thus, the evolution equation for $a(z)$ can again be obtained from the effective potential (33), the corresponding effective mass being $m_{\text{eff}}^{(2)} = 35/8\pi^2 \approx 0.443$. Its drastic difference from $m_{\text{eff}}^{(1)}$, corresponding to the ansatz (51), and from $m_{\text{eff}}^{(0)} \equiv 1$, corresponding to the traditional ansatz, is noteworthy. The change in the curve $L(E)$ produced by the new value of the effective mass again amounts to stretching, this time by a factor $(m_{\text{eff}}^{(1)})^{-1/2} \approx 1.502$, yielding curve 3 in fig. 2. An immediate conclusion is that the new curve is much worse than the previous ones at $E \leq 2$; in the range $2 \leq E \leq 3.5$ the numerical data fall between curves 1 and 3; and at $E \geq 4$ the modified ansatz (48) definitely gives a better approximation.

To directly illustrate the strong compression of the soliton, we display in fig. 3 its intensity profile $|u(\tau)|^2$ at a point close to the optimum compression length, for $E = 5.5$. As one sees, this profile is reasonably well approximated by the modified ansatz (48), while the traditional ansatz (13) predicts in this case a profile which is completely off the actual one.

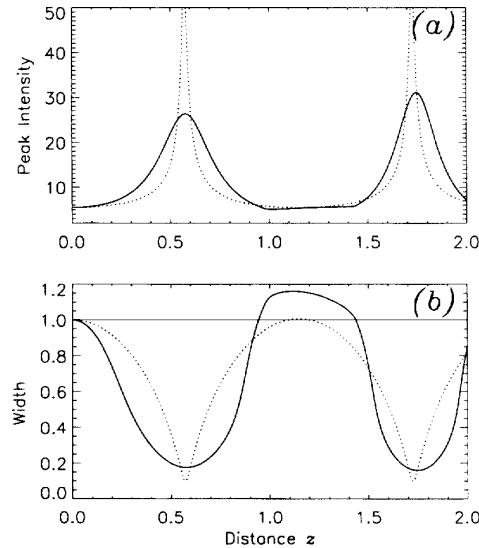


Fig. 4. (a) Peak power and (b) width of a pulse with energy $E = 5.5$ vs. propagation distance. The solid and dotted curves display, respectively, direct numerical results and analytical predictions produced by the modified variational ansatz (48). Two full compression–dilatation cycles are shown.

Further information about the accuracy (or inaccuracy) of the modified version of VA is given by the dependences of the pulse’s peak intensity and width on the propagation distance, displayed in fig. 4 for $E = 5.5$. A general inference suggested by these plots is that, at this quite large degree of compression, the modified VA overestimates the peak intensity very close to the optimum compression point, but, otherwise, provides a reasonable analytical approximation, and is quite accurate in predicting the optimum compression length, which is most important for applications.

In a recent work, Smyth [2000] has revisited detailed comparison of direct numerical simulations of the compression problem with results predicted by VA, adding the above-mentioned sophisticated version of VA worked out by Kath and Smyth [1995], which includes the small radiation background. A conclusion was that, while the modified ansatz (48) and the ansatz including the radiation predict the optimum compression length equally accurately for large values of the compression degree, the latter ansatz predicts the amplitude and width of the compressed pulse, and the phase distribution in it, essentially better.

Lastly, it is relevant to mention the problem of soliton compression in conjugation with the action of localized or distributed amplification, which is described by the modified NLS equation (20). Detailed investigations performed

by Quiroga-Teixeiro, Anderson, Andrekson, Berntson and Lisak [1996] and by Chu, Malomed and Peng [1996] have demonstrated that VA based on the ansatz of the usual type (13), taking into account the effective variable nonlinear coefficient (24), provides for sufficiently accurate predictions for compression of the soliton in such a setting.

2.1.5. Compression of a soliton in a three-fiber configuration

The pulse-compression technique described in the previous subsection does not make it possible to transform a given soliton into a compressed *fundamental* soliton corresponding to the smaller value of the dispersion coefficient. Instead, it produces a vibrating chirped pulse. The problem of compression of solitons without disturbing their fundamental character is of great interest. As follows from the general expression (6) for the soliton, its width can be presented in terms of the energy as $W \equiv \sqrt{D}/\eta = D/\gamma E$; hence, if the fundamental soliton is compressed by lowering the dispersion coefficient from D_1 to D_2 , without energy loss and at a constant value of the nonlinearity coefficient, the ideal compression factor is

$$\left(\frac{W_1}{W_2}\right)_{E=\text{const.}} = \frac{D_1}{D_2}. \quad (56)$$

One possibility to achieve nearly ideal compression is to use a *dispersion-decreasing* fiber with a gradually decreasing local dispersion coefficient, which is able to perform adiabatic compression of a soliton, as described below in § 5.1. However, a much simpler possibility is to use the configuration proposed by Anderson, Lisak, Malomed and Quiroga-Teixeiro [1994], in which an intermediate fiber segment, with a value \tilde{D} of its dispersion coefficient taking some specially chosen value between the initial and final values D_1 and D_2 , is inserted between the incoming and outgoing fibers.

In terms of the standard VA, the incoming soliton corresponds to a particle resting at the bottom of the potential well (see fig. 1) corresponding to $D = D_1$. In passing to the second fiber, and then to the third, the soliton jumps from one potential well into another, corresponding to a different value of D (it is assumed that the nonlinear coefficient is the same in all the fibers involved). The energy E , width a , and chirp b of the pulse must be continuous across the jump. According to eq. (31), the continuity of b implies that the combination $D^{-1}da/dz$ must keep its value, as does a , across the jump, while the derivative da/dz itself changes its value by a jump.

Within the framework of this description, an *ideal* transformation of an incoming fundamental soliton, which was adjusted to the dispersion coefficient $D = D_1$,

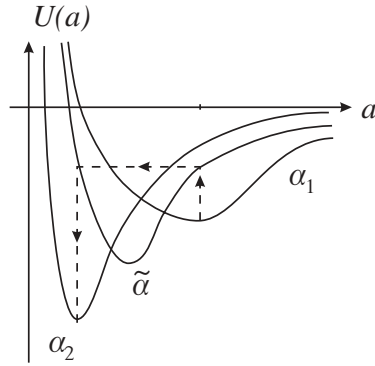


Fig. 5. Potential wells corresponding to three different values of the dispersion coefficient (here denoted α) for a fixed value of the soliton energy. The dashed trajectory demonstrates the possibility for ideal compression of the input soliton into an output soliton, keeping its fundamental character.

into an outgoing fundamental soliton, adjusted to $D = D_2$, is achieved if the value \tilde{D} of the dispersion in the intermediate fiber and its length L_* are selected in such a way that after the jump from the first potential well into the second the soliton performs exactly half a cycle of oscillations in the second well, hits its wall, and at this point jumps into the third potential well corresponding to $D = D_2$, as illustrated by fig. 5. An elementary calculation at constant energy yields

$$\tilde{D} = \frac{2D_1D_2}{D_1 + D_2}, \quad L_* = \frac{\pi^2 (D_1 + D_2)^2}{8\sqrt{D_1D_2}E^2} \quad (57)$$

(here, the nonlinear coefficient is $\gamma \equiv 1$). In this approximation, the same result is expected if the soliton passing the intermediate segment performs any odd number of half-cycles of the oscillations.

This prediction was checked against direct simulations. To estimate the efficiency of the scheme, the soliton was passed through the intermediate segment with the value \tilde{D} taken as per eq. (57) with different values of its length. The soliton component in the energy of the output pulse was determined as corresponding to the discrete eigenvalue obtained from the numerical solution of the ZS equations for this pulse. Figure 6 shows the most essential numerical result, viz., the share of the input soliton's energy which is kept by the output soliton at different values of the dispersion ratio D_1/D_2 , vs. the length of the intermediate segment measured in units of the length L_* predicted by eq. (57). The last curve, corresponding to $D_1/D_2 = 10$, includes two optimum-compression points corresponding to both one and three half-cycles of the

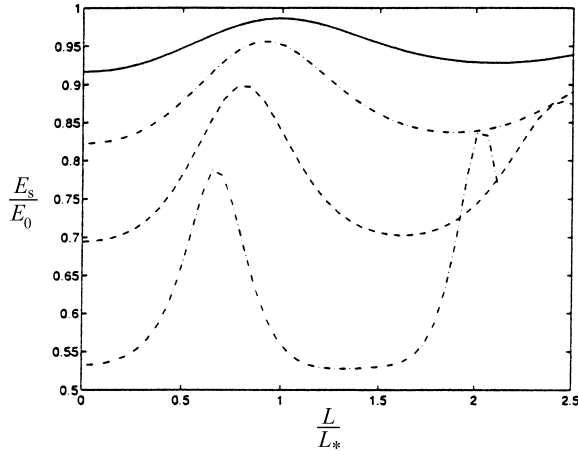


Fig. 6. Results of direct simulations for the energy of the compressed soliton, E_s , normalized to the energy E_0 of the input soliton, vs. the length of the intermediate segment L normalized to the optimum-compression length L_* predicted by VA (eq. 57). The four curves displayed pertain to dispersion ratios $D_1/D_2 = 2, 3, 5, 10$.

oscillations. It is noteworthy that, although degradation of compression quality does occur in direct simulations with increasing dispersion ratio, the degradation is not catastrophic: even at a very large value of the dispersion contrast, $D_1/D_2 = 10$, as much as 84% of the input energy is kept in the soliton component of the output pulse (and the best result is achieved at the *second* optimum-compression point). It is interesting too that the actual value of the (first) optimum-compression length decreases with increasing of the dispersion ratio.

In the same work by Anderson, Lisak, Malomed and Quiroga-Teixeiro [1994], a related problem was analyzed by means of VA, viz., “tunneling” of a soliton through a finite segment of a purely linear fiber inserted between two nonlinear ones. Predictions produced by VA for this problem (e.g., the critical length of the linear segment behind which the soliton gets completely destroyed) were compared to direct simulations, resulting in good agreement.

The three-fiber compression scheme was tested in a real experiment by Bertilsson, Aakjer, Quiroga-Teixeiro, Andrekson and Hedekvist [1995]. For instance, an input fundamental soliton with width 11 ps was successfully compressed to a fundamental soliton with width 2.4 ps, when the soliton was passed from a fiber with $D_1 = 5 \text{ ps}/(\text{km} \cdot \text{nm})$ to one with $D_2 = 1 \text{ ps}/(\text{km} \cdot \text{nm})$ through a 20 km-long intermediate segment with dispersion $D = 1.7 \text{ ps}/(\text{km} \cdot \text{nm})$, which is quite close to that predicted for this case by eq. (57). The compression

factor achieved, $W_1/W_2 \approx 4.6$, is quite close to the ideal one, $D_1/D_2 = 5$, predicted by eq. (56).

2.1.6. Resonant excitation of soliton internal vibrations by periodic amplification

A realistic model of a fiber communication link should take into account losses, periodic amplification, and filtering, which makes it necessary to consider a perturbed NLS equation,

$$iu_z + \frac{1}{2}u_{\tau\tau} + |u|^2u = i\alpha(z)u + i\beta u_{\tau\tau}, \quad (58)$$

where we set $D = \gamma \equiv 1$, the term $\sim \beta$ accounts for the filtering (which is taken in the distributed approximation, averaging the discretely placed filters along the fiber link), and the function $\alpha(z)$ combines the uniformly distributed losses and periodic amplification as per eq. (21). Stationarity of the soliton transmission regime requires the mean net rate of attenuation and amplification for the soliton, averaged over long distance, to be zero. Neglecting filtering losses, as well as emission of radiation by the soliton, this condition amounts to setting $gz_a = \alpha_0$ in eq. (21). When the additional losses are taken into account, they must be compensated by $\alpha(z)$ having a residual positive mean value $\bar{\alpha}$. Therefore, in the general case it is natural to split the function $\alpha(z)$ into a mean value and a variable part $\alpha(z)$ with zero average value,

$$\alpha(z) \equiv \bar{\alpha} + \alpha_1(z). \quad (59)$$

The dissipative term $\sim \alpha$ in eq. (58) can be converted into a variable coefficient in front of the nonlinear term by means of the transformation (22). In the present case, it is reasonable to apply this transformation only to the variable part of $\alpha(z)$, leaving the mean value $\bar{\alpha}$ aside, which leads to the equation

$$iv_z + \frac{1}{2}v_{\tau\tau} + e^{2\Lambda(z)}|v|^2v = i(\bar{\alpha}v + \beta v_{\tau\tau}), \quad (60)$$

where $\Lambda \equiv \int \alpha_1(z) dz$.

Periodic perturbation of a soliton obeying eq. (60), a physical origin of which is the periodic amplification of the soliton in a long fiber link, may get into a *resonance* with the free internal vibrations of a deformed soliton described above. This problem was considered, by means of VA, in a paper by

Malomed [1996]. The exact resonance takes place if the period of the small vibrations of a perturbed soliton, which is

$$z_0 \equiv \frac{2\pi}{K_0} = \frac{\pi^2}{E^2}, \quad (61)$$

with K_0 given by eq. (36) (recall that now $D = \gamma = 1$), is equal to the amplification spacing z_0 , see eq. (21). Proximity to the resonance is determined by a *detuning parameter*,

$$\epsilon \equiv \frac{\pi^2}{(E^2 z_a)} - 1. \quad (62)$$

The result takes the form of the variational equations derived above, in which the energy is replaced by $E(z) \equiv E \exp(2\Lambda(z))$, and, additionally, the filtering term gives rise to an effective friction force that should be added to eq. (32), so that it becomes

$$\frac{d^2 a}{dz^2} = \frac{4}{\pi^2} \left[\frac{1}{a^3} - \frac{E e^{2\Lambda(z)}}{a^2} \right] - \frac{16(6 + \pi^2)}{3\pi^3} E^2 \beta \frac{da}{dz} \quad (63)$$

(strictly speaking, the friction force takes this simple form only for small-amplitude oscillations near the bottom of the potential well, see fig. 1). Besides, the relation between the chirp b and the varying width a changes against eq. (31):

$$b = \frac{1}{2a} \frac{da}{dz} - \frac{4\alpha_1(z)}{\pi^2 a^2}$$

[recall that $\alpha_1(z)$ is the variable part of α defined in eq. (59)].

In eq. (63), z -periodic functions can be decomposed into Fourier series, and nonlinearities are to be expanded, assuming oscillations with a small amplitude near the bottom of the potential well. Keeping quadratic and cubic nonlinear terms in the latter expansion, it was demonstrated that the final equation can be mapped into the standard equation for a resonantly driven nonlinear oscillator, provided that the detuning (62) is small enough. Using well-known results for the latter equation (Landau and Lifshitz [1975]), the amplitude of established oscillations can be found, and their stability can be examined. In particular, a *bistability* region was found in the parametric space, where two different solutions for the driven internal vibrations of the soliton may exist, being

simultaneously stable. The expression for the bistability region takes a simple form when the filtering is disregarded, $\beta = 0$:

$$\epsilon < - \left(\frac{9g}{\pi^2} \right)^{2/3} \quad (64)$$

[recall that g is the gain parameter from eq. (21), and ϵ is the detuning (62)]. The difference between two coexisting stable propagation modes of the soliton in the bistable range is in the size of the chirp: one mode is characterized by low chirp, while the other has relatively large chirp.

Moreover, it was shown that a *subharmonic* resonance, which takes place when the period (61) of small vibrations of the perturbed soliton is close to $2z_a$, also gives rise to a bistability. Thus, the soliton may propagate along the fiber link in the state of *persistent* internal vibrations, which are resonantly driven by the periodic amplification.

2.2. A spatial soliton in a periodically inhomogeneous planar waveguide

2.2.1. A stationary soliton

A peculiarity of physically relevant problems for spatial solitons is that they may interact with an effective external potential, as per eq. (5). For the simplest case, with a potential of parabolic shape, VA was applied to the corresponding spatial soliton by Michinel [1995], who used a Gaussian ansatz including a degree of freedom accounting for a possible shift of the soliton off the waveguide's center. In particular, it was demonstrated that this ansatz generated decoupled evolution equations for the internal vibrations of the soliton, and for oscillations of its center about the center of the waveguide.

A model with great potential for applications to photonics introduces a periodically inhomogeneous nonlinear waveguide that may be a basis for a switchable multichannel system guiding light signals. The basic version of this model postulates a simple sinusoidal spatial modulation of the waveguide, so that eq. (5) takes the form

$$iu_z + \frac{1}{2}u_{xx} + \epsilon \cos(qx) \cdot u + |u|^2 u = 0, \quad (65)$$

where $L \equiv 2\pi/q$ and ϵ are the period and amplitude of the modulation; using the invariance of eq. (65), it is possible to set $L = 1$, i.e., $q = 2\pi$, which will be assumed below. As a matter of fact, the same equation (65) also describes a planar array of densely packed nonlinear waveguides, a medium in which actual experiments with the spatial solitons have been performed (Eisenberg,

Silberberg, Morandotti, Boyd and Aitchison [1998]). Indeed, a chain of coupled-mode equations for the array reduces, in the dense-packing approximation, to the NLS equation in which the residual discreteness manifests itself in the form of an effective harmonic *Peierls–Nabarro* potential (Kivshar and Campbell [1993]), i.e., exactly eq. (65).

This model was analyzed in detail by means of a combined analytical (VA-based) and direct numerical methods by Malomed, Wang, Chu and Peng [1999]. The first objective of the analysis was to find stationary one-soliton solutions of the form

$$u(x, z) = \exp(ikz) U(x) \quad (66)$$

with a real propagation constant k and real $U(x)$. The solution describes a solitary beam trapped in a trough (one of the channels induced by the periodic spatial modulation).

Substitution of eq. (66) into eq. (65) leads to an ODE,

$$\frac{1}{2} U'' + [\epsilon \cos(2\pi x) - k] U + U^3 = 0, \quad (67)$$

which can be derived from the Lagrangian

$$L = \int_{-\infty}^{+\infty} [(U')^2 + (2k - \epsilon \cos(2\pi x)) U^2 - U^4] dx. \quad (68)$$

The solution is approximated by a simple ansatz, $U = A \operatorname{sech}(\eta x)$. Placing the center of the soliton at $x = 0$, one assumes $\epsilon > 0$ in eq. (65), then $x = 0$ is a local potential minimum for the soliton. Substituting the ansatz into the Lagrangian and performing the integration, the variation in A and η leads to

$$\eta^2 - 2\pi^2 \epsilon \frac{[2\pi^2 \cosh(\pi^2/\eta) - 3\eta \sinh(\pi^2/\eta)]}{\eta^2 \sinh^2(\pi^2/\eta)} = 2k, \quad (69)$$

$$A^2 = \frac{1}{4} \left[\eta^2 + 6k - \frac{6\pi^2 \epsilon}{\eta \sinh(\pi^2/\eta)} \right]. \quad (70)$$

Equations (69) and (70) have exactly one solution at any $\epsilon > 0$ and any $k > 0$. In particular, the asymptotic form of the solution for very small and very large k is $A^2 = \eta^2 = 2k$.

Comparison of the VA prediction for the soliton shape with numerical solutions of eq. (67) is presented in fig. 7. Note that, at small k , the width of the soliton is essentially larger than the modulation period. This explains the wavy

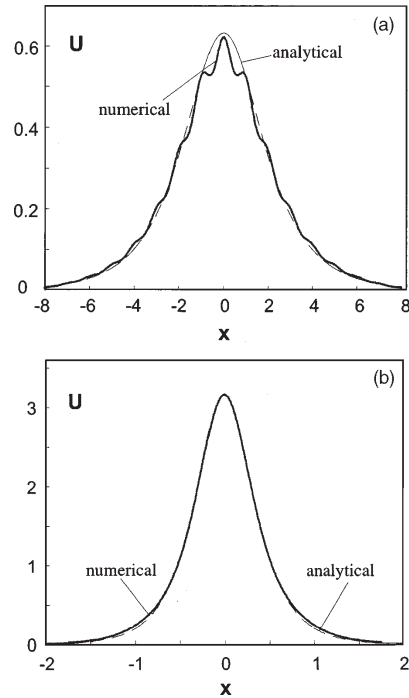


Fig. 7. Comparison between the one-soliton solutions to eq. (67) at $\epsilon = 1$ with (a) $k = 0.2$ and (b) $k = 5.0$, obtained numerically (solid curves) and by means of VA (dashed curves).

shape of the soliton in fig. 7a with $k = 0.2$. Of course, this feature is not included in the simple ansatz adopted above, which explains some disagreement between VA and the numerical results at small k : at $k = 0.2$, the amplitude predicted by eq. (70) differs by less than 2% from the numerical value $U(x = 0) = 0.622$. At larger k , the soliton becomes narrower, and it is then very close to the shape predicted by VA, see fig. 7b.

2.2.2. Soliton stability and the Vakhitov–Kolokolov criterion

Numerical simulations of the full PDE (65), using an ansatz with the width and amplitude (69) and (70) predicted by VA as an initial configuration, have demonstrated that, at all values of ϵ and k , the initial configuration gives rise to *stable solitons*. Actually, VA makes it possible to predict the stability by means of a criterion proposed by Vakhitov and Kolokolov [1973] (the VK criterion). According to this criterion, one should calculate the power of the solitary beam, $F = \int_{-\infty}^{+\infty} |u|^2 dx$, which is thus obtained as a function of ϵ and k . The VK cri-

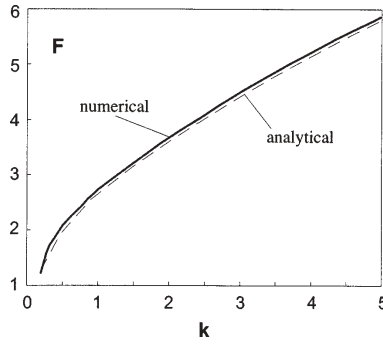


Fig. 8. Solitary-beam power F vs. propagation constant k for the one-soliton state in model (65): shape found numerically (solid curve) and shape predicted by VA (dashed curve).

terion states that a necessary (but, generally, not sufficient) condition for the stability of the soliton is $\partial F/\partial k > 0$. A typical example of the dependence $F(k)$ evaluated on the basis of both numerical and variational solutions is displayed in fig. 8, which clearly shows that the numerical and variational results are fairly close, both showing that the slope $\partial F/\partial k$ is positive everywhere.

An issue crucially important for the use of this model as a multichannel system is the existence and stability of *two-soliton* states, with the solitary beams trapped in two adjacent channels. The two-soliton state can be destabilized by the mutual attraction of the two beams, which can lead to their merging into one beam. Malomed, Wang, Chu and Peng [1999] had found a stability region for two-soliton states by means of direct simulations.

2.2.3. Switching a soliton between adjacent channels

A more sophisticated problem that was also considered by Malomed, Wang, Chu and Peng [1999] is to model controllable switching of the soliton from a given trough into an empty adjacent one (the principal possibility of switching spatial solitons was demonstrated experimentally by Shalaby and Barthelemy [1991]). To this end, one may assume that a laser beam launched in the direction transverse to the planar waveguide is focused on a small spot with coordinates $(x = x_0, z = 0)$ somewhere between the two troughs [$0 < x_0 < 1$; recall $q \equiv 2\pi$ in eq. (65)]. Through cross-phase modulation (XPM), the bright spot gives rise to an attraction center, which is described by an additional localized perturbation added to eq. (65):

$$iu_z + \frac{1}{2}u_{xx} + \epsilon \cos(2\pi x) \cdot u + |u|^2 u = -\mu \delta(x - x_0) \delta(z) \cdot u, \quad (71)$$

μ being proportional to the intensity of the transverse beam. The attracting spot has a chance to throw the soliton over the dividing potential barrier into the adjacent trough.

To analyze this possibility, the change of the soliton induced by the perturbation concentrated at the spot can be found in an exact form. Indeed, representing the soliton solution as $u(x, z) = a(z, x) \exp(i\phi(x, z))$ with real amplitude a and phase ϕ , it is straightforward to see that the spot does not introduce any instantaneous change of the amplitude, while the change of the phase is

$$\Delta\phi(x, z) \equiv \phi(x, z=+0) - \phi(x, z=-0) = \mu \delta(x - x_0). \quad (72)$$

Further analysis can be carried out by means of perturbation theory, treating both ϵ and μ as small parameters, and the soliton as a particle. The unperturbed NLS soliton should be taken in the general “walking” form (7), which, in the present case, corresponds to $a(x, z) = \sqrt{2k} \operatorname{sech}(\sqrt{2k}(x - cz - \xi))$, where k is the propagation constant introduced in eq. (66), the small “velocity” c is, in fact, a ramp of the solitary beam in the (x, z) plane, and ξ is the coordinate of the beam center at $z = 0$. With regard to the definition (11) of the momentum of the “walking” soliton, it may be interpreted as a particle with the following momentum, kinetic energy, and mass:

$$P = Mc, \quad E_{\text{kin}} = \frac{P^2}{2M}, \quad M = 2\sqrt{2k}. \quad (73)$$

We consider the situation in which the beam at $z < 0$ was trapped in the given channel (trough), so that it has $c = \xi = 0$. As follows from the general expression (11) for the momentum, the instantaneous phase change (72) gives rise to a jump of the momentum from 0 to a value that can be found in exact form:

$$P = \int_{-\infty}^{+\infty} a^2(x) \Delta\phi'(x) dx = \mu \int_{-\infty}^{+\infty} a^2(x) \delta'(x - x_0) dx \equiv -2\mu a(x_0) a'(x_0). \quad (74)$$

The substitution of the unperturbed soliton form, $\sqrt{2k} \operatorname{sech}(\sqrt{2k}x)$, into eq. (74) yields an explicit result for P . Thus, the localized perturbation plays the role of a sudden push that lends the particle a kinetic energy, which can be found at the first order of perturbation theory, using eqs. (73) and (74),

$$E_{\text{kin}} = \mu^2 (2k)^{5/2} \sinh^2(\sqrt{2k}x_0) \operatorname{sech}^6(\sqrt{2k}x_0). \quad (75)$$

The interaction of the unperturbed soliton with the periodically modulated refractive index is described by an effective periodic potential $W(\xi)$, which is generated by the corresponding part of the Lagrangian (68),

$$W(\xi) \equiv -\epsilon \int_{-\infty}^{+\infty} \cos(2\pi x) \cdot a^2(x) dx = -\frac{\pi^2 \epsilon}{\sinh\left(\pi/\sqrt{2k}\right)} \cos(2\pi\xi). \quad (76)$$

According to eq. (76), the height of the potential barrier separating two adjacent troughs is

$$\Delta W = \frac{2\pi^2 \epsilon}{\sinh\left(\pi/\sqrt{2k}\right)}. \quad (77)$$

The soliton set in “motion” (physically, given the ramp c) by the sudden push will pass the separating barrier and get into the adjacent trough if $E_{\text{kin}} > \Delta W$. Substitution of equations (75) and (77) into this inequality shows that the attracting spot created at the point x_0 is able to switch the solitary beam into the adjacent channel if its strength μ^2 exceeds a threshold value

$$\mu_{\text{thr}}^2 = \frac{2\pi^2 \epsilon}{(2k)^{5/2}} \cdot \frac{\cosh^6\left(\sqrt{2k}x_0\right)}{\sinh\left(\pi/\sqrt{2k}\right) \sinh^2\left(\sqrt{2k}x_0\right)}. \quad (78)$$

In particular, μ_{thr}^2 , considered as a function of x_0 , takes a minimum value at the point where $\cosh^2\left(\sqrt{2k}x_0\right) = \frac{3}{2}$.

In the framework of the lowest approximation of the perturbation theory, the soliton kicked out from the trough where it was originally trapped will not be trapped by the adjacent trough, but will keep moving farther. However, radiative losses not taken into account in the lowest approximation are likely to help trapping the soliton. Direct simulations demonstrate that radiative losses take place indeed, and the soliton can be trapped by the adjacent trough after having been pushed by the spot (Malomed, Wang, Chu and Peng [1999]).

2.3. Interactions and bound states of solitons

2.3.1. Potential of interaction between two far-separated solitons

2.3.1.1. *General analysis.* The variational methods can also be quite efficiently used for the description of multi-soliton complexes, the simplest and most important example of which is a pair of far-separated solitons. In the case of

the unperturbed NLS equation, the interaction force between two distant solitons was calculated analytically by Karpman and Solov'ev [1981] on the basis of the perturbation theory for a single soliton, which treated the overlapping between one soliton and a vanishing tail of the other as a small perturbation (similar work was done by Gordon [1983]). Essentially the same results were obtained by Anderson and Lisak [1986a] by means of VA, postulating an ansatz in the form of a linear superposition of two solitons.

The interaction force between solitons, predicted by Karpman and Solov'ev [1981], was directly measured by Mitschke and Mollenauer [1987] in an experiment with solitons in an optical fiber. Interactions between spatial solitons are also amenable to direct experimental studies, as first demonstrated by Reynaud and Barthelemy [1990] and Aitchison, Weiner, Silberberg, Leaird, Oliver, Jackel and Smith [1991].

Following these ideas, it is natural to consider two far-separated solitons as particles, describing their interaction in terms of the corresponding effective potential. It will be shown below, following Malomed [1998a], that VA makes it possible to find the effective interaction potential in a very general and fairly simple analytical form.

For two far-separated solitons, the wave field is assumed to be a superposition of their individual fields u_1 and u_2 ,

$$u(z, \tau) = u_1(z, \tau) + u_2(z, \tau). \quad (79)$$

Note, however, that a weak "tail" of one soliton can be essentially distorted where it overlaps with the "body" of the other soliton. The general analysis outlined below does *not* neglect this distortion. The configuration with two solitons to be considered here is defined so that the center of the first soliton is set at $\tau = 0$, and that of the second is at $\tau = -T$, where T is a large separation between the solitons.

The interaction potential is, with the minus sign, part of the Lagrangian produced by the overlapping of each soliton with the small tail belonging to the other. Substituting the superposition (79) into the Lagrangian, one arrives in the first approximation at the following general expression for the potential:

$$U_{\text{int}} = \left\{ - \int \left(\left[\left(\frac{\delta \mathcal{L}}{\delta u^*} \right) \Big|_{u=u_1} - \frac{\partial}{\partial z} \left(\frac{\partial \mathcal{L}}{\partial u_z^*} \right) \Big|_{u=u_1} \right] \cdot u_2^* + \left(\frac{\partial \mathcal{L}}{\partial u_\tau^*} \right) \Big|_{u=u_1} \cdot (u_2^*)_\tau \right) d\tau \right. \\ \left. + \text{c.c.} \right\} + \{1 \Rightarrow 2\}, \quad (80)$$

where c.c. stands for the complex conjugate expression, the integral is taken over a vicinity of the first soliton where the tail of the other one is small, and $\{1 \rightleftharpoons 2\}$ stands for a symmetric contribution from a vicinity of the second soliton. The presence of $\partial/\partial z$ in one of the terms of the integrand implies that the z -derivative was transferred, in that term, from the multiplier u_2^* as per integration by parts with respect to z , which is implied because the Lagrangian $L = \int_{-\infty}^{+\infty} \mathcal{L} dz$ should be further inserted into the action, $\int_{-\infty}^{+\infty} L dz$.

If integration by parts (with respect to τ) is applied to the last term in the integrand in eq. (80), one arrives at the following integral expression:

$$\int \left[\left(\frac{\delta \mathcal{L}}{\delta u^*} \right) - \frac{\partial}{\partial z} \left(\frac{\partial \mathcal{L}}{\partial u_z^*} \right) - \frac{\partial}{\partial \tau} \left(\frac{\partial \mathcal{L}}{\partial u_\tau^*} \right) \right]_{u=u_1} \cdot u_2^* d\tau, \quad (81)$$

which is *exactly equal to zero*, as the one-soliton solution (for the first soliton) is obtained from the Lagrangian exactly in the form stating that the expression in the square brackets in eq. (81) is zero. Therefore, the only nonzero contribution to the interaction potential in its general form (80) comes from the integration limits when integrating by parts the last term in the integrand in eq. (80):

$$U_{\text{int}} = \frac{1}{2} D(z) \left[(u_1)_\tau u_2^* + \text{c.c.} \right] \Big|_{\tau=-\tau_0}^{\tau=+\infty} + \{1 \rightleftharpoons 2\}. \quad (82)$$

As the integral in eq. (80) is to be taken over a vicinity of the first soliton, the lower integration limit τ_0 is realized here as some value of τ such that

$$\eta^{-1} \ll \tau_0 \ll T, \quad (83)$$

where η^{-1} is the width of the soliton (see below), and T is the large separation between the solitons defined above. The condition $\eta^{-1} \ll \tau_0$ is very helpful, as it makes it possible to approximate, in the expression (82), the wave forms of *both* solitons by asymptotic expressions for their tails, which can be readily obtained from the linearized version of the underlying NLS equation, as will be shown below. It is also evident that this approach avoids the above-mentioned complication, viz., distortion of the soliton's tail in the region when it overlaps with the body of the other soliton. An important result is that, as will be seen below, the final expression for the interaction potential does *not* depend on the arbitrary value of the intermediate temporal coordinate τ_0 .

2.3.1.2. Calculation of the soliton's "tails". In a realistic case, the corresponding NLS equation describing a long fiber-optic communication link must include

the gain/loss term as in eq. (20), and also a filtering term, so that the linearized form of the perturbed NLS equation becomes (cf. eq. 97 considered below)

$$iu_z + \frac{1}{2}D(z)u_{\tau\tau} = i\alpha(z)u + i\beta(z)u_{\tau\tau}. \quad (84)$$

Here, β is the filtering coefficient, and the most general case is considered, in which D , α and β may all be periodically modulated, in order to take into account, respectively, possible dispersion management, periodic alternation of the losses and gain, and discrete allocation of filters in a real *lumped* model (as opposite to the simplified *distributed* model, which assumes the filtering to be uniformly “smeared” along the fiber link). Accordingly, these coefficients may assume the forms

$$D(z) = \bar{D} + \frac{d\Delta(z)}{dz}, \quad \alpha(z) = \bar{\alpha} + \frac{dA(z)}{dz}, \quad \beta(z) = \bar{\beta} + \frac{dB(z)}{dz}, \quad (85)$$

where overbars indicates average values, and the terms represented by the derivatives account for the purely variable parts with zero mean values (in particular, $\Delta(z)$ is called *accumulated dispersion*, which is defined so that it does not include a contribution from the average part of the dispersion coefficient).

A solution to the linearized equation (84) for an exponentially decaying tail may be sought for as

$$u_{\text{tail}}(z, \tau) = A \exp[-\phi(z) + i\psi(z) - (\eta + i\chi)|\tau|], \quad (86)$$

where A , η and χ are real constants. In fact, A and η , the latter constant determining a characteristic soliton’s width $\sim \eta^{-1}$, may only be found by matching the tail (86) to the soliton solution of the full (nonlinear) perturbed NLS equation, so in the solution (86) they figure as arbitrary real constants, while χ must be found along with $\phi(z)$ and $\psi(z)$. The final form of the solution is simplified due to the fact that the dissipative terms on the rhs of eq. (84) may be treated as small perturbations.

The solution must satisfy the condition that the function $\phi(z)$ in (86) may oscillate in z , but may neither decay nor grow systematically, as the interaction between established (quasi-stationary) solitons is considered. This condition yields, at first order of perturbation theory,

$$\chi = \frac{\bar{\alpha} + \bar{\beta}\eta^2}{\bar{D}\eta}, \quad (87)$$

and then one finds

$$\phi(z) = \eta\chi\Delta(z) - [A(z) + \eta^2B(z)], \quad \psi(z) = \frac{1}{2}\eta^2 [Dz + \Delta(z)] + \psi_0, \quad (88)$$

where $\Delta(z)$, $A(z)$ and $B(z)$ are the oscillating functions defined in eq. (85), and ψ_0 is an arbitrary real constant.

2.3.1.3. Interaction potential for two solitons in an optical communication link.

The solution (86) for the tails of both solitons u_1 and u_2 can be inserted into the general expression (82) for the interaction potential (80). Because the condition for equilibrium between gain and losses selects the same parameters A and η for all solitons in the system, it is sufficient to consider the case of interaction between identical solitons. One can then immediately check that the contribution from the outer integration limit with respect to both solitons, i.e. at $\tau = +\infty$, vanishes, while the contribution from the intermediate limit $\tau = -\tau_0$ has mutually cancelling exponential factors $\exp(\pm\eta\tau_0)$ produced by the expressions (86) for the tails of u_1 and u_2 , so that the effective potential does not depend on the arbitrary value of τ_0 :

$$U_{\text{int}}(T, \Delta\psi) = -2A^2\eta D(z) \exp(-2\phi(z) - \eta T) \cos(\chi T) \cos(\Delta\psi), \quad (89)$$

where $\Delta\psi \equiv \psi_0^{(1)} - \psi_0^{(2)}$ is the phase difference between the two solitons. A remarkable feature of this expression is that the potential does not decay monotonically with the separation T between the solitons, but shows oscillations accounted for by the multiplier $\cos(\chi T)$, as seen in fig. 9. As first shown by Malomed [1991b], this opens the way to the existence of stationary bound states of the two solitons at values of T corresponding to extrema of the potential (89),

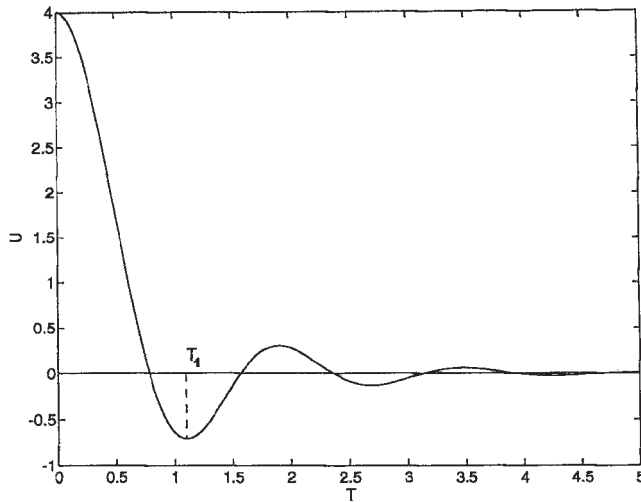


Fig. 9. Schematic form of the potential of the interaction (89) between two solitons for $\Delta\phi = \pi$. The point $T = T_1$ corresponds to the first bound state generated by the potential, see eq. (90).

i.e., $\cot(\chi T) = -\chi/\eta$. The first bound state corresponds to the smallest possible separation between the solitons, which is

$$T_1 = \frac{1}{\chi} \left[\frac{\pi}{2} + \tan^{-1} \left(\frac{\chi}{\eta} \right) \right] \approx \frac{\pi}{2\chi} \quad (90)$$

(see fig. 9), where it is taken into account that $|\chi/\eta| \ll 1$ as per eq. (87). However, the stability of those bound states is a tricky problem, which will be considered in the next subsection.

It should be noted that the general expression (82) for the interaction potential was obtained for a model that has the Lagrangian representation (81). In fact, the analysis outlined above remains completely correct in the presence of loss and gain, as they can be easily included in the Lagrangian by means of the transformation based on eqs. (22) and (24). Contrary to this, the use of the potential is not quite consistent in the presence of filtering, for which a simple Lagrangian representation is not available. Nevertheless, the concept of the effective potential may be employed in the case when filtering acts as a small perturbation. Note also that the oscillations in the shape of the potential (89), which represent its most nontrivial feature, demand the presence of loss and gain, as is obvious from eqs. (90) and (87), but not necessarily the presence of filtering.

The general approach to the calculation of an effective interaction potential between two far-separated solitons outlined above was generalized by Malomed [1998c] for two- and three-dimensional solitons. As well as in the 1D case, the integral contribution to the potential can be eliminated by means of integration by parts, which, in the multidimensional situation, takes the form of the Gauss theorem, that reduces the potential to a contribution from the corresponding surface term, taken along circumferences (in the 2D case) or spheres (in the 3D case) of a large radius ρ surrounding each soliton. The radius ρ is chosen so that $r_0 \ll \rho \ll R$ (cf. eq. 83), where r_0 is the size of the solitons, and R is the separation between them. Then, the surface term can be easily calculated in a general explicit form, as both solitons are represented in it by their asymptotic tails. The final expression for the interaction potential, which is (cf. eq. 89) $U_{\text{int}} \sim R^{-(D-1)/2} \exp(-R/r_0) \cos(\Delta\psi)$ (in the purely conservative model), where $D = 2$ or 3 is the dimension, does not depend on the intermediate radius ρ_0 , similar to the fact that expression (89) does not contain the intermediate time scale τ_0 . A similar result was obtained by Malomed, Maimistov and Desyatnikov [1999] for the interaction of multidimensional solitons belonging to different components in a two-component model.

2.3.1.4. *Generalization for dissipative systems.* The concept of the effective interaction potential generated by the overlapping of the tail of each soliton with the body of the other can also be applied to purely dissipative systems that admit representation in the *gradient* (pseudo-Hamiltonian) form [cf. the Hamiltonian representation (17)]:

$$u_t = -\frac{\delta\Lambda}{\delta u^*}, \quad \Lambda = \int_{-\infty}^{+\infty} \lambda(u, u^*, u_x, u_x^*) dx, \quad (91)$$

where the variational derivative acts on the *Lyapunov functional* Λ with a real density λ . An obvious consequence of eq. (91) is $d\Lambda/dt \leq 0$, hence the dynamical evolution described by eq. (91) drives the system to a state with a minimum value of the Lyapunov functional.

A physically interesting example of the gradient system is a parametrically driven Ginzburg–Landau (GL) equation, which was introduced by Coulet, Lega and Pomeau [1991] [cf. the parametrically driven damped NLS equation (29)]:

$$u_t = u - |u|^2 u + u_{xx} + \gamma u^*, \quad (92)$$

that can be derived from the Lyapunov functional with the density

$$\Lambda = \int_{-\infty}^{+\infty} \left(|u_x|^2 - |u|^2 + \frac{1}{2}|u|^4 - \frac{1}{2}[u^2 + (u^*)^2] \right) dx, \quad (93)$$

γ being a real parameter. Equation (92) has an exact solution in the form of a *Bloch domain wall* (BDW), alias kink,

$$\operatorname{Re} u = \sigma \sqrt{1 + \gamma} \tanh(\sqrt{2\gamma}x), \quad \operatorname{Im} u = \sigma \mu \sqrt{1 - 3\gamma} \operatorname{sech}(\sqrt{2\gamma}x), \quad (94)$$

where $\sigma = \pm 1$ and $\mu = \pm 1$ are two independent polarities of the kink. BDW is stable in its existence interval $0 < \gamma < \frac{1}{3}$, which gives rise to a natural problem of the interaction between two BDWs with a large separation L between them.

The interaction is accounted for by a part in the Lyapunov functional (93) that is generated by overlapping between the two kinks. This part of the functional will be referred to as a *pseudopotential* of the interaction. Linearizing the integrand in the integral expression for the pseudopotential with respect to the fields representing weak tails of the kinks, and taking into account the fact that an isolated BDW is an exact solution to eq. (92), which is generated by the Lyapunov functional as per eq. (91), it was shown by Malomed

and Nepomnyashchy [1994] that applying integration by parts reduces the pseudopotential \mathcal{U}_{int} to a general expression similar to eq. (82),

$$\mathcal{U}_{\text{int}} = [(u_1^*)_{x} u_2 + \text{c.c.}] \Big|_{x=-x_0}^{x=+\infty} + \{1 \rightleftharpoons 2\}, \quad (95)$$

where x_0 is an intermediate point similar to τ_0 in eq. (82).

The substitution of straightforward asymptotic expressions for the tails of the two BDWs (94) into the general expression (95) yields an effective interaction pseudopotential that, as well as its counterpart (89) in the conservative model, does not depend on the choice of the intermediate point:

$$\mathcal{U}_{\text{int}}(L) = 16\sqrt{\frac{2}{3}} \left[(1 - 3\gamma)\lambda_1\lambda_2 \exp\left(-\sqrt{\frac{2}{3}}L\right) - \frac{14}{3} \exp\left(-2\sqrt{\frac{2}{3}}L\right) \right] \quad (96)$$

(recall that $\lambda_{1,2}$ are intrinsic polarities of the two kinks). In expression (96), it is taken into account that $\sigma_1\sigma_2 \equiv -1$ for two adjacent kinks.

This result is most interesting in the case when $(1 - 3\gamma)$ is small: then the pseudopotential (96) combines attraction at $L < L_0 \approx \sqrt{\frac{3}{2}} |\ln(1 - 3\gamma)|$ and repulsion at $L > L_0$. Therefore, one may conclude that a periodic array of BDWs in an infinite system, or in a long one subject to periodic boundary conditions, is stable if the array spacing exceeds L_0 (Malomed and Nepomnyashchy [1994]).

2.3.2. Full analysis of bound states of solitons in a realistic model of an optical communication link

For a full description of the interactions between solitons (in particular, for the analysis of the stability of their bound states), it is necessary to consider the interactions by means of direct perturbation theory, rather than limiting the analysis to finding the effective interaction potential. The model takes into account, as above, losses, gain, and filtering, but in the distributed approximation, so that the accordingly perturbed NLS equation actually takes the form of the complex Ginzburg–Landau (GL) equation with constant coefficients. In the GL model, soliton-like pulses have, in accordance with eq. (86), tails which decay exponentially with oscillations, in contrast to the monotonically decaying tails of the NLS soliton (6).

In the simplest GL equation with a cubic nonlinearity, solitary pulses are obviously unstable, as the zero solution, i.e., the soliton's background, is unstable in that equation due to the presence of the linear gain. Therefore, interactions between solitons and their bound states can be studied in a consistent way, as was

done by Afanasjev, Malomed and Chu [1997] in the framework of the *cubic–quintic* (CQ) GL equation, which combines linear loss, cubic gain, and quintic loss:

$$iu_z + \frac{1}{2}u_{\tau\tau} + |u|^2 u = -i\alpha u + i\beta u_{\tau\tau} + i\epsilon |u|^2 u - i\Gamma |u|^4 u. \quad (97)$$

Here, we set $D = \gamma = 1$, and the positive parameters α , β , ϵ and Γ account for, respectively, linear losses, spectral filtering, nonlinear gain, and stabilizing higher-order nonlinear losses (a model of this type was first introduced by Petviashvili and Sergeev [1984]). The linear and quintic losses provide for the linear stability of the zero solution and for the global stability of the model, respectively. The nonlinear gain, accounted for by the term $\sim \epsilon$ in eq. (97), can be produced, in a fiber-optic communication link, by a combination of the usual linear amplifiers with nonlinear saturable absorbers, see, e.g., the book by Hasegawa and Kodama [1995]. As demonstrated first in an appendix to the paper by Malomed [1987], in the case when the gain and dissipation terms in eq. (97) are small perturbations, which is relevant for the application to optical fibers, the CQ model gives rise to two different stationary soliton-like pulses which are close to the NLS soliton:

$$u = \eta \operatorname{sech}[\eta(\tau - T)] \exp\left[i\left(\frac{1}{2}\eta^2 z + \phi\right)\right], \quad (98)$$

$$\eta^2 = (16\Gamma)^{-1} \left[5(2\epsilon - \beta) \pm \sqrt{25(2\epsilon - \beta)^2 - 480\alpha\Gamma} \right], \quad (99)$$

where T and ϕ are arbitrary constants. The upper and lower signs in eq. (99) correspond, respectively, to stable and unstable pulses. Besides selecting the definite value of the soliton's amplitude, which is arbitrary in the case of the NLS soliton proper, the small dissipative perturbations in eq. (97) also cause the asymptotic form of the soliton far from its center to be oscillating (cf. eq. 86),

$$u \approx 2\eta \exp(-\eta|\tau| + i\chi|\tau|), \quad (100)$$

where $\chi = \alpha\eta^{-1} + \beta\eta$ [cf. eq. (87); the small parameter χ is absent in the zero-order approximation (98)].

To consider the interaction between pulses with equal amplitudes η , it is convenient to define the normalized propagation distance $x \equiv 2\sqrt{2}\eta^2 z$, the separation between the pulses, $r \equiv \eta(T_1 - T_2)$, and the phase difference between

them, $\psi \equiv \psi_1 - \psi_2$. Considering overlapping between the solitons as another small perturbation, one can derive a system of evolution equations for r and ψ :

$$\frac{d^2 r}{dx^2} + \frac{\sqrt{2}}{3} \beta \frac{dr}{dx} + e^{-r} [\cos(br) + b \sin(br)] \cos \psi = 0, \quad (101)$$

$$\frac{d^2 \psi}{dx^2} + \frac{\lambda}{\sqrt{2}} \frac{d\psi}{dx} - e^{-r} \cos(br) \sin \psi = 0, \quad (102)$$

where the four original control parameters combine into three final ones:

$$\beta, \quad \lambda \equiv \frac{1}{15} \sqrt{25(2\epsilon - \beta)^2 - 480\alpha\Gamma}, \quad b \equiv \frac{-\alpha + \beta\eta^2}{\eta^2}. \quad (103)$$

Notice that $\cos(br)$ and $\sin(br)$ in eqs. (101) and (102) are induced by the oscillations in the soliton's tail as per eq. (100).

Equations (101) and (102) may be regarded as equations of motion for a mechanical system with two degrees of freedom, r and ψ , in the presence of friction, in the potential $U(r, \psi) = -e^{-r} \cos(br) \cos \psi$, which has a set of local extrema at

$$br_0 = \tan^{-1} b + \frac{1}{2} \pi(1 + 2n), \quad \psi_0 = \pi m \quad (104)$$

(cf. eq. 90), where $n = 0, 1, 2, \dots$, and $m = \pm 1, \pm 2, \dots$. Normally, points of the potential minimum would be stable fixed points (FPs) of the underlying dynamical system and, thus, they would produce stable bound states of the two pulses. However, a peculiarity of the system (101) and (102) is that, while the effective mass corresponding to the coordinate r is $+1$, the mass corresponding to ψ is -1 . The presence of the *negative* effective mass drastically changes the stability of the FPs: all the local extrema (104) are *saddles*. It is easy to find a pair of eigenvalues that determine the character of the saddle FP (so that small perturbations around the static solution are growing as $\exp(\sigma z)$):

$$\sigma_{1,2} = \pm b \sqrt{\frac{3}{\beta\lambda}} e^{-r_0}. \quad (105)$$

Due to the assumed smallness of the parameters on the rhs of eq. (97), the coordinate r_0 of the FP given by eq. (104) is large, hence the eigenvalues (105) are exponentially small. Notice that, in the framework of the fourth-order system (101) and (102), the FP must have four eigenvalues. Two others that are missing

in (105) are negative, and they are not exponentially small, i.e., they correspond to quickly decaying (stable) small perturbations around the FP.

Besides the saddles (104), eqs. (101) and (102) also have another set of FP's,

$$br_0 = \frac{1}{2}\pi(1+2n), \quad \psi_0 = \frac{1}{2}\pi(1+2m). \quad (106)$$

Comparing FP's (104) and (106), one concludes that, for the same value of n , they have nearly equal separation r between the bound pulses, but the relative phase ψ differs by $\frac{1}{2}\pi$. Stability analysis of the FP's (106) reveals that they have two relatively large negative eigenvalues corresponding to rapidly decaying perturbations [as well as in the case of FP (104)], and two exponentially small complex eigenvalues

$$\sigma_{1,2} = \pm ib \sqrt{\frac{3}{\beta\lambda}} e^{-r_0} + \frac{3}{2} \left(\frac{b}{\beta\lambda} \right)^2 \left(\sqrt{2}\beta + \frac{3}{\sqrt{2}}\lambda \right) e^{-2r_0}; \quad (107)$$

hence, the FPs (106) are unstable spirals.

Thus, we obtain two types of unstable bound states in the CQ GL model: depending on the phase difference between the pulses, their bound state are unstable as the saddle or as the spiral. Exactly this was observed in numerical experiments performed at *non-small* values of the perturbation parameters (and with *normal* dispersion, i.e., with the opposite sign in front of the dispersion term) by Afanasjev and Akhmediev [1996]. Therefore, one may conjecture that the above analytical results should plausibly remain valid even when the perturbation theory cannot be applied.

Returning to perturbative analysis, one can notice a very important difference of eq. (107) from eq. (105). Namely, for the same n , i.e., nearly the same r_0 , the real part of the eigenvalue (107), accounting for the instability of the spiral, is proportional to the *square* of the exponentially small factor $\exp(-r_0)$, while in the case of the saddle the growth rate of the instability is linear in this factor.

Thus, the instability of the spiral is extremely weak. Nevertheless, it is an issue of fundamental interest to explore the result of a developing instability at extremely large propagation distances. To this end, it is necessary to take into account that the fourth-order system (101) and (102) implies relatively quick decay of the perturbations corresponding to the above-mentioned relatively large (non-exponential) stable eigenvalues, and very slow evolution of perturbations corresponding to the exponentially small eigenvalues (105) and (107). In this connection, a natural simplification of the full system is to project it onto the two-dimensional space of the slow modes, eliminating two rapidly decaying ones.

Technically, this implies treating the second derivatives in eqs. (101) and (102) as small perturbations. In the zeroth approximation, one simply omits the second derivatives, so that eqs. (101) and (102) reduce to

$$\frac{dr}{dx} = -\frac{3}{\sqrt{2}\beta} e^{-r} [\cos(br) + b \sin(br)] \cos \psi, \quad (108)$$

$$\frac{d\psi}{dx} = \frac{\sqrt{2}}{\lambda} e^{-r} \cos(br) \sin \psi. \quad (109)$$

Within the framework of this system, FP (104) remains the saddle, while (106) is neutrally stable.

At the next step, one restores the second-derivative term by means of the identity $\frac{d^2\psi}{dx^2} \equiv \frac{d}{dx} \left(\frac{d\psi}{dx} \right)$, and similarly for r , making use of the expressions (109) and (108) for $d\psi/dx$ and dr/dx . To perform the second differentiation, one can use eqs. (108) and (109) once again. Retaining essential corrections to eqs. (108) and (109) produced by this procedure, one arrives at the system

$$\frac{dr}{dx} = -\frac{3}{\sqrt{2}\beta} e^{-r} [\cos(br) + b \sin(br)] \left[\cos \psi + \frac{3}{\beta\lambda} e^{-r} \cos(br) \sin^2 \psi \right] = 0, \quad (110)$$

$$\begin{aligned} \frac{d\psi}{dx} = & \frac{\sqrt{2}}{\lambda} e^{-r} \cos(br) \sin \psi \\ & - \frac{3}{\sqrt{2}\lambda^2\beta} b e^{-2r} [\cos(br) + b \sin(br)] \sin(br) \sin(2\psi). \end{aligned} \quad (111)$$

It is straightforward to verify that the reduced system (110) and (111) has exactly the same FPs (104) and (106) as the full system (101) and (102), with the eigenvalues given by the same expressions (105) and (107). However, unlike the complicated full system, it is very easy to understand the general character of the dynamical trajectories on the phase plane of the reduced system. Indeed, one can check that the saddles (104) are connected by a rectangular grid of dynamical trajectories of the form $r \equiv r_0$, $\psi = \psi(x)$, and $r = r(x)$, $\psi \equiv \psi_0$, where r_0 and ψ_0 are the values of r and ψ at FPs (104). These trajectories are stable and unstable separatrices of the saddles, and they are exact solutions to both eqs. (101, 102) and (110, 111). From this fact, and from the knowledge of the eigenvalues of the FPs, there follows a phase portrait of the reduced system shown in fig. 10. Looking at the figure, one concludes that the spirals, except for those corresponding to $n = 0$ in eq. (106), asymptotically approach, at $x \rightarrow \infty$, infinite-period limit cycles coinciding with an elementary cell of the separatrix grid. The spirals corresponding to $n = 0$, i.e., to the bound states with the smallest possible

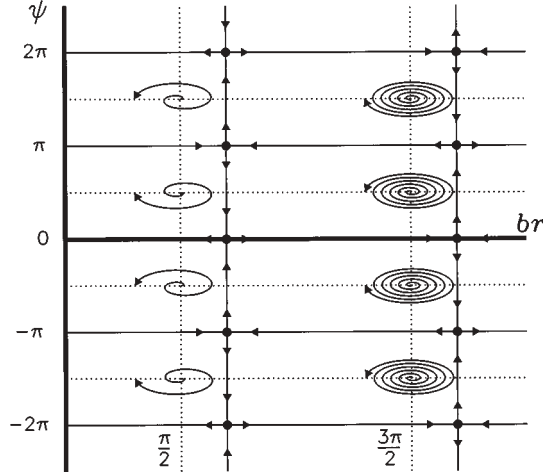


Fig. 10. Phase portrait of the reduced dynamical system (108) and (109), showing the long-distance evolution of the bound state of two solitons in the cubic–quintic Ginzburg–Landau model.

separation between the pulses, formally also asymptotically tend to a similar cycle, that, however, passes through $r = 0$, which implies a *collision* between the two pulses. The latter event is not described by the above approximation. It is natural to expect that the colliding pulses will undergo fusion into a single pulse.

These conclusions have been checked by direct simulations of the full four-dimensional system (101) and (102), with the conclusion that the full system always produces results virtually identical to those obtained from the reduced system, even if the perturbation parameters are not really small (Afanasjev, Malomed and Chu [1997]). Thus, a general conclusion is that the spiral-type bound states of the pulses in the CQ GL model are either practically stable in the usual sense, if one may neglect the exponentially weak instability, or stable as dynamical states corresponding to the limit cycle.

2.4. Dark and “symbiotic” solitons

This review focuses on “bright” solitons, which are represented by solutions vanishing at infinity. It is, nevertheless, necessary to mention another class of solutions, in the form of dark solitons (DSs), which look like a hole in a uniform continuous-wave (CW) background. As is well known, the DS solution exists and is stable in the usual NLS equation (2) in the case of normal dispersion ($D < 0$):

$$u_{\text{dark}} = a \exp(i\epsilon a^2 + i\phi_0) \tanh\left(\sqrt{\frac{\epsilon}{|D|}} a(\tau - \tau_0)\right), \quad (112)$$

where a is the amplitude of the background supporting DS, and ϕ_0 and τ_0 are arbitrary phase and position constants. DSs were first observed in a nonlinear optical fiber by Krökel, Halas, Giuliani and Grischkowsky [1988].

The description of the dynamics of perturbed DSs is essentially complicated by the presence of the fixed-amplitude background. In any perturbation-theory approach, separation of the internal DS degrees of freedom and the background is a crucial issue (Kivshar and Yang [1994], Kivshar and Królikowski [1995]; see also a review by Kivshar and Luther-Davies [1998]). Moreover, a perturbed dark soliton can easily generate waves propagating on top of the background. Due to strong radiative losses generated by these waves, the dark soliton actually has no effective “quasimode” of its internal vibrations, contrary to the Anderson quasimode of the bright soliton described above. An appropriately modified version of VA for DS was developed by Kivshar and Królikowski [1995]; it also includes the possibility of having nonlinearities in the corresponding NLS equation different from the cubic nonlinearity in eq. (2), and other perturbation terms. The technique was applied to various problems, notably the interaction (in fact, repulsion) between two DSs.

VA for moving DSs was developed, with an emphasis on the stability problem, by Barashenkov and Panova [1993]. A necessary stability criterion for moving DSs, obtained in that work in a fairly simple form, states that the properly defined momentum of the DS must be a *decreasing* function of its velocity; this was later rigorously proved by Barashenkov [1996] by means of a *Lyapunov functional* (i.e., an integral functional with the property that it may only decrease as a result of the evolution of the fields) which can be introduced in this problem.

Another known model that gives rise to DS is a system of NLS equations coupled by the nonlinear cross-phase-modulation terms, that will be considered (for bright solitons) in detail below in § 4. If the two equations correspond to two carrier waves with different wavelengths copropagating in a fiber, it is quite possible to encounter a case where one carrier wave (typically, that with the larger wavelength) has anomalous dispersion, while the other wave has normal dispersion. Then, it is interesting to consider a bound state consisting of a bright soliton in one subsystem and a DS in the other. Detailed analysis shows that the only possible bound state of this type has the bright-soliton component in the *normal*-dispersion wave, and the DS component in the *anomalous*-dispersion wave (Trillo, Wabnitz, Wright and Stegeman [1988], Afanasjev, Dianov and Serkin [1989], Wang and Yang [1990]). Because such soliton components, obviously, cannot exist in isolation, the bound state was given the name “symbiotic soliton” by Lisak, Höök and Anderson [1990], who studied it in detail by means of an accordingly modified version of VA. Note, however,

that symbiotic solitons are always unstable, as the CW background, which is necessary to support its DS component in the anomalous-dispersion subsystem, cannot be stable.

§ 3. Variational approximation for the inverse scattering transform

As mentioned in the introduction, the NLS equation, which is the most important model for nonlinear optical fibers and waveguides, is amenable to an exact solution by means of IST. In the context of this method, the first step is to find *scattering data* corresponding to a given initial pulse $u(\tau)$, solving the ZS (Zakharov and Shabat [1971]) linear equations for the two-component complex *Jost function* $(\psi^{(1)}(x), \psi^{(2)}(x))$,

$$i\psi_{\tau}^{(1)} + \lambda\psi^{(1)} + u^*(\tau)\psi^{(2)} = 0, \quad (113)$$

$$i\psi_{\tau}^{(2)} - \lambda\psi^{(2)} + u(\tau)\psi^{(1)} = 0, \quad (114)$$

where the asterisk indicates complex conjugation, and λ is the spectral parameter which takes values in the upper complex half-plane. The most important characteristic of the pulse, viz., its *soliton content*, is determined by discrete eigenvalues λ_n , each giving rise to a soliton (7) with amplitude $\eta = 2 \operatorname{Im}(\lambda_n)$ and velocity shift $c = 4 \operatorname{Re}(\lambda_n)$, provided that $D = \gamma \equiv 1$ in eq. (2).

Note that, as was discovered by Ablowitz, Kaup, Newell and Segur [1973, 1974] (see also books by Ablowitz and Segur [1981] and Newell [1985]), the ZS equations are used in application of IST not only to the NLS equation, but also to other integrable equations, including, in particular, those describing self-induced transparency in an optical medium filled with two-level atoms (Ablowitz, Kaup and Newell [1974], Kaup [1977]). Thus, it is quite important to develop methods for solving ZS equations.

There are very few field configurations for which the ZS equations can be solved exactly. These include a rectangular box without chirp (Manakov [1973b]), and a pulse of the form $u_0(\tau) = A[\operatorname{sech}(a\tau)]^{1+i\mu}$ with real a and μ (Maimistov and Sklyarov [1987], Grünbaum [1989]). In other cases, numerical methods had to be used (Boffeto and Osborne [1992]); in some cases, a WKB- (Wentzel–Kramers–Brillouin)-like analytical approximation can be applied to the ZS equations (Lewis [1985]). In particular, an important problem which requires numerical calculation is the influence of chirp on the soliton content of pulses, as the increase of the chirp gives rise to bifurcations, generating new solitons and then pushing solitons apart by lending them opposite velocities (Hmurcik

and Kaup [1979], Kaup and Scacca [1980]). The problem can be solved in the simplest way for a rectangular box with the chirp accounted for by the phase function $\phi(\tau) = b|\tau|$, with $b = \text{const.}$, so that all of the initial chirp is concentrated at the soliton's center (Kaup, El-Reedy and Malomed [1994]).

On the other hand, the ZS equations have a natural variational representation, which was used by Kaup and Malomed [1995] to develop VA for a semi-analytical calculation of the discrete eigenvalues λ , an account of which is given below. Independently, essentially the same was done by Desaix, Anderson and Lisak [1994] and by Desaix, Anderson, Lisak and Quiroga-Teixeiro [1996] (in the latter work, rectangular-box, sech^3 , and Gaussian initial pulses were considered).

Multiplying eq. (113) by $\psi^{(2)}$ and integrating the result over $d\tau$, one can obtain the following representation for the spectral parameter:

$$\lambda = -\frac{L}{N}, \quad (115)$$

$$L \equiv \int_{-\infty}^{+\infty} \left\{ \frac{i}{2} (\psi_{\tau}^{(1)} \psi^{(2)} - \psi_{\tau}^{(2)} \psi^{(1)}) + \frac{1}{2} [u^* (\psi^{(2)})^2 - u (\psi^{(1)})^2] \right\} d\tau, \quad (116)$$

$$N \equiv \int_{-\infty}^{+\infty} \psi^{(1)} \psi^{(2)} d\tau. \quad (117)$$

Varying expression (115) with respect to $\psi^{(1)}$ and $\psi^{(2)}$ produces equations (113) and (114), i.e., eqs. (115)–(117) give an effective Lagrangian for the ZS equations. It is noteworthy that this Lagrangian exactly coincides with the eigenvalue sought for; a similar fact is well known in quantum mechanics, where the linear Schrödinger equation can be obtained by varying a functional which is the energy eigenvalue (Landau and Lifshitz [1977]). However, an essential difference from quantum mechanics is that the functional (115) is not real.

Note that the terms in expression (116) containing τ -derivatives cancel mutually if $\psi^{(1)}$ is proportional to $\psi^{(2)}$. Thus, variational *ansätze* for these components should be functionally different. For example, if one uses Gaussian trial functions, it is necessary to allow the two Gaussians to have shifted centers, so that the ratio $\psi^{(1)}/\psi^{(2)}$ would be τ -dependent.

As a first example, one can take a rectangular pulse with an internal phase jump $\Delta\phi = 2\epsilon$:

$$u(\tau) = \begin{cases} 0 & \text{if } |\tau| > 1, \\ A \exp(i\epsilon \text{sgn } \tau) & \text{if } |\tau| < 1. \end{cases} \quad (118)$$

Here A is the real amplitude, and the width of the pulse can always be scaled to be 2, as implied in eq. (118). The simplest possible ansatz for the Jost functions corresponding to this pulse is

$$\psi^{(1)}(\tau) = \begin{cases} 2 \exp(-\mu(\tau - 1)) & \text{if } \tau > 1, \\ \tau + 1 & \text{if } |\tau| < 1, \\ 0 & \text{if } \tau < -1. \end{cases} \quad (119)$$

$$\psi^{(2)} = \begin{cases} 0 & \text{if } \tau > 1, \\ B(1 - \tau) & \text{if } |\tau| < 1, \\ 2B \exp(\mu(\tau + 1)) & \text{if } \tau < -1. \end{cases} \quad (120)$$

The integrals (116) and (117) calculated with this ansatz are

$$L = 2iB + \frac{1}{6}A [B^2 (e^{-i\epsilon} + 7e^{i\epsilon}) - (7e^{i\epsilon} + e^{-i\epsilon})], \quad N = \frac{4}{3}B; \quad (121)$$

note that they do not depend on μ .

Substitution of expressions (121) into eq. (115) and varying the only nontrivial parameter B yields $B = \pm i$. Inserting this back into eq. (115), one obtains the eigenvalues

$$\text{Im } \lambda = -\frac{3}{2} \pm 2A \cos \epsilon, \quad \text{Re } \lambda = \mp \frac{3}{2}A \sin \epsilon. \quad (122)$$

Since only the eigenvalue with $\text{Im } \lambda > 0$ is meaningful, eq. (122) shows that, with increasing area $S \equiv 2A$ of the pulse (118), the soliton appears, with an infinitesimal amplitude and finite velocity $c = -\frac{9}{2} \tan \epsilon$, at the threshold value

$$S_{\text{thr}} = \frac{3}{2 \cos \epsilon}. \quad (123)$$

In the case $\epsilon = 0$, when the ZS equations for the pulse (118) have an exact solution, eq. (123) yields the threshold area $\frac{3}{2}$, while the exact result is $\pi/2$ (Manakov [1973b]). Thus, the present crude approximation, using a single variational parameter, gives an error $< 5\%$. This approximation fails to predict additional solitons which appear with a further increase of the area, the total number of solitons produced by the rectangular box with $\epsilon = 0$ being $[(2S - \pi)/2\pi] + 1$ (Manakov [1973b]).

Equation (123) predicts that S_{thr} diverges in the limit $2\epsilon = \pi$, when the pulse (118) turns into a combination of two pulses with opposite signs. For this case, an improved ansatz with an additional free parameter yields the

result that the two-box configuration may produce only a pair of solitons with equal amplitudes and opposite velocities, provided that A exceeds a threshold value $3/2^{3/2}$.

VA may also be applied for predicting the soliton content in the practically important case of a chirped Gaussian pulse,

$$u_0(\tau) = B \exp [-(\sigma^2 + i\beta)\tau^2], \quad (124)$$

with real B , β and σ . A natural form for the Jost-function ansatz is also Gaussian,

$$\psi^{(n)} = B_n \exp [-(W_n \tau^2 + 2\zeta_n \tau)], \quad n = 1, 2, \quad (125)$$

where the variational parameters B_n , W_n and ζ_n may be complex, provided that $\text{Re } W_n > 0$. The subsequent calculation of the effective Lagrangian and variation can be done analytically, but the expressions are cumbersome. Final results are presented in fig. 11 as plots of the soliton amplitude η vs. the area of the initial pulse at different fixed values of the initial chirp β (in all cases shown,

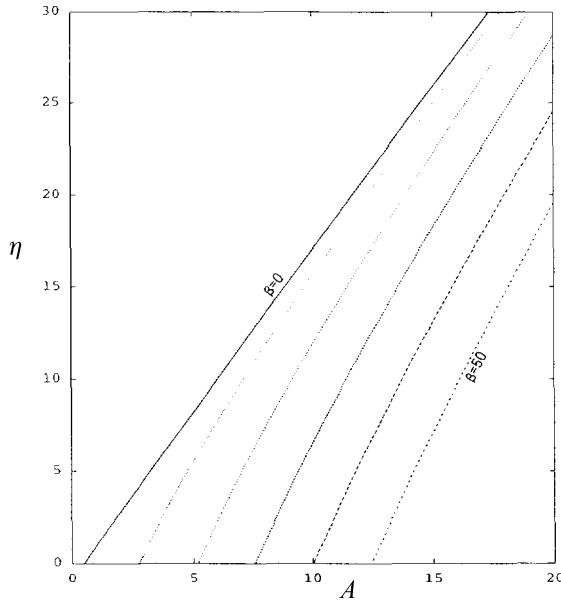


Fig. 11. Amplitude of the single soliton generated by an initial Gaussian chirped pulse (124) vs. its effective area $A \equiv B/(\sqrt{\pi}\sigma)$ for $\sigma = 1$ and different values of the initial chirp, $\beta = 0, 10, 20, 30, 40, 50$.

exactly one soliton is generated). These curves are almost the same as those obtained numerically for the same problem by Kaup and Scacca [1980]. Note that the plots clearly show the increase of the area necessary for the formation of the soliton with an increase of the initial chirp.

§ 4. Internal dynamics of vector (two-component) solitons

4.1. General description

An important aspect of nonlinear fiber optics is copropagation of two or several modes in one fiber. Although standard fibers are designed to admit propagation of a single mode determined by its transverse structure (Agrawal [1995]), the polarization of light makes the fiber bimodal. Another very important possibility is to launch different modes carried by different wavelengths, which is the basis of the wavelength-division multiplexing (WDM) technique. WDM is the cornerstone of the present-day development of optical telecommunications, as it allows to create many parallel channels in a single fiber core. In the latter case, the most essential dynamical process is collision between two solitons belonging to different channels. In the application to optical telecommunications, quasi-random collisions in a multi-channel system are very detrimental, as they generate random walk (*temporal jitter*) of the solitons, which interferes with data transmission. VA can be naturally applied to the collision problem, reducing it to interaction of particles, as was shown for a two-channel system in an early work by Anderson and Lisak [1986b], and for multi-soliton states in multi-channel systems by Ablowitz, Biondini, Chakravarty and Horne [1998].

A related problem appears when two copropagating waves have their frequencies on opposite sides of the fiber's zero-dispersion point, so that one wave has normal dispersion, and the other propagates at anomalous dispersion. While only the latter wave can carry bright solitons, the normal-dispersion channel can be used to launch a periodic structure (which, loosely, may be realized as a periodic array of dark solitons). This *support structure* in the normal-dispersion channel induces, through the XPM interaction, an effective periodic potential in the soliton-carrying anomalous-dispersion channel (Shipulin, Onishchukov and Malomed [1997], Malomed and Shipulin [1999]). The periodic potential may be quite useful, helping to stabilize the temporal position of solitons against the jitter (random walk) induced by interaction of a soliton with optical noise in the fiber. The suppression of the jitter by the periodic support structure has

been considered using a combination of variational and numerical methods. In particular, the soliton dynamics reduce to an equation of motion for a particle in a periodic potential under the action of a random driving force, which, in turn, gives rise to the corresponding Fokker–Planck equation.

From the standpoint of applications of VA, the case of a bimodal system corresponding to two polarizations in a nonlinear fiber is more interesting, as it allows one to consider different types of vector two-component solitons and their internal vibrations. Vector solitons in bimodal systems are considered below.

A basic model of a bimodal nonlinear fiber includes two nonlinearly coupled NLS equations (see a detailed derivation by Menyuk [1987] and a book by Agrawal [1995]) for the amplitudes $u(z, t)$ and $v(z, t)$ of the electromagnetic waves in two linearly polarized modes,

$$iu_z + icu_\tau + ku + \frac{1}{2}u_{tt} + (|u|^2 + \frac{2}{3}|v|^2)u + \frac{1}{3}v^2u^* = \lambda v, \quad (126)$$

$$iv_z - icv_\tau - kv + \frac{1}{2}v_{tt} + (|v|^2 + \frac{2}{3}|u|^2)v + \frac{1}{3}u^2v^* = \lambda u, \quad (127)$$

where the asterisk stands for complex conjugation, and the terms $\sim \pm c$ and $\pm k$ take into account, respectively, the group-velocity and phase-velocity birefringence due to deviation of the fiber's cross-section from the ideal circular shape (usually, the group-velocity birefringence is much weaker than its phase-velocity counterpart). The nonlinear cross-coupling terms preceded by the coefficient $\frac{2}{3}$ are insensitive to the phase difference between the u and v fields, and represent the *cross-phase modulation* (XPM) between the two polarizations, induced by the Kerr effect. The phase-sensitive terms preceded by the coefficient $\frac{1}{3}$ account for another manifestation of the Kerr effect in a multimode system, viz., *four-wave mixing*. Lastly, the linear-coupling terms (with real λ) on the rhs of the equations take into regard possible *twist* of the fiber, which causes linear mixing between the two linear polarizations (Trillo, Wabnitz, Banyai, Finlayson, Seaton, Stegeman and Stolen [1989]).

Equations (126) and (127) can be derived from the Lagrangian density

$$\begin{aligned} L = & \frac{1}{2} [(u^*u_z + v^*v_z + icu^*u_\tau - icv^*v_\tau) + \text{c.c.}] \\ & + k (|u|^2 - |v|^2) - \frac{1}{2} (|u_\tau|^2 + |v_\tau|^2) + \frac{1}{4} (|u|^4 + |v|^4) \\ & + \frac{2}{3}|u|^2|v|^2 + \frac{1}{6} [u^2(v^*)^2 + v^2(u^*)^2], \end{aligned} \quad (128)$$

hence VA can be applied here. The dynamics of two-component solitons governed by eqs. (126) and (127) are rather complicated if four-wave mixing is taken into account, as the phase difference between the components will play

the role of an additional degree of freedom, along with the widths of the two components and the separation between their centers, see below. This problem was analyzed by means of VA, neglecting the group-velocity birefringence and twist-induced linear coupling, in the works of Muraki and Kath [1989, 1991] and Anderson, Kivshar and Lisak [1991], and a generalization for a case when the birefringence coefficient varies randomly along the fiber was developed by Ueda and Kath [1992]. A similar analysis based on VA which, however, took into account the group-velocity birefringence and linear coupling between the polarizations was independently developed by Malomed [1991a]. In all these works, the variational ansatz was based on sech, and results were presented in the form of normal forms of various modes of intrinsic vibrations of two-component solitons. As demonstrated by Malomed [1991a], in the presence of the group-velocity birefringence, VA also makes it possible to explain another interesting dynamical phenomenon: internal degrees of freedom of the two-component soliton get coupled to the motion of its center of mass, so that the internal vibrations generate periodic oscillations of the velocity at which the soliton propagates (this effect had been known from direct numerical simulations of eqs. (126) and (127) reported by Trillo, Wabnitz, Wright and Stegeman [1989] and Wright, Stegeman and Wabnitz [1989]).

However, in a realistic situation the fiber birefringence is so strong that the corresponding length of beatings between two polarization components is much smaller than any propagation length relevant to the evolution of solitons, hence both the four-wave-mixing nonlinear and twist-induced linear phase-dependent coupling are negligible. Thus, the most fundamental model is based on the simplified version of eqs. (126) and (127),

$$iu_z + \frac{1}{2}u_{tt} + (|u|^2 + \frac{2}{3}|v|^2)u = 0, \quad (129)$$

$$iv_z + \frac{1}{2}v_{tt} + (|v|^2 + \frac{2}{3}|u|^2)v = 0, \quad (130)$$

in which the birefringence terms are dropped because they may be readily eliminated in the absence of the phase-dependent couplings. The dynamics of two-component solitons in this simplified model will be considered below, following works by Ueda and Kath [1990], Kaup, Malomed and Tasgal [1993], and Malomed and Tasgal [1998].

Notice that the XPM coefficient $\frac{2}{3}$ in eqs. (129) and (130) is relatively close to its special value 1, at which the two coupled NLS equations constitute a model integrable by means of IST, as was found by Manakov [1973a]. The proximity to the Manakov system can be used to develop a perturbative approach based on a

combination of the Lagrangian and Hamiltonian representations of the equations (Malomed [1991a]).

Before proceeding to detailed consideration of vector solitons, it is relevant to mention another problem which appears in the model of a bimodal fiber, in the case when the dispersion is normal, and NLS equations for two waves with opposite *circular* polarizations are used. In this case, the XPM coefficient in the coupled NLS equations is 2 (the same as for the interaction between waves at different wavelengths) rather than $\frac{2}{3}$, see eqs. (129) and (130). While bright solitons are impossible with normal dispersion, it was demonstrated by Malomed [1994a] that another nonlinear structure occurs in this case, viz., an *optical domain wall*, separating two temporal domains filled with waves having opposite circular polarizations. Variational methods are quite useful in the study of these domain walls and interactions between them.

4.2. Solitons in a bimodal birefringent fiber

4.2.1. Ansatz and stationary states

A general ansatz for vector solitons must make it possible to describe solitons with different widths of their two components, as well as independent vibrations of the two widths. Because a product of hyperbolic secants with different widths cannot be integrated in analytical form, the only option is to adopt a Gaussian-based approximation, as was first done by Kaup, Malomed and Tasgal [1993]. The ansatz for vector solitons generated by eqs. (129) and (130) is

$$u(z, t) = A_u \exp \left[-\frac{1}{2} \left(\frac{t - y_u}{W_u} \right)^2 \right] \exp \{ i [\phi_u + b_u(t - y_u) + c_u(t - y_u)^2] \}, \quad (131)$$

$$v(z, t) = A_v \exp \left[-\frac{1}{2} \left(\frac{t - y_v}{W_v} \right)^2 \right] \exp \{ i [\phi_v + b_v(t - y_v) + c_v(t - y_v)^2] \}, \quad (132)$$

where, as usual, all the free parameters are real and are assumed to be functions of z . The ansatz accommodates a pulse with arbitrary amplitudes (A_u, A_v), widths (W_u, W_v), and central positions (y_u, y_v). Each component is also allowed to have arbitrary phase (a_u, a_v), central frequency (b_u, b_v), and frequency chirp (c_u, c_v). Note that the ansatz admits splitting of the vector soliton into single-component ones.

The VA technique yields a set of equation for the twelve parameters of the ansatz. The set includes four dynamical invariants and six evolutionary

equations which are written below as three second-order equations. There are also equations for the phases ϕ_u and ϕ_v which involve other variables but do not themselves influence anything else, so they are not displayed below. The dynamical invariants are the energies in the two modes and their net momentum,

$$E_u \equiv \frac{1}{2} \int_{-\infty}^{\infty} |u|^2 dt = \frac{\sqrt{\pi}}{2} A_u^2 W_u, \quad (133)$$

$$E_v \equiv \frac{1}{2} \int_{-\infty}^{\infty} |v|^2 dt = \frac{\sqrt{\pi}}{2} A_v^2 W_v, \quad (134)$$

$$\begin{aligned} P &\equiv \int_{-\infty}^{\infty} \frac{i}{2} (u_t u^* - u u_t^* + v_t v^* - v v_t^*) dt = \frac{d}{dz} (E_u y_u + E_v y_v) \\ &\equiv -(E_u b_u + E_v b_v), \end{aligned} \quad (135)$$

and the Hamiltonian of eqs. (129) and (130), which is not needed in an explicit form. It is convenient to define the soliton's polarization angle θ , by $\tan^2 \theta \equiv E_v/E_u$.

The equations of motion for the widths $W_{u,v}$ and relative position $y \equiv y_u - y_v$ of the components of the vector soliton are

$$\begin{aligned} \frac{d^2}{dz^2} W_u &= W_u^{-3} - \frac{E_u}{\sqrt{2\pi}} W_u^{-2} \\ &\quad - \frac{4}{3\sqrt{\pi}} E_v W_u (W_u^2 + W_v^2)^{-3/2} \left(1 - \frac{2y^2}{W_u^2 + W_v^2}\right) \exp\left(-\frac{y^2}{W_u^2 + W_v^2}\right), \end{aligned} \quad (136)$$

$$\begin{aligned} \frac{d^2}{dz^2} W_v &= W_v^{-3} - \frac{E_v}{\sqrt{2\pi}} W_v^{-2} \\ &\quad - \frac{4}{3\sqrt{\pi}} E_u W_v (W_u^2 + W_v^2)^{-3/2} \left(1 - \frac{2y^2}{W_u^2 + W_v^2}\right) \exp\left(-\frac{y^2}{W_u^2 + W_v^2}\right), \end{aligned} \quad (137)$$

$$\begin{aligned} \frac{d^2}{dz^2} y &= \frac{d}{dz} (-b_u + b_v) \\ &= -\frac{4B}{3\sqrt{\pi}} (E_u + E_v) (W_u^2 + W_v^2)^{-3/2} y \exp\left(-\frac{y^2}{W_u^2 + W_v^2}\right), \end{aligned} \quad (138)$$

and $c_u = (2W_u)^{-1}(d/dz)W_u$, $c_v = (2W_v)^{-1}(d/dz)W_v$.

Fixed points (FPs) of eqs. (136)–(138) correspond to steady-state vector solitons with $y = c_u = c_v = 0$. The corresponding stationary values of the widths were first found, by means of VA, in a paper by Kaup, Malomed and Tasgal

[1993] (independently, the same family of general stationary solitons was found in a purely numerical form by Haelterman, Sheppard and Snyder [1993]):

$$W_u = \frac{\sqrt{\pi/2}}{E_u} \left[1 - \frac{2}{3} r^4 \left(\frac{2}{r^2+1} \right)^{3/2} \right] \bigg/ \left[1 - \frac{4}{9} \left(\frac{2r}{r^2+1} \right)^3 \right], \quad (139)$$

$$W_v = \frac{\sqrt{\pi/2}}{E_v} \left[1 - \frac{2}{3} r^{-1} \left(\frac{2}{r^2+1} \right)^{3/2} \right] \bigg/ \left[1 - \frac{4}{9} \left(\frac{2r}{r^2+1} \right)^3 \right], \quad (140)$$

where the width ratio $r \equiv W_u/W_v$ is determined by

$$\frac{2}{3} \left(\frac{2}{1+r^2} \right)^{3/2} \left(r^4 - \frac{E_u}{E_v} \right) + \frac{E_u}{E_v} r - 1 = 0. \quad (141)$$

Thus, the energies of the two modes E_u and E_v are free parameters of the stationary vector soliton, which determine its amplitudes A_u and A_v and widths W_u and W_v according to the above equations. While the relative frequency $(b_u - b_v)$ is zero at the fixed point, the mean frequency $(b_u + b_v)/2$ can take any constant value, a nonzero one adding a net momentum to the soliton, making it “walking”.

Table 1 summarizes the VA predictions for the parameters of the stationary vector soliton in a range of polarization angles. The values of the widths in the table refer to either the Gaussian ansatz with net energy $E \equiv E_u + E_v = \sqrt{\pi/2}$, or (see below) a *hybrid* Gaussian–sech ansatz with $E = 1$. Note that the negativeness of the Hamiltonian is a necessary existence condition for the soliton (if the Hamiltonian is positive, the pulse will decay into radiation). The stationary widths for other values of the energies can be obtained from table 1: in either ansatz, the widths scale as the reciprocal of the net energy, so, to obtain the widths for arbitrary net energy E , the values in table 1 should be multiplied by

Table 1

Widths of the two components predicted for the stationary vector soliton by the variational approximation based on the Gaussian ansatz with total energy $E = \sqrt{\pi/2}$ or the sech ansatz with total energy $E = 1$, for different values of the vector soliton’s polarization angle θ

Polarization	θ (°)								
	0	5	10	15	20	25	30	40	45
W_u	1.0000	1.0038	1.0149	1.0330	1.0571	1.0860	1.1175	1.1774	1.2000
W_v	n/a	1.1881	1.1930	1.2003	1.2089	1.2168	1.2220	1.2150	1.2000

$(\sqrt{\pi/2}/E)$ or $(1/E)$, for the Gaussian or sech ansatz, respectively. For polarization angles $> 45^\circ$, one should take the complement of the angle and interchange u and v .

4.2.2. A hybrid ansatz

In the exactly solvable cases, $v = 0$ or $u = v$, when the coupled system degenerates into a single NLS equation, and in the Manakov system, exact vector-soliton solutions have $|u| = A^{\text{sech}} \text{sech}(t/W^{\text{sech}})$, with width and amplitude related to those predicted by the Gaussian ansatz in a simple way:

$$W^{\text{sech}} = \sqrt{\frac{2}{\pi}} W^{\text{Gauss}}, \quad A^{\text{sech}} = \sqrt{\frac{\pi}{2^{3/2}}} A^{\text{Gauss}}, \quad (142)$$

provided that the energy of the soliton, $E \equiv (A^{\text{sech}})^2 W^{\text{sech}}$, is equal to that of the Gaussian ansatz. This relation suggests that making the same adjustment in the *final* results produced by the Gaussian-based VA, i.e., replacing the Gaussian by the sech pulse with the parameters rescaled according to eq. (142), may help to get the approximate vector-soliton shape closer to the true pulse shape. To estimate the importance of the adjustment, one can note that, in the solvable cases, the standard FWHM width predicted by the Gaussian approximation differs from that of the exact sech soliton with the same energy by a factor $(\sqrt{2} \cosh^{-1} \sqrt{2})/\sqrt{\pi \ln 2} \approx 0.845$.

Thus, to improve the accuracy of VA, one may take a solution to eqs. (136)–(138), which govern the evolution of the parameters of the Gaussian ansatz, and insert the solution not into the Gaussian ansatz but rather into

$$u(z, t) = A_u^{\text{sech}} \text{sech}\left(\frac{t - y_u}{W_u^{\text{sech}}}\right) \exp[i(\phi_u + b_u(t - y_u) + c_u(t - y_u)^2)], \quad (143)$$

$$v(z, t) = A_v^{\text{sech}} \text{sech}\left(\frac{t - y_v}{W_v^{\text{sech}}}\right) \exp[i(\phi_v + b_v(t - y_v) + c_v(t - y_v)^2)], \quad (144)$$

with the widths and amplitudes rescaled according to eq. (142).

Comparison with numerical simulations clearly shows advantages offered by the hybrid ansatz. It was observed that, starting with the initial conditions corresponding to the FP (139)–(141), predicted by the Gaussian-based VA, more than 99% of the initial energy is ultimately retained by the soliton, with the exact size of the radiative losses slightly depending on the soliton's polarization angle θ . So, by this measure – the share of the net energy going into the soliton – the predictions of the Gaussian VA are very good. However, in terms of the

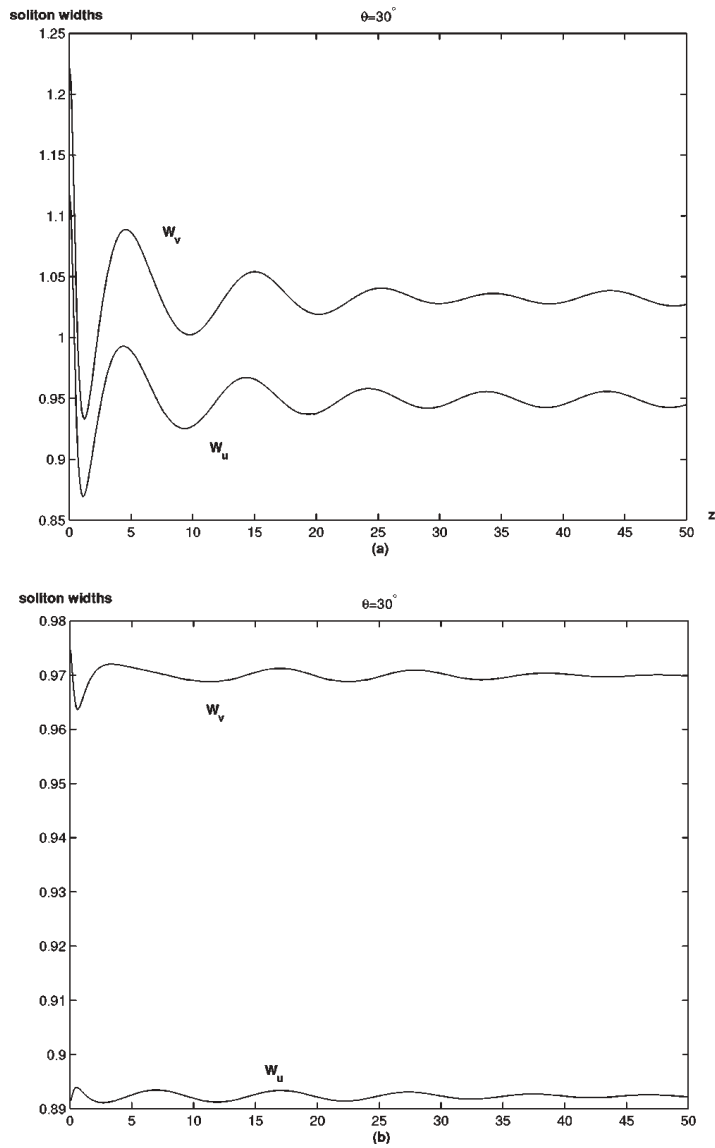


Fig. 12. (a) Evolution of the vector soliton widths produced by simulations of eqs. (129) and (130), starting from the initial condition predicted by the usual Gaussian approximation for the vector soliton with polarization $\theta = 30^\circ$ and energy $E = \sqrt{\pi/2}$. (b) Same, starting from the initial conditions predicted by the hybrid Gaussian-sech approximation, based on eqs. (142)–(144). The larger and smaller widths pertain to the less energetic and more energetic components of the vector soliton, respectively.

eventual widths of the vector solitons, the agreement of the same version of VA with the numerical results is worse, with a relative error of about $\frac{1}{6}$. To illustrate, fig. 12a shows the numerically simulated evolution of the pulse widths, starting from the fixed point of the usual Gaussian approximation, with total energy $E = \sqrt{2\pi}$ and polarization $\theta = 30^\circ$.

The hybrid approximation, based on eqs. (142)–(144), yields much more accurate predictions for the widths of the stationary states than the usual Gaussian VA: even in the worst case the relative error is below 1%, while in most cases the accuracy is even higher than that. The radiative energy shed by the evolving vector soliton starting from the hybrid ansatz was too small to measure, being much less than 1%, which is another drastic improvement offered by the hybrid VA model. Figure 12b illustrates this, showing the evolution of the widths in the simulations, starting from the stationary solution as predicted by the hybrid model with total energy $E = \sqrt{2\pi}$ and polarization $\theta = 30^\circ$.

4.2.3. Intrinsic vibrations of a vector soliton

For small oscillations around the stationary vector soliton, linearization of eqs. (136)–(138) shows that small vibrations of the separation y between the two components decouple from vibrations of the widths W_u and W_v . Two distinct eigenmodes of the width vibrations can be identified: one “in-phase”, with both widths oscillating synchronously, the other “out-of-phase”, with the two widths oscillating with a phase shift π (Kaup, Malomed and Tasgal [1993]).

For the case $\theta = 45^\circ$, when the energy of the vector soliton is equally divided between its two components, the y - and in-phase width oscillation eigenmodes were first identified by Ueda and Kath [1990]. In this case, the eigenfrequencies of the separation (y -), in-phase-width, and out-of-phase-width vibration modes, calculated by means of the sech ansatz, are

$$(k_y^{\text{sech}}, k_{\text{in}}^{\text{sech}}, k_{\text{out}}^{\text{sech}}) = (0.50, 0.69, 0.99) \cdot \frac{2E^2}{\pi}. \quad (145)$$

The same eigenfrequencies were found from direct simulations by Malomed and Tasgal [1998] to be

$$(k_y^{\text{num}}, k_{\text{in}}^{\text{num}}, k_{\text{out}}^{\text{num}}) = (0.53, 0.54, 0.56) \cdot \frac{2E^2}{\pi}. \quad (146)$$

Comparison with eq. (145) shows a large error of the VA-based prediction for the in-phase-width mode, and a very large error for the out-of-phase-width mode.

The stability and instability of different oscillation modes of the perturbed vector soliton can be predicted by considering the unperturbed one as a nonlinear structure that protects itself from decay into radiation by placing its eigenfrequency in a *spectral gap* in which radiation modes do not exist. In other words, the unperturbed soliton is, essentially, a gap soliton, as defined in the review by de Sterke and Sipe [1994]. In particular, for the case $\theta = 45^\circ$, the gaps in the spectra of the spatial frequencies k for u - and v -components are identical, and they can easily be found in exact form from eqs. (129) and (130) linearized around the stationary soliton, without resorting to VA:

$$|k| < 0.5454 \cdot \frac{2E^2}{\pi}. \quad (147)$$

If the mode's eigenfrequency lies inside the continuous spectrum (outside the band gap), the oscillation mode couples to the radiation and is therefore subject to decay. Comparing the eigenfrequencies (146) with the spectral gap (147), one concludes that the predicted frequency of the separation oscillations k_y belongs to the gap, and the frequency of the in-phase-width oscillations is located virtually exactly at the edge of the gap. In contrast with these, the frequency of the out-of-phase-width oscillations lies deep inside the continuous spectrum. These conclusions suggest that the oscillations of the separation between the two components of the vector soliton should be the stablest eigenmode, while the out-of-phase width oscillations should be unstable.

The system of ODEs (136)–(138) produced by VA also predicts the possibility of dynamical chaos if the vector-soliton's internal vibrations have sufficiently large amplitude. However, in the corresponding PDE simulations, the degree of freedom corresponding to the out-of-phase-width oscillations dies out quickly, which actually prevents the appearance of chaos (Malomed and Tasgal [1998]).

It is relevant to mention work by Yang [1997a] (see also Yang [1997b]), who studied the vibrations of vector solitons and emission of radiation from them via a different method, based on numerical algorithms for determining the true form of the small vibrations. This work provides a considerable advance in detailed understanding of the dynamics of small vibrations in vector solitons; in particular, the out-of-phase mode of the width vibrations was identified there with a combination of radiation modes, which accords with the results outlined above.

Vector solitons with more than two components can also be considered in a model of several waves carried by different frequencies and interacting via XPM. By means of a combination of variational and numerical methods, a three-component vector soliton of this type was considered by Tran, Sammut and Samir [1994].

4.3. Resonant splitting of a vector soliton in a bimodal fiber with periodically modulated birefringence

It is quite easy to fabricate a bimodal optical fiber with periodically modulated birefringence, which gives rise to a model with a group-velocity difference between two polarization modes that changes sign periodically. This suggests a possibility of a resonance between the separation mode of internal vibration of the vector soliton, considered above, and the periodic modulation of the birefringence.

This model was introduced by Malomed and Smyth [1994]. It is based on coupled equations (cf. eqs. 126 and 127)

$$iu_z + ic(z)u_\tau + \frac{1}{2}u_{tt} + (|u|^2 + B|v|^2)u = 0, \quad (148)$$

$$iv_z - ic(z)v_\tau + \frac{1}{2}v_{tt} + (|v|^2 + B|u|^2)v = 0, \quad (149)$$

where physically relevant values of the XPM coefficient are $B = \frac{2}{3}$ and $B = 2$ corresponding, as explained above, to linear and circular polarizations. The group-velocity difference between the polarizations is assumed to be modulated as

$$c(z) = \varepsilon \sin(kz). \quad (150)$$

In what follows, we set $k \equiv 1$, which can always be achieved by obvious rescaling.

In order to derive equations for internal oscillations of the vector soliton, the following ansatz is adopted (cf. eqs. 131 and 132):

$$u = A(z) \operatorname{sech}\left(\frac{\tau - y(z)}{W(z)}\right) \exp[i\phi_1(z) + i\Omega(z)(\tau - y(z)) + ib(z)(\tau - y(z))^2], \quad (151)$$

$$v = A(z) \operatorname{sech}\left(\frac{\tau + y(z)}{W(z)}\right) \exp[i\phi_2(z) - i\Omega(z)(\tau + y(z)) + ib(z)(\tau + y(z))^2]. \quad (152)$$

Straightforward VA-based calculations lead to the following equations of motion for the separation $y(z)$ between the centers of the two components and their common width $W(z)$:

$$\frac{d^2y}{dz^2} = 2BKW^{-2}F'\left(\frac{2y}{W}\right) + \varepsilon \cos z, \quad (153)$$

$$\frac{d^2W}{dz^2} = \frac{4}{\pi^2} \left\{ W^{-3} - KW^{-2} - 3BKW^{-2} \left[F\left(\frac{2y}{W}\right) + \frac{2y}{W}F'\left(\frac{2y}{W}\right) \right] \right\}, \quad (154)$$

where $K \equiv A^2 W$ is the dynamical invariant which represents the conserved energy in each polarization (the notation K for energy is used instead of E in this section), and $F(x) \equiv (x \cosh x - \sinh x) / \sinh^3 x$.

At $\varepsilon = 0$, the system of equations (153) and (154) has a fixed point (FP) at $y = 0$, $W = (1 + B)^{-1} K^{-1}$, which corresponds to the stationary vector soliton. Linearizing the equations in a vicinity of the FP, one readily finds two eigenfrequencies of small oscillations in the absence of the periodic modulation:

$$q_y^2 = \frac{16}{15} B(1 + B)^3 K^4, \quad (155)$$

$$q_W^2 = \frac{4}{\pi^2} (1 + B)^4 K^4, \quad (156)$$

where the subscript indicates the type of the corresponding eigenmode.

Several different types of resonance between the internal vibrations of the vector soliton and the periodic modulation of the birefringence are possible. The simplest (fundamental) resonance is expected for the value of the soliton's energy at which

$$K^{-4} = \frac{16}{15} B(1 + B)^3, \quad (157)$$

when, according to eq. (155), the eigenfrequency q_y coincides with the modulation wave number (which is 1 in the notation adopted). A second-order resonance may take place at

$$K^{-2} = \frac{(1 + B)^2}{\pi}, \quad (158)$$

when $q_W = 2$ according to eq. (156). Indeed, eq. (153) shows that in this case the variable y is driven at the frequency 1, and, in turn, it resonantly drives the variable W through eq. (154) at the frequency 2.

In order to realize how the resonances predicted by considering small internal vibrations of the vector soliton manifest themselves, the system of equations (153)–(154) was simulated numerically. It was found that, with increasing modulation amplitude ε , the driven vibrations of the vector soliton become more and more chaotic and, finally, the vector soliton is split into two single-component ones, which corresponds to $y \rightarrow \infty$ at $z \rightarrow \infty$ in terms of eqs. (153) and (154), at a certain critical value ε_{cr} . Figure 13 shows an example of the evolution of the separation $y(z)$, finally resulting in splitting, in the case when ε slightly exceeds ε_{cr} .

A numerically found dependence of ε_{cr} on energy K is shown (for $B = 2$, i.e., circular polarizations) in fig. 14. In this case, eqs. (157) and (158) predict the

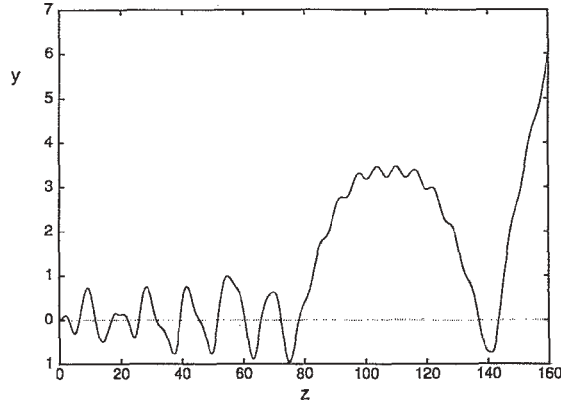


Fig. 13. Example of the splitting of a vector soliton into two single-component solitons under the action of a periodically modulated birefringence, as predicted by simulations of eqs. (153) and (154) with $B = \frac{2}{3}$ (i.e., for linear polarizations), at $K = 0.8$ and $\varepsilon = 0.13$ (slightly above the splitting threshold).

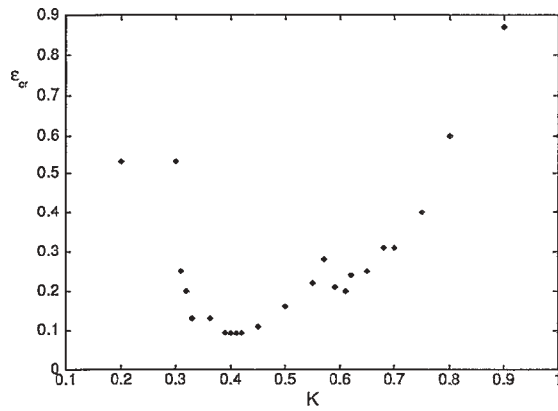


Fig. 14. Critical amplitude of birefringence modulation, ε_{cr} , vs. soliton energy K , as obtained from simulations of eqs. (153) and (154) with $B = 2$ (i.e., for circular polarizations).

fundamental and second resonances at $K = 0.363$ and $K = 0.591$, respectively. The plot in fig. 13 indeed has the deepest and second-deepest minima fairly close to these two points. The accuracy with which the positions of the minima are predicted by eqs. (157) and (158) is remarkable, as the analytical results were obtained from the consideration of small oscillations, while the splitting implies indefinitely large amplitudes of the oscillations prior to the splitting.

§ 5. Spatially nonuniform fibers and dispersion management

5.1. Dispersion-decreasing fibers

As was explained in detail in § 2.1.4, the problem of compression of a pulse in an optical fiber without disturbing the pulse's fundamental-soliton character is of great practical importance. If the original pulse is already sufficiently narrow in the temporal domain, and/or the fiber's dispersion is high enough, so that the soliton period (see eq. 8) is not too large, a natural idea is to pass the soliton through a long piece of fiber with a gradually decreasing dispersion coefficient (Kuehl [1988]). If the length of the piece essentially exceeds the soliton period, one may hope that the pulse will adiabatically follow the decreasing dispersion coefficient, while remaining the fundamental soliton. This idea was realized in *dispersion-decreasing fibers* (DDF), in which the variable dispersion is created by *tapering* the fiber, i.e., gradually varying the diameter of its core. Experimentally, high-quality strong compression of fundamental solitons by means of DDF has been demonstrated in a number of works, e.g., by Chernikov, Dianov, Richardson and Payne [1993].

DDF may find a particular application in improvement of the amplification of (sufficiently narrow) solitons in a long fiber-optic communication link, as proposed by Malomed [1994b]. A problem is that, as a matter of fact, a linear (erbium-doped) amplifier instantaneously multiplies the soliton temporal profile by an amplification factor, transforming the fundamental soliton into a "lump", that will later split into an amplified soliton proper and a noisy radiation component. However, the amplified pulse may be fed immediately into a fiber with a higher dispersion value, for which it will remain a fundamental soliton, and then DDF can adiabatically transform it into a fundamental soliton adjusted to the value of the dispersion in the system (bulk) fiber.

5.2. Formation of a soliton from a pulse passing a zero-dispersion point

An interesting realization of the situation considered above is when the dispersion is varied along the propagation length so that it changes from normal to anomalous. As proposed by Malomed [1993], in that case a pulse launched in the normal-dispersion part of the fiber may self-trap into a soliton after passing the zero-dispersion point (ZDP). The process can be analyzed by means of VA, using the general equations (32) and (33) with the variable $D(z)$. The most essential prediction is that formation of a soliton is possible if the pulse's energy exceeds a certain threshold, which is proportional to the value of the slope dD/dz at ZDP.

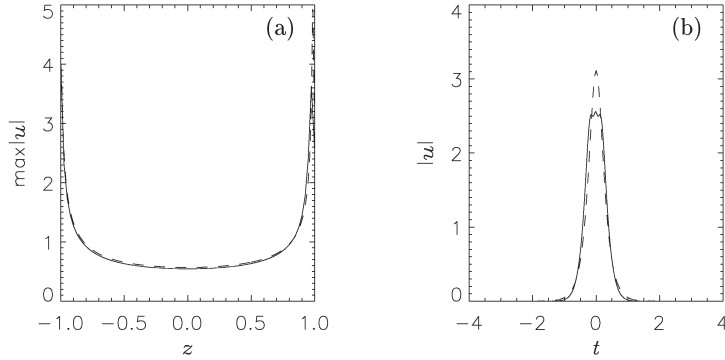


Fig. 15. Comparison of results produced by direct simulations of the NLS equation (solid curves) with the variable dispersion coefficient passing through zero and simulations of the variational equation (32) (dashed curves) in the same case. For energy $E = 4$ and area $M = \pi/2$ of the initial pulse (159), we show (a) the evolution of the field amplitude $|u|$ at the center of the pulse, $\tau = 0$, and (b) the temporal shape of the pulse, $|u(\tau)|$, at the point $z = 1$.

This process was simulated numerically by Clarke, Grimshaw and Malomed [2000], within the framework of eq. (2) with $\gamma \equiv 1$ and $D(z)$ taken in the simplest form providing for the continuous passage through ZDP (at $z = 0$): $D(z) \equiv \text{sgn}(z)$ at $|z| > 1$, and $D(z) = z$ at $|z| < 1$. In fact, the simulations commenced at $z = -1$ with the initial pulse

$$u(z = -1, \tau) = A \operatorname{sech}(h\tau). \quad (159)$$

Thus, the possible outcomes of the process are controlled by two positive parameters A and h introduced in eq. (159), i.e., by the energy and area of the initial pulse, which are $E = 2A^2/h$ and $M = \pi A/h$ according to eqs. (10) and (9) [in this section, the definition of energy does not include the factor $\frac{1}{2}$ in front of the integral in eq. (10), and the symbol for the area is M (“mass” of the soliton) instead of S].

Comparison of direct PDE simulations with those of the variational dynamical equation (32) has demonstrated that the agreement between them is quite good for sufficiently narrow initial pulses, for which VA is expected to be applicable, see fig. 15 for an example. Results of many simulations are summarized in a diagram showing qualitatively different outcomes of the pulse evolution for different values of the initial area and energy (fig. 16). These outcomes may be: decay of the pulse into radiation, formation of a single fundamental soliton, formation of a higher-order soliton (*breather*), and also formation of a pair of two separating fundamental solitons. A noticeable feature of the diagram is a

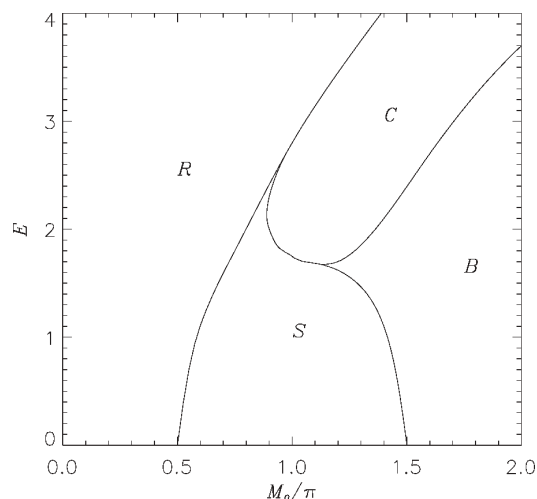


Fig. 16. Chart showing different outcomes of the evolution of a pulse (159) passing from normal to anomalous dispersion, for different values of the pulse's initial area $M = \pi A^2/h$ and energy $E = 2A^2/h$. Symbols: *R*, decay into radiation; *S*, formation of a single fundamental soliton; *B*, formation of a breather; *C*, formation of a pair of separating fundamental solitons.

virtually direct transition from the single-soliton state to the pair of separating solitons (regions *S* and *C* in fig. 16), although, in theory, the transition may only occur via an intermediate breather state. Plausibly, the intermediate layer is so thin that it cannot be seen in the computer-generated diagram.

5.3. Fibers with periodically modulated dispersion

5.3.1. Variational analysis

The fact that VA predicts persistent internal vibrations of a perturbed soliton, described in the exact parametric form by eq. (38) or in the approximation of small oscillations by eq. (36), suggests a possibility of resonances between these vibrations and a periodic modulation of the local dispersion coefficient along the fiber. This problem was considered first by Malomed, Parker and Smyth [1993], who assumed the simplest sinusoidal form of the modulation,

$$D(z) = 1 + \varepsilon \sin z, \quad (160)$$

where it is implied that the period of the modulation may always be made equal to 2π by means of a rescaling of the NLS equation (2). Possible nonlinear

resonances were studied analytically, assuming $\varepsilon \ll 1$, expanding the dynamical equation (32) around the equilibrium position (35), and retaining quadratic and cubic nonlinear terms in the expansion. The fundamental resonance corresponds to the case when the spatial frequency K_0 of free small oscillations near the equilibrium position (see eq. 36) is close to the spatial modulation frequency, which is 1 in eq. (160). Also considered in detail were the first subharmonic resonance, corresponding to K_0 close to $\frac{1}{2}$, and the second-order resonance, which takes place for K_0 close to 2.

The main subject of the analysis was possible destruction of the soliton under the action of the periodic dispersion modulation. VA based on the simple ansatz (13) predicts destruction of the soliton if a corresponding solution to eq. (32) has $a(z) \rightarrow \infty$ at $z \rightarrow \infty$: this means the soliton becomes infinitely broad, decaying into radiation.

Of course, the consideration of resonances in the small vibrations of the soliton near its equilibrium configuration does not make it possible to produce solutions which give rise to the destruction of the soliton. In order to predict a possible decay, the full dynamical equation (32) with $D(z)$ in the form (160) was solved numerically. In an interval of soliton energies covering both the above-mentioned first subharmonic resonance and the second-order resonance, it was found that oscillations driven by the sinusoidal modulation are anharmonic but still periodic at very small values of the amplitude, typically $\varepsilon \approx 0.01$. They become nonperiodic (possibly quasiperiodic) at larger values of the modulation amplitude, $\varepsilon \approx 0.05$; with a subsequent increase of ε , the oscillations get apparently chaotic (at $\varepsilon \lesssim 0.20$), and, finally, a critical value ε_{cr} can be found such that, at ε slightly larger than ε_{cr} , the particle performs a rather large number of irregular oscillations inside the potential wall, but is finally kicked out of the trapped state and escapes to infinity. As explained above, this result implies eventual decay of the soliton into radiation. In all the cases considered, the critical modulation amplitude took values

$$0.20 < \varepsilon_{\text{cr}} < 0.25. \quad (161)$$

The sequence of different dynamical regimes observed with increasing ε is illustrated by a set of typical plots in fig. 17, which pertain to the case $K_0 = 2$, i.e., $E = \sqrt{\pi}$, when eq. (36) predicts the second-order resonance.

When the modulation amplitude ε is small, the rate of direct emission of radiation by the soliton can be calculated by means of perturbation theory, as done by Abdullaev, Caputo and Flytzanis [1994]; the role of radiation loss in the destruction of the soliton is considered in detail in the next subsection.

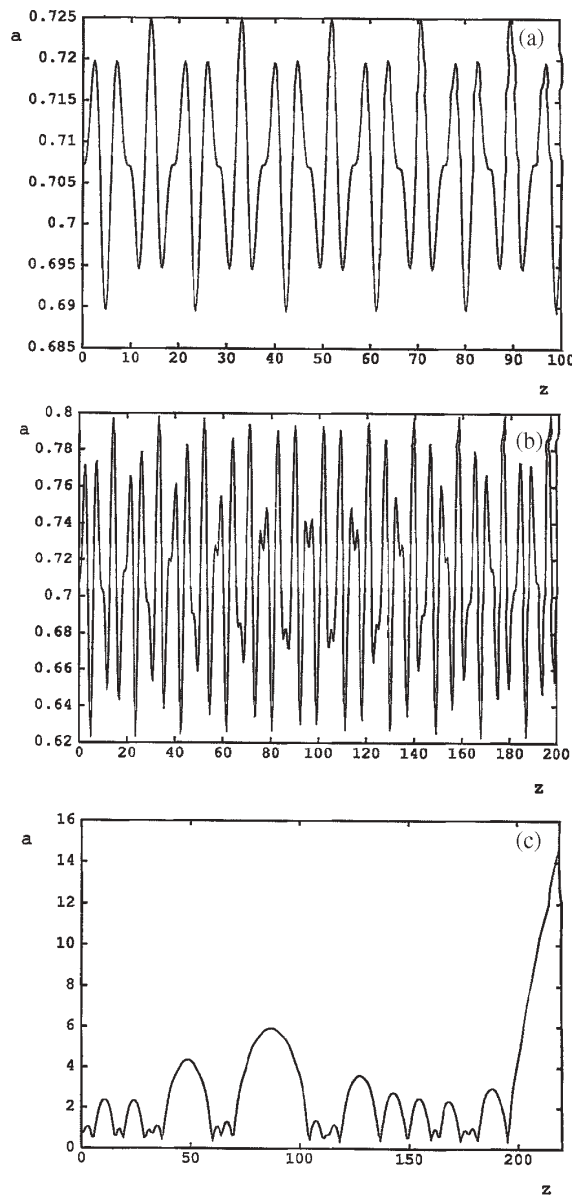


Fig. 17. Typical solutions to eq. (32), with the effective potential (33) and $D(z)$ taken as per eq. (160). The energy of the soliton is $E = \sqrt{\pi}$, which corresponds to the frequency $K_0 = 2$ of small free vibrations (36) of the soliton near its equilibrium shape. The modulation amplitude is (a) $\varepsilon = 0.01$, (b) $\varepsilon = 0.05$, and (c) $\varepsilon = 0.25$, the latter value being slightly larger than the critical amplitude which gives rise to destruction of the soliton.

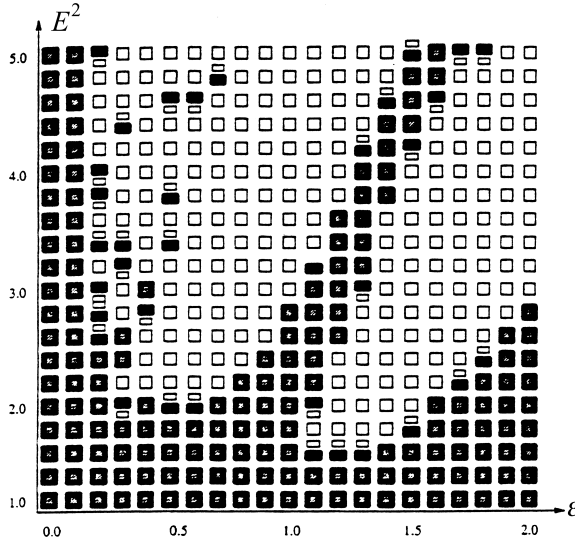


Fig. 18. Phase diagram in the parametric plane (ϵ, E^2) of the NLS equation with the local dispersion modulated as per eq. (160). The solid and open rectangles correspond, respectively, to stable and splitting solitons.

5.3.2. Comparison with direct simulations

Grimshaw, He and Malomed [1996] compared the VA predictions for a soliton in a fiber with sinusoidally modulated dispersion with results of direct simulations of the NLS equation (2) with $\gamma \equiv 1$ and $D(z)$ taken as per eq. (160). Results of systematic simulations are summarized in fig. 18. Two gross features of this diagram roughly comply with the predictions of VA. Firstly, destruction of the soliton may take place if the modulation amplitude exceeds a critical value, which varies, essentially, within the interval $0.15 < \epsilon_{cr} < 0.20$, that should be compared to the interval (161) predicted by VA. Secondly, destruction of the soliton actually takes place, for ϵ not too large, if the initial squared soliton energy E^2 exceeds a minimum value E_{min}^2 varying between 1.8 and 2.0, which may be compared with the value $E^2 = \frac{1}{2}\pi$ that, according to eq. (36), gives rise to the fundamental resonance between small vibrations of the perturbed soliton and the periodic modulation (160).

The most essential qualitative difference between the assumptions on which VA was based and numerical results is that the fundamental mode of the soliton destruction under the action of the sinusoidally modulated dispersion is not decay into radiation, but *splitting* of the soliton into two apparently stable secondary solitons, which is also accompanied by emission of a considerable amount of

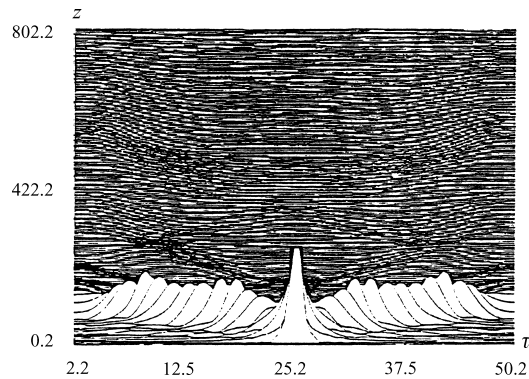


Fig. 19. Typical example of the splitting of a fundamental soliton into two secondary ones in the NLS equation with sinusoidally modulated dispersion, observed at $\varepsilon = 0.3$ and $E^2 = 2.9$, cf. fig. 18.

radiation. A typical example of this splitting is displayed in fig. 19. Obviously, the ansatz (13) does not admit any splitting; nevertheless, VA predicts the basic characteristics of the destruction of the soliton qualitatively and semi-quantitatively correctly, even if the actual destruction mode is different from that implied by VA.

Detailed inspection of the numerical results presented by Grimshaw, He and Malomed [1996] shows that, prior to splitting, the soliton performs a number of irregular vibrations, which resembles the picture produced by VA, see fig. 17c. In accordance with that picture, the vibrational stage preceding the destruction of the soliton is quite long if the splitting takes place at ε slightly exceeding ε_{cr} .

The soliton stability diagram for the sinusoidally modulated model, displayed in fig. 18, has a number of other interesting features, such as a “stability isthmus” and general restabilization of the soliton at large ε [note that for $\varepsilon > 1$, the local dispersion becomes sign-changing according to eq. (160)]. However, these features are found too far outside the domain of applicability of VA.

Very interesting additional results concerning the comparison between VA and direct simulations in the above model were obtained by Abdullaev and Caputo [1998]. They have also found that the destruction of the soliton takes place via splitting into two secondary ones, and demonstrated that agreement between VA and direct simulations is fair as long as the frequency K_0 of the small vibrations (see eq. 36) remains smaller than the modulation spatial frequency (equal to 1 in the present notation). At $K_0 \gtrsim 1$, intensive emission of radiation takes place (even without complete destruction of the soliton), which, naturally, strongly deteriorates the agreement with VA, that completely disregards the radiation component of the field. These conclusions are illustrated by figs. 20 through 22,

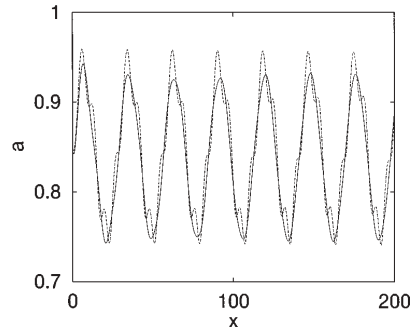


Fig. 20. Comparison between oscillations of the soliton width as predicted by VA (dashed curve) and found by Abdullaev and Caputo [1998] from direct simulations of the NLS equation (solid curve) with sinusoidally modulated dispersion at $K_0 = \frac{1}{4}$ and $\varepsilon = 0.1$.

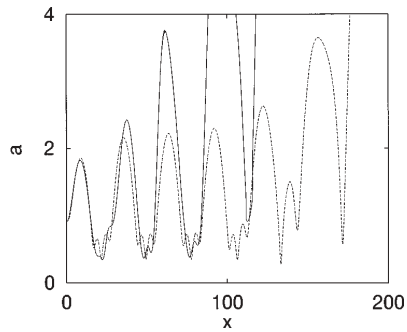


Fig. 21. Same as fig. 20, but for $\varepsilon = 0.6$. Both VA and direct simulations predict destruction of the soliton in this case.

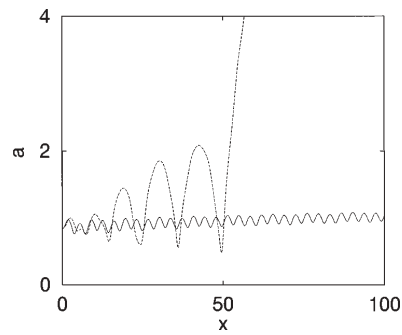


Fig. 22. Same as fig. 20, but for $K_0 = 1$ and $\varepsilon = 0.2$. In this case, VA predicts decay of the soliton, but in direct simulations it remains stable, as the internal vibrations predicted by VA are strongly damped by radiation losses.

which compare the analytical and direct numerical results for different values of K_0 and ε . Note that the destruction of the soliton in the case shown in fig. 21 actually proceeds via splitting. Another important numerical finding reported by Abdullaev and Caputo [1998] is that, in cases when the variational and direct numerical results are generally close, a more subtle (and quite natural) effect of radiation losses is strong suppression of higher harmonics in the soliton's internal vibrations predicted by VA.

5.4. Dispersion management

In application to real optical telecommunications, the concept of variable sign-changing dispersion has gained great popularity under the name of dispersion management (DM). For long fiber-optic links, however, the use of fibers with harmonically modulated dispersion, as in eq. (160), is impractical. A much simpler possibility, which is DM proper, is to build a long link composed of periodically alternating segments with positive (normal) and negative (anomalous) dispersion, so that the *path-average dispersion* (PAD) is close to zero. It is necessary to stress that this concept, in the form of periodic *dispersion compensation*, has been known for a long time, and has been implemented in existing telecommunication networks, in application to the linear regime of optical signal transmission (Lin, Kogelnik and Cohen [1980]). However, a great deal of interest in the propagation of optical solitons in dispersion-compensated links has arisen not long ago, starting with works by Smith, Knox, Doran, Blow and Bennion [1996] and others (in particular, Knox, Forsyiaik and Doran [1995], Suzuki, Morita, Edagawa, Yamamoto, Taga and Akiba [1995], Nakazawa and Kubota [1995], Gabitov and Turitsyn [1996]).

VA is a natural technique for the analysis of DM schemes; therefore it was used in numerous works (see papers by Berntson, Anderson, Lisak, Quiroga-Teixeiro and Karlsson [1996], Gabitov, Shapiro and Turitsyn [1997], Matsumoto [1997], Malomed [1997], Turitsyn [1997], Lakoba, Yang, Kaup and Malomed [1998], Turitsyn, Gabitov, Laedke, Mezentsev, Musher, Shapiro, Schäfer and Spatschek [1998], Kutz, Holmes, Evangelides and Gordon [1998], Berntson, Doran, Forsyiaik and Nijhof [1998], and Turitsyn, Aceves, Jones, Zharnitsky and Mezentsev [1999]). Very recently, the approach proposed originally by Kath and Smyth [1995] in order to incorporate the radiative component of the field into VA for the usual NLS equation was generalized by Yang and Kath [2001] for the case of DM. A common feature of different forms of VA developed for DM models is that they are based on the Gaussian (rather than sech) ansatz, as

the Gaussian provides for an exact solution to the *linear* Schrödinger equation in the dispersion-compensated model, see below, and is therefore the most natural basis for VA.

When PAD is close to zero, it may be necessary to take into account third-order dispersion (TOD). The VA technique for a DM system including TOD was worked out by Hizanidis, Efremidis, Malomed, Nistazakis and Frantzeskakis [1998] (the TOD coefficient was assumed to be constant). Comparison with direct simulations has demonstrated that VA makes it possible to take TOD into account in quite an accurate form.

It is relevant to mention that description of DM solitons may be based not directly on the corresponding NLS equation in the temporal domain, but rather on its integral counterpart in the frequency domain, as shown by Ablowitz and Biondini [1998] (see also a work by Paré, Roy, Lesage, Mathieu and Bélanger [1999]). In relation to this, an interesting version of VA for the DM model was proposed by Paré and Bélanger [2000]: using the fact that the above-mentioned integral equation can be derived from its own Lagrangian, VA can be applied to this equation. In fact, contrary to the usual approach, this implies approximating the DM soliton by means of an ansatz (for which the Gaussian form was adopted) not continuously along the fiber link, but only at junctions between the DM cells. It was demonstrated that results produced by this version of VA are in fairly good agreement with direct simulations.

The version of VA for DM pulses which is presented below follows, chiefly, the works by Lakoba, Yang, Kaup and Malomed [1998] and Malomed and Berntson [2002]. The NLS equation governing pulse propagation in the DM transmission line is

$$iu_z + \frac{1}{2}\delta(Z)u_{TT} + |u|^2u = 0, \quad (162)$$

where $\delta(Z)$ is the local piecewise-constant dispersion coefficient, so that

$$\delta(Z) = \begin{cases} \delta_1, & 0 < Z < \tilde{L}_1, \\ \delta_2, & \tilde{L}_1 < Z < \tilde{L}_1 + \tilde{L}_2 \equiv L_{\text{map}}, \end{cases} \quad (163)$$

which is repeated periodically, L_{map} being the DM period. The most interesting case is then the *strong-DM regime*, corresponding to the situation with $L_{\text{map}} \ll 1/P_0$ and $\tau_p^2 \ll |\delta_1 \tilde{L}_1| \approx |\delta_2 \tilde{L}_2|$, where P_0 and τ_p are the peak power and width of the pulse. In terms of rescaled variables, $z \equiv Z/L_{\text{map}}$, $\tau \equiv T/\sqrt{\tilde{L}_1 \tilde{L}_2 |\delta_1 - \delta_2|/L_{\text{map}}}$, eq. (162) takes the form

$$iu_z - \frac{1}{2}\beta(z)u_{\tau\tau} + \left(-\frac{1}{2}\beta_0 u_{\tau\tau} + |u|^2u\right) = 0, \quad (164)$$

with

$$\beta_0 \equiv -\frac{\delta_1 \tilde{L}_1 + \delta_2 \tilde{L}_2}{\tilde{L}_1 \tilde{L}_2 |\delta_1 - \delta_2|}, \quad (165)$$

$$\beta(z) = \begin{cases} D_1 = \text{sgn}(\tilde{D}_1 - \tilde{D}_2) \cdot L_1, & 0 < z < L_1, \\ D_2 = \text{sgn}(\tilde{D}_2 - \tilde{D}_1) \cdot L_2, & L_1 < z < 1 \end{cases} \quad (166)$$

(which is repeated with period 1), where β_0 is PAD and $L_{1,2} \equiv \tilde{L}_{1,2}/L_{\text{map}}$, so that the coefficients are subject to normalizations

$$D_1 L_1 + D_2 L_2 = 0, \quad |D_1 L_1| = |D_2 L_2| = 1. \quad (167)$$

In the strong-DM case, PAD and nonlinearity are much weaker than the local dispersion, hence the expression in brackets in eq. (164) is a small perturbation. A well-known *exact* solution of eq. (164) in zero-order approximation, when the perturbation is omitted, is the Gaussian pulse

$$u_0 = \sqrt{\frac{P_0}{1 + 2i(\Delta(z)/\tau_0^2)}} \exp\left[-\frac{\tau^2}{(\tau_0^2 + 2i\Delta(z))} + i\phi\right]. \quad (168)$$

Here P_0 and τ_0 are, respectively, the peak power and minimum width of the pulse over one DM period, $\Delta(z) = \Delta_0 - \int_0^z \beta(z') dz'$ is *accumulated dispersion* (from which a contribution produced by PAD is subtracted), and Δ_0 and ϕ are real constants. To better realize the meaning of the parameters introduced in the above expression, one can compare it to the standard form of the Gaussian pulse,

$$u_0 = a(z) \exp\left[-\frac{\tau^2}{W^2(z)} + ic(z) \tau^2 + i\phi\right]; \quad (169)$$

then its amplitude $a(z)$, width $W(z)$ and chirp $c(z)$ are expressed in terms of the parameters introduced in eq. (168) as follows:

$$a(z) = \sqrt{\frac{P_0}{1 + 2i(\Delta(z)/\tau_0^2)}}, \quad W(z) = \frac{\sqrt{\tau_0^4 + 4\Delta(z)^2}}{\tau_0}, \quad c(z) = \frac{2\Delta(z)}{\tau_0^4 + 4\Delta(z)^2}. \quad (170)$$

The parameter τ_0 , which is dimensionless in view of the normalization conditions (167), plays a dominant role below; in works on this topic, another constant is frequently used, called *DM strength*,

$$S \equiv \frac{1.443}{\tau_0^2} \quad (171)$$

(Berntson, Doran, Forysiak and Nijhof [1998]; the factor 1.443 appears due to the use of the FWHM definition of the width of the Gaussian pulse).

The exact solution (168) of the linear-DM model is used as the variational ansatz for the nonlinear model. The application of VA yields the following evolution equations for the parameters of the ansatz:

$$\frac{d\tau_0}{dz} = \sqrt{2} \frac{E \tau_0 \Delta(z)}{W^3(z)}, \quad (172)$$

$$\frac{d\Delta_0}{dz} = -\beta_0 + \frac{E [4\Delta^2(z) - \tau_0^4]}{2\sqrt{2} W^3(z)}, \quad (173)$$

where, as usual, the soliton's energy $P_0 \tau_0 \equiv E$ is the dynamical invariant. In fact, E plays the role of a small parameter measuring the relative weakness of the nonlinearity in comparison with the local dispersion.

An issue of fundamental interest is to find conditions allowing for the *stationary propagation* of the pulse, i.e., a dynamical regime in which the parameters τ_0 and Δ_0 return to their initial values after passing one DM period. Because, as seen from eqs. (172) and (173), changes of τ_0 and Δ_0 within one period are small $\sim (\beta_0, E)$, in first approximation one may insert unperturbed values of τ_0 and Δ_0 into the rhs of eqs. (172) and (173), and demand that (recall the DM period is 1 in the present notation)

$$\int_0^1 \frac{d\tau_0}{dz} dz = \int_0^1 \frac{d\Delta_0}{dz} dz = 0. \quad (174)$$

This yields the stationary-propagation conditions for the Gaussian pulse in an explicit form:

$$\Delta_0 = -\frac{1}{2}, \quad \beta_0 = \frac{\sqrt{2}}{4} A^2 \tau_0^4 \left[\ln \left(\sqrt{1 + \frac{1}{\tau^4}} + \frac{1}{\tau^2} \right) - \frac{2}{\sqrt{\tau_0^4 + 1}} \right]. \quad (175)$$

The meaning of the condition $\Delta_0 = -\frac{1}{2}$ is quite simple: it requires the pulse to have zero chirp at the midpoint of each fiber segment.

The second of conditions (175) predicts that the DM soliton propagates steadily at anomalous PAD, $\beta_0 < 0$, provided that $\tau_0^2 > (\tau_0^2)_{\text{cr}} \approx 0.30$, at $\beta_0 = 0$ if $\tau_0^2 = (\tau_0^2)_{\text{cr}}$, and at normal PAD, $\beta_0 > 0$, if $(\tau_0^2)_{\text{min}} \approx 0.148 < \tau_0^2 < (\tau_0^2)_{\text{cr}}$. The latter case is quite interesting, as the classical NLS soliton cannot exist at normal dispersion. Further analysis of eq. (175) shows that, in this case, the solution exists in a limited interval of the normal-PAD values,

$$0 \leq \frac{\beta_0}{E} \leq \left(\frac{\beta_0}{E} \right)_{\text{max}} \approx 0.0127. \quad (176)$$

Inside this interval, eq. (175) yields *two* different values of the minimum width τ_0 for a given value of β_0/E , while in the anomalous-PAD region, τ_0 is a uniquely

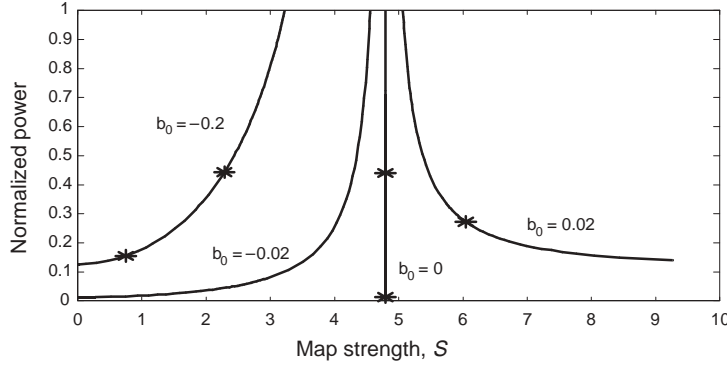


Fig. 23. Peak power of the stationary DM soliton vs. map strength at different values of the path-average dispersion β_0 ($\equiv b_0$), as predicted by the variational approximation based on eq. (175). Asterisks mark particular cases for which the corresponding model with *random DM* was investigated in detail, see § 5.5.

defined function of β_0/E . It can be concluded that the DM soliton corresponding to the larger value of τ_0 is *stable*, while that corresponding to smaller τ_0 is *unstable*. The border between the stable and unstable solitons corresponds to $\beta_0/E = (\beta_0/E)_{\max}$ (see eq. 176), and it is located at $\tau_0^2 = (\tau_0^2)_{\min} \approx 0.148$ [i.e., all stable and unstable solitons have, respectively, $\tau_0^2 > (\tau_0^2)_{\min}$ and $\tau_0^2 < (\tau_0^2)_{\min}$]. The results concerning the stability of these two solitons were reproduced in a mathematically rigorous form by Pelinovsky [2000].

Translating τ_0^2 into the standard DM-strength parameter S according to eq. (171), one concludes that VA predicts the following:

- stable DM solitons at anomalous PAD if $S < S_{\text{cr}} \approx 4.79$;
- stable DM solitons at *zero* PAD if $S = S_{\text{cr}} \approx 4.79$;
- stable DM solitons at *normal* PAD if $4.79 < S < S_{\text{max}} \approx 9.75$;
- no stable DM soliton if $S > S_{\text{max}} \approx 9.75$.

The normalized power of the DM soliton, which is $P \equiv 4 \cdot 1.12P_0$ (the factor 1.12 is the ratio of the FWHM widths for the sech-shaped and Gaussian pulses) vs. the DM strength at different fixed values of PAD, β_0 , is shown, as predicted by eq. (175), in fig. 23. A counterpart of the same dependence, obtained by Berntson, Doran, Forsysiak and Nijhof [1998] from direct simulations of eq. (164), is displayed in fig. 24. In fig. 23 the curves are shown only in the region $S < 9.75$, where the solitons are expected to be stable. The curves in fig. 24 corresponding to normal PAD ($\beta_0 > 0$) terminate at points where the DM soliton becomes unstable.

Comparison of figs. 23 and 24 shows that VA yields acceptable results for

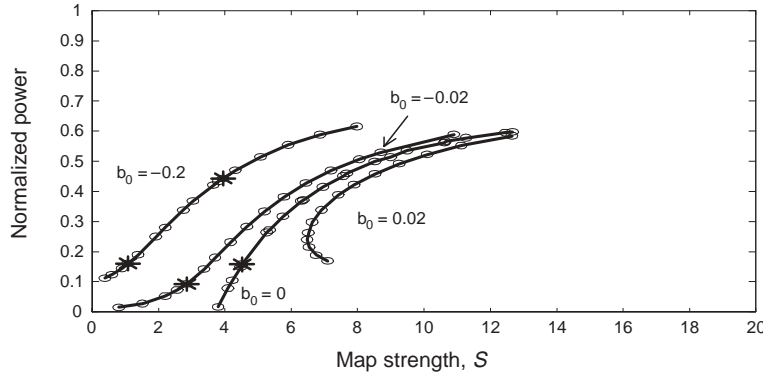


Fig. 24. Counterpart of fig. 23, obtained by direct numerical simulations of eq. (164). Asterisks mark particular cases for which the corresponding model with *random DM* was investigated in detail.

relatively small values of the soliton power, where the above approximation, which treated the nonlinearity as a weak perturbation, should be relevant. In particular, the VA-predicted value $S_{\text{cr}} \approx 4.79$ is different from, but reasonably close to, the critical DM strength $S_{\text{cr}} \approx 4$ which was found from direct simulations for the small-power case. With increasing power, the numerically found S_{cr} grows. It is also noteworthy that the value $S_{\text{max}} \approx 9.75$, predicted by VA as the stability limit for DM solitons, is indeed close to the result of direct simulations for small powers, see fig. 24.

5.5. Random dispersion management

Existing terrestrial optical telecommunication webs are patchwork systems, which include links with very different lengths (Agrawal [1997]). This circumstance of practical importance suggests to consider *random DM*. A short account of recent results obtained for random DM by Malomed and Berntson [2002] by means of VA is given here, the most salient feature being a sharp difference between robust and unstable soliton propagation regimes. A random-DM model of a different type was considered by Abdullaev and Baizakov [2000] (see also work by Abdullaev, Bronski and Papanicolaou [1999]), where the local values of the dispersion, rather than the fiber-segment lengths, were distributed randomly. In these works, the above-mentioned drastic difference between stable and unstable regimes of soliton transmission was not reported.

The basic equation and normalizations are the same as in the previous section, i.e., they are given by eqs. (164) and (167). In the case of random DM, the normalizations must be applied to mean values of the random lengths. Limiting

the consideration to the case when the mean lengths of the segments with anomalous and normal dispersion are equal, $\overline{L_1} = \overline{L_2}$, eqs. (167) yield $\overline{L_{1,2}} = \frac{1}{2}$ and $|D_{1,2}| = 2$. To comply with the former condition, one may assume that the random lengths $L_{1,2}$ are distributed uniformly in the interval $0.1 < L < 0.9$. The minimum length 0.1 is introduced because, in reality, the length can neither be very large (say, larger than 200 km) nor be very small (shorter than 20 km).

The same ansatz (168) and variational equations (172 and 173) may be used with the randomly distributed lengths. As explained above, the change of the soliton's parameters, $\tau_0 \rightarrow \tau_0 + \delta\tau_0$, $\Delta_0 \rightarrow \Delta_0 + \delta\Delta_0$, within one DM cell is small. Therefore, the evolution of the pulse passing many cells is approximated by smoothed differential equations, $d\tau_0/dz = \delta\tau_0 / (L_1^{(n)} + L_2^{(n)})$ and $d\Delta_0/dz = \delta\Delta_0 / (L_1^{(n)} + L_2^{(n)})$ (here n is the cell's number), which take the following form,

$$\frac{d\tau_0}{dz} = \frac{\sqrt{2}E\tau_0^4}{8(L_2 + L_1)} \left[\frac{1}{\sqrt{\tau_0^4 + 4\Delta_0^2}} + \frac{1}{\sqrt{\tau_0^4 + 4(\Delta_0 + 2L_2 - 2L_1)^2}} - \frac{2}{\sqrt{\tau_0^4 + 4(\Delta_0 + 2L_2)^2}} \right], \quad (177)$$

$$\begin{aligned} \frac{d\Delta_0}{dz} = & -\beta_0 \\ & + \frac{\sqrt{2}E\tau_0^3}{8(L_2 + L_1)} \left[\frac{2\Delta_0}{\sqrt{\tau_0^4 + 4\Delta_0^2}} + \frac{2(\Delta_0 + 2L_2 - 2L_1)}{\sqrt{\tau_0^4 + 4(\Delta_0 + 2L_2 - 2L_1)^2}} \right. \\ & - \frac{4(\Delta_0 + 2L_2)}{\sqrt{\tau_0^4 + 4(\Delta_0 + 2L_2)^2}} - \frac{1}{2} \ln \left(2\Delta_0 + \sqrt{\tau_0^4 + 4\Delta_0^2} \right) \\ & - \frac{1}{2} \ln \left(2(\Delta_0 + 2L_2 - 2L_1) + \sqrt{\tau_0^4 + 4(\Delta_0 + 2L_2 - 2L_1)^2} \right) \\ & \left. + \ln \left(2(\Delta_0 + 2L_2) + \sqrt{\tau_0^4 + 4(\Delta_0 + 2L_2)^2} \right) \right]. \quad (178) \end{aligned}$$

The most essential characteristic of the pulse propagation at given values of β_0 and E is the cell-average pulse's width,

$$\overline{W} \equiv \frac{1}{L} \int_{\text{cell}} W(z) dz. \quad (179)$$

Simulations of eqs. (177) and (178) reveal that there are two drastically different dynamical regimes. If the soliton's energy is sufficiently small (hence

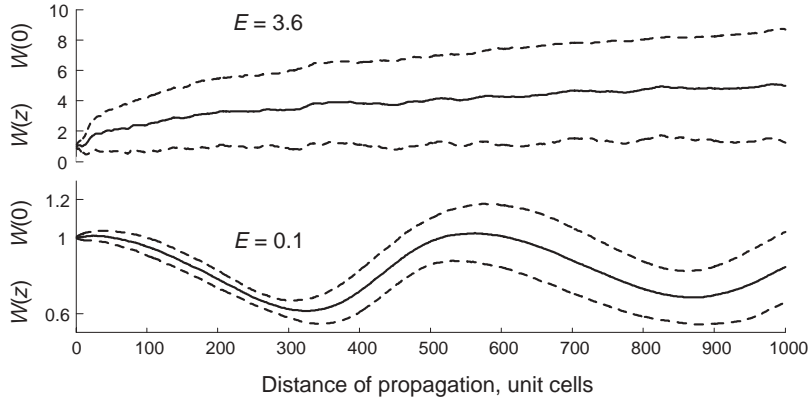


Fig. 25. Evolution of the soliton's cell-average pulse width (normalized to its initial value) in the random-dispersion-management model with zero PAD. The mean values (solid curve) and standard deviations (dashed curves) are produced by averaging over 200 different realizations of the random-length set. The propagation distance is given in units of the average DM cell length. The bottom and top plots correspond to the DM solitons with low energy $E = 0.1$ and high energy $E = 3.6$, respectively.

the approximation outlined in the previous section is relevant) and PAD is anomalous or zero, i.e., $\beta_0 \leq 0$ (especially, if $\beta_0 = 0$), the pulse performs random vibrations but remains, in fact, fairly stable over long propagation distances. When the energy is larger, as well as when PAD is normal, $\beta_0 > 0$, the pulse demonstrates fast degradation.

Typical examples of the propagation are displayed in fig. 25 for the zero-PAD case, which is the best in terms of the soliton stability. Simulations of eqs. (177) and (178) have been performed with 200 different realizations of the random-length set, chosen so that $L_1^{(n)} \equiv L_2^{(n)}$ (equal lengths of the anomalous- and normal-dispersion segments inside each DM cell). Figure 25 shows the evolution of $\langle \bar{W}(z) \rangle$, i.e., the mean value of the width (179) averaged over the 200 random realizations, along with the corresponding normal deviations from the mean value. The figure demonstrates that some systematic slow evolution takes place on top of the random vibrations, which are eliminated by averaging over 200 realizations. Systematic degradation (broadening) of the soliton takes place too, but it is extremely slow if the energy is small. In the case shown in the bottom part of fig. 25, the pulse survives with very little degradation in propagation over more than 1000 average cell lengths (in fact, as long as the simulations could be run). It is not difficult to understand this: in the limit of zero power, i.e., in the linear random-DM model, an exact solution for the pulse is available in essentially the same form as given above for periodic DM,

see eq. (168). If PAD is exactly zero, this exact solution predicts no systematic broadening of the pulse.

If the soliton's energy is larger, further simulations of eqs. (177) and (178) show that, after having passed a very large distance, the sluggish spreading out of the soliton suddenly ends in a blowup (complete decay into radiation). This seems to be qualitatively similar to what was predicted by VA for periodic sinusoidal modulation of the dispersion, see § 5.3.1. and fig. 17c: a long span of chaotic but nevertheless quasi-stable vibrations is suddenly ended by rapid irreversible decay.

In fact, the case $\beta_0 = 0$ is a point of *sharp optimum*: at any finite anomalous PAD, i.e., $\beta_0 < 0$, the degradation of the pulses is essentially faster, especially for those with larger energy, and at any small normal value of PAD, $\beta_0 > 0$, very rapid decay always takes place, virtually at all values of energy.

Malomed and Berntson [2002] have also performed a comparison of the results predicted by VA with direct simulations of the same random-DM model. The direct numerical results prove to be quite similar to what was predicted by VA. In particular, the most stable propagation is again observed at zero PAD, the soliton's broadening is faster at nonzero anomalous PAD, and all solitons decay very quickly at nonzero normal PAD. The soliton's stability in the direct simulations drastically deteriorates with increasing energy, as also predicted by VA.

Detailed comparison shows that, surprisingly, the direct simulations yield somewhat *better* results for the soliton's stability than VA: the actual broadening rate may be ~20% smaller than that predicted by VA. The slow long-scale oscillations, clearly seen in fig. 25, are less pronounced in the direct simulations. The sudden decay into radiation, predicted by VA after very long propagation, does not take place in the direct simulations; instead, the soliton eventually splits into two smaller ones, quite similar to what is observed in direct simulations of the model with periodically modulated dispersion, see fig. 19.

5.6. Interactions between dispersion-managed solitons

5.6.1. Collisions between solitons belonging to different channels in wavelength-division-multiplexed systems

Wavelength-division multiplexing (WDM), i.e., creation of a large number of channels in the same fiber, carried by different wavelengths, is the most important direction in the development of optical telecommunications. In soliton-based systems, the most serious problem related to WDM is *crosstalk* due to collisions of pulses belonging to different channels. Collisions are inevitable, as the

inherent dispersion of the fiber gives rise to different group velocities of the carrier waves in different channels.

Very promising results are produced by a combination of WDM and DM, especially with respect to the suppression of collision-induced effects, as shown in simulations reported by Niculae, Forysiak, Gloag, Nijhof and Doran [1998]. Here, an account of VA-based analysis of collisions in the combined WDM/DM system will be given, following a work by Kaup, Malomed and Yang [1999].

The simplest two-channel system is described by the following equations (cf. eq. 164):

$$i(u_z + cu_\tau) + \frac{1}{2}D(z)u_{\tau\tau} + \left[\frac{1}{2}\bar{D}_u u_{\tau\tau} + \gamma(|v|^2 + 2|u|^2)u\right] = 0, \quad (180)$$

$$i(v_z + \frac{1}{2}D(z)v_{\tau\tau} + \left[\frac{1}{2}\bar{D}_v v_{\tau\tau} + \gamma(|u|^2 + 2|v|^2)v\right] = 0, \quad (181)$$

where c is the inverse group-velocity difference between the channels, $D(z)$ is the main part of the dispersion (with zero average), which may be assumed the same in both channels, $\bar{D}_{u,v}$ are the values of PAD in the two channels, which are different in general, and the nonlinear terms represent, as usual, the self-phase modulation (SPM) and cross-phase modulation (XPM) effects.

The analysis uses the same ansatz (168) for the solitons as above. However, in order to describe the dynamics of the interacting pulses, the ansatz may be taken in a more general form, which is obtained from eq. (168) by the Galilean boost,

$$u(z, \tau) = u_0(z, \tau - T(z)) \exp(-i\omega\tau + i\psi(z)), \quad (182)$$

where ω is an arbitrary frequency shift, and the corresponding position shift is generated by the following equation:

$$\frac{dT}{dz} = -\omega (D(z) + \bar{D}_u). \quad (183)$$

In the absence of interaction, the parameters of solitons in both channels are selected by the conditions (175). Since these conditions were obtained treating the SPM nonlinearity as a small perturbation, the XPM-induced interaction between solitons may also be considered as a perturbation in the Lagrangian of eqs. (180) and (181) (the Lagrangian representation of XPM-coupled equations

was considered in § 4). This approach makes it possible to derive the following evolution equation for the soliton's frequency shift in the presence of XPM:

$$\frac{d\omega}{dz} = \frac{2^{3/2}P_\nu\tau_0^4 cz}{[\tau_0^4 + 4\Delta^2(z)]^{3/2}} \exp\left(-\frac{c^2\tau_0^2 z^2}{[\tau_0^4 + 4\Delta^2(z)]}\right), \quad (184)$$

where P_ν is the peak power of the pulse in the ν -channel. In the same approximation, the evolution of the position is governed by the unperturbed equation (183). Equation (184) implies that the centers of the two solitons coincide at $z = 0$.

In a two-channel model without DM, a dynamical equation similar to (184) was derived by Ablowitz, Biondini, Chakravarty and Horne [1998]). However, there is a principal difference between the collision in the system with DM and that in the system with constant dispersion: as the coefficient $D(z)$ in eq. (183) periodically changes sign, it is easy to see that, in the strong-DM regime, colliding pulses pass through each other many times before separating.

It is necessary to distinguish between *complete* and *incomplete* collisions. In the former (generic) case, the solitons are far separated before the collision, while in the latter case, which takes place when the collision occurs close to the input point, the solitons overlap strongly at the beginning of the interaction. In either case, the most important result of the collision is a net shift of the soliton's frequency $\delta\omega$, which can be calculated as

$$\delta\omega = \int_{z_0}^{+\infty} \frac{d\omega}{dz} dz, \quad (185)$$

where $d\omega/dz$ should be taken from eq. (184). The lower limit of the integration in expression (185) is finite in the case of the incomplete collision, while a complete collision corresponds to $z_0 = -\infty$. The net frequency shift is very detrimental, as, through the dispersion, it gives rise to a change of the soliton's velocity. If the soliton picks up a "wrong" velocity, information carried by the soliton stream in the fiber-optic telecommunication link may be lost completely.

An estimate of physical parameters for *dense* WDM arrangements, with a wavelength separation between channels of $\delta\lambda < 1$ nm (this is the case of paramount practical interest) shows that the group-velocity mismatch c may be regarded as a small parameter, hence the function cz varies slowly in comparison with the rapidly oscillating accumulated dispersion $\Delta(z)$. In this case, the integral (185) and similar integrals can be calculated in a fully analytical form, as shown by Kaup, Malomed and Yang [1999]. In particular, the net

frequency shift is zero for the complete collision, which shows the ability of DM to suppress collision-induced effects. In fact, the zero net shift is a result of the multiple character of the collision (see above): each elementary collision may generate a finite frequency shift, but they sum up to zero.

Once the net frequency shift is zero, the collision is characterized by a net position shift, which is a detrimental effect too, but less dangerous than the frequency shift. The position shift can be found from eq. (183):

$$\delta T \equiv \int_{-\infty}^{+\infty} \frac{dT}{dz} dz = \epsilon \bar{D} \int_{-\infty}^{+\infty} z \frac{d\omega}{dz} dz + \int_{-\infty}^{+\infty} \Delta(z) \frac{d\omega}{dz} dz, \quad (186)$$

where integration by parts was performed. Then, substituting the expression (184) for $d\omega/dz$, one can perform the integrations analytically, to obtain a very simple final result (for definiteness, it is written for the soliton in the u -subsystem):

$$\delta T_u = \sqrt{2\pi} \bar{D}_u P_v \frac{\tau_0}{c^2}. \quad (187)$$

Note that this result contains a product of two small parameters, namely, $\text{PAD} \bar{D}_u$ and the power P_v (the latter is small as it measures the nonlinearity in the system, and it was assumed from the very beginning that the nonlinearity is a small perturbation).

The net frequency shift generated by the incomplete collision can be found similarly. In this case, the worst (largest) result is obtained for the configuration with the centers of the two solitons coinciding at the launching point $z = 0$:

$$(\delta\omega)_{\max} = \sqrt{2} \frac{P_v}{cS} \ln(S + \sqrt{1 + S^2}), \quad (188)$$

where S is the DM strength defined by eq. (171).

These analytical results obtained by means of VA were compared with numerical simulations. First of all, simulations show that the net frequency shift induced by complete collisions is very small indeed (much smaller than in the case of incomplete collisions at the same values of the parameters). As for the position shift in the case of complete collision, the analytical prediction (187) is compared to numerical results in fig. 26, showing reasonable agreement.

In the case of incomplete collisions, simulations yield a nonzero frequency shift, which was compared to the analytical prediction (188) by Kaup, Malomed and Yang [1999]. In this case, there is acceptable agreement again. However, in contrast to the case of complete collision (fig. 26), the difference between the

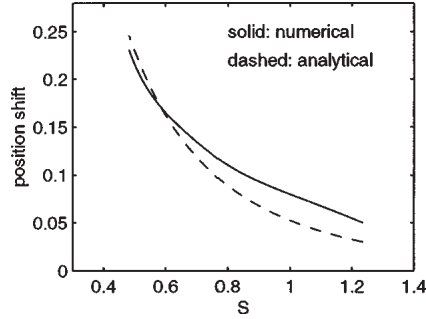


Fig. 26. Analytically and numerically found position shift of the soliton induced by complete collision in the two-channel model described by eqs. (180) and (181) with $L_1 = 0.4$, $L_2 = 0.6$, $D_1 = \frac{5}{2}$, $D_2 = -\frac{5}{3}$, $c = 0.3$, and peak powers of the colliding pulses $P_u = P_v = 0.1$.

analytically predicted and numerically found results (this time, the frequency shifts) *decreases* with increasing DM strength S .

5.6.2. Interactions between solitons inside one channel

As demonstrated in the previous subsection, DM makes it possible to suppress the crosstalk between solitons in different channels of the WDM system. Thus, the most serious remaining limiting factor in the strong-DM regime is the interaction of pulses in the same channel, as demonstrated by Yu, Golovchenko, Pilipetskii and Menyuk [1997]. In fact, in this regime the intrachannel interactions turn out to be stronger than in the absence of DM, which suggests that it may be optimal to use a *moderate-DM* regime rather than strong DM.

Analysis of the interactions inside one channel can be effectively performed by means of VA, although a particular variational technique which yields good agreement with direct simulations turns out to be rather cumbersome. Below, main results for the intrachannel interactions between solitons are presented, following the paper by Wald, Malomed and Lederer [1999].

Earlier, VA based on the Gaussian ansatz was applied to this problem by Georges [1998], Matsumoto [1998] and Malomed [1998a,b] (see also a related paper by Kumar, Wald, Lederer and Hasegawa [1998]). It was shown that this simple version of VA correctly describes the interactions in the strong-DM regime, despite the fact that the Gaussian ansatz approximates only the cores of the DM solitons adequately, but not their “tails”, whose genuine form is exponential rather than Gaussian (Ablowitz and Biondini [1998]). The incorrect approximation for the tails is not significant in the case of strong-DM, as the

huge periodic spreadings of the pulses lead to strong overlapping between them, involving their cores rather than tails. In the moderate-DM case, however, the tails play a dominant role in the interactions (Malomed [1998a]), and the simple Gaussian ansatz fails in this case.

To describe the interaction of two separated pulses, one may substitute $u(z, \tau) = u_1(z, \tau) + u_2(z, \tau)$ into eq. (164), which describes the one-channel DM model, and split it, following Karpman and Solov'ev [1981], into *separate* NLS equations for the two pulses, treating the interaction between them as a small perturbation,

$$i \frac{\partial u_n}{\partial z} - \frac{1}{2} \beta(z) \frac{\partial^2 u_n}{\partial \tau^2} + |u_n|^2 u_n = -u_n^2 u_{3-n}^* + 2|u_n|^2 u_{3-n}, \quad n = 1, 2. \quad (189)$$

These equations can be derived from the Lagrangian density $\mathcal{L} = \mathcal{L}_1 + \mathcal{L}_2$, where (cf. eq. 15)

$$\mathcal{L}_n = \left[\frac{i}{2} \left(u_n^* \frac{\partial u_n}{\partial z} - u_n \frac{\partial u_n^*}{\partial z} \right) + \frac{1}{2} \left(\beta \left| \frac{\partial u_n}{\partial \tau} \right|^2 + |u_n|^4 \right) \right] + |u_n|^2 (u_n u_{3-n}^* + u_n^* u_{3-n}), \quad (190)$$

the last term accounting for the interaction. An ansatz which proves to be adequate for the description of the interactions between solitons is

$$u_n(z, \tau) = A_n(z) f(t_n) \exp \left[i \Phi_n(z) - i \kappa_n(z) t_n + i b_n(z) f^{-1} \frac{\partial^2 f}{\partial t_n^2} \right], \quad (191)$$

$$f(t_n) \equiv \exp \left[-\sqrt{a_n(z) + t_n^2} \right], \quad t_n \equiv q(\tau - T_n(z)), \quad (192)$$

where real variational parameters are $A_{1,2}$, $\Phi_{1,2}$, $\kappa_{1,2}$, $b_{1,2}$, $a_{1,2}$ and $T_{1,2}$, while q is an auxiliary constant that is *not* to be varied, see below. This ansatz combines a Gaussian-like core and exponentially decaying tails, as $f(t_n) \approx \exp(-|t_n|)$ as $|t_n| \rightarrow \infty$. The shape of the pulses is controlled by the parameters $a_n(z)$: the larger a_n , the more Gaussian-like the pulse is.

Calculating the full Lagrangian $L = \int_{-\infty}^{+\infty} (\mathcal{L}_1 + \mathcal{L}_2) d\tau$ with the ansatz (191)–

(192) in analytical form is not possible, therefore the resulting variational equations for the parameters of the ansatz are cast into the following form:

$$\begin{aligned} \frac{da_n}{dz} &= \beta q^2 b_n Q_1(a_n), & \frac{dT_n}{dz} &= \beta q \kappa_n, \\ \frac{db_n}{dz} &= \frac{1}{2} [-\beta q^2 + \beta q^2 b_n^2 Q_2(a_n) + E_n Q_3(a_n)], \\ \frac{d\kappa_n}{dz} &= -\frac{2q}{E_n} A_n^3 A_{3-n} \\ &\times \int_{-\infty}^{+\infty} f^3(t_n) f(t_{3-n}) \left[\frac{3t_n \cos \Delta\phi}{\sqrt{a_n + t_n^2}} + (-1)^n b_n \frac{\partial}{\partial t_n} \left(\frac{1}{f(t_n)} \frac{\partial^2 f}{\partial t_n^2} \right) \sin(\Delta\phi) \right] d\tau. \end{aligned} \quad (193)$$

Here, $E_n \equiv A_n^2 \int_{-\infty}^{+\infty} f^2(\tau, a_n) d\tau = 2A_n^2 \sqrt{a} K_1(2\sqrt{a})$, with K_1 the modified Bessel function, are the energies of the two pulses, which are conserved separately in the approximation used here. Further,

$$\begin{aligned} \Delta\phi &\equiv \kappa_1 t_1 - \kappa_2 t_2 + \frac{b_2}{f(t_2)} \frac{\partial^2 f}{\partial t_2^2} - \frac{b_1}{f(t_1)} \frac{\partial^2 f}{\partial t_1^2}, \\ Q_1(a) &\equiv \frac{I_0 I_1}{\Delta}, \quad Q_2(a) \equiv \frac{I_1 I'_0 - I_0 I'_1}{\Delta}, \quad Q_3(a) \equiv \frac{2I_2 I'_0 - I_0 I'_2}{\Delta}, \end{aligned} \quad (194)$$

$$I_1(a) \equiv \int_{-\infty}^{+\infty} \left(\frac{1}{f} \frac{\partial^3 f}{\partial \tau^3} - \frac{1}{f} \frac{\partial f}{\partial \tau} \frac{\partial^2 f}{\partial \tau^2} \right)^2 d\tau, \quad I_2(a) \equiv \int_{-\infty}^{+\infty} f^4(\tau) d\tau, \quad (195)$$

$$I_3(a) \equiv \int_{-\infty}^{+\infty} \left(\frac{\partial f}{\partial \tau} \right)^2 d\tau,$$

$$I_0(a) \equiv 2\sqrt{a} K_1(2\sqrt{a}), \quad \Delta \equiv I_0 I'_3 - I_3 I'_0.$$

The evolution equations (193) were solved numerically, and the results were compared to direct simulations of the interaction between two solitons in eq. (164) with DM taken in the simplest symmetric form (cf. eq. 166),

$$\beta(z) = \begin{cases} \beta_1, & 0 \leq z \leq \frac{1}{2}z_1, \\ \beta_2, & \frac{1}{2}z_1 < z \leq z_2 + \frac{1}{2}z_1, \\ \beta_1, & z_2 + \frac{1}{2}z_1 < z \leq z_1 + z_2, \end{cases} \quad (196)$$

and the launch point in the middle of one of the segments. In the simulations, the lengths of the DM segments in eq. (196) were $z_1 = z_2 = 0.1$, and the initial FWHM width was fixed to be $2 \ln(1 + \sqrt{2}) \approx 1.763$, i.e., the same as that of the pulse $A \operatorname{sech} \tau$. To keep this fixed value of the width for an arbitrary initial

value $a_{1,2}(0) \equiv a_0$ of the parameter $a(z)$ in the ansatz (191), (192), the constant q in eq. (191) was chosen so that

$$q^2 = \frac{\ln 2}{1.763^2} (\ln 2 + 4\sqrt{a_0}) \approx 0.155 + 0.892\sqrt{a_0} \quad (197)$$

(recall that q was defined as a *nonvariational* auxiliary parameter). Note that, in this notation, the expression for the DM strength is

$$S \equiv \frac{\beta_1 z_1 - \beta_2 z_2}{1.763^2} \quad (198)$$

instead of eq. (171).

First, eqs. (193) were applied to an isolated pulse. The objective was, solving numerically the first two equations of the system (193), to find the initial values a_0 and $\eta_0 \equiv A(0) \exp(-\sqrt{a_0})$ that provide for a stationary DM pulse, i.e., strictly periodic evolution of $a(z)$ and $b(z)$ [in other words, an analog of the conditions (175) obtained for the simple Gaussian ansatz (168)]. Because of the presence of *two* unknown initial values [with q taken as per eq. (197)], the simulations generate a whole set of values (a_0, η_0) that give rise to a stationary pulse (in fact, the η_0 thus found is nearly constant, while a_0 may vary within broad limits). This implies that an extra optimization condition may be imposed, in order to select a unique set of values that gives rise to the most accurate approximation for the DM soliton.

The extra condition was the demand that not only the transmission of the isolated pulse, but also *interactions* between identical pulses must be correctly described by the full system of variational equations (193). To this end, the full system was solved numerically, and the *collision distance* predicted by this solution, i.e., the value of the propagation distance z at which a collision of two solitons has to take place, was compared to the actual collision distance obtained from direct numerical simulations of eq. (164). This procedure, repeated at many different values of parameters, has yielded an empirical result giving the value of a_0 , optimized against the description of the interactions, as a function of the DM strength S (see eq. 198),

$$a_0(S) = 1.2 + 5.8S^2, \quad (199)$$

in the range $S \lesssim 1.5$ (i.e., for *moderate* DM).

Detailed results reported by Wald, Malomed and Lederer [1999] show that the ansatz based on eqs. (191) and (192) and optimized as outlined above, although being somewhat cumbersome, generates a shape for an isolated DM soliton

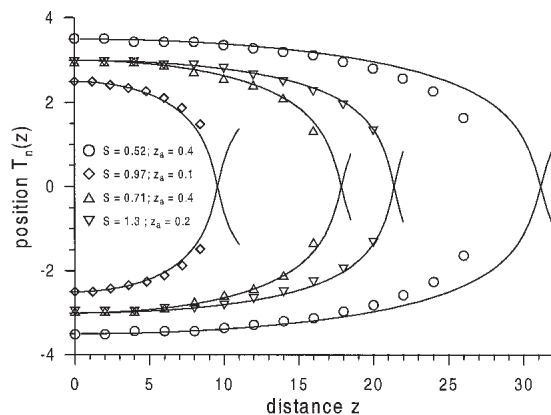


Fig. 27. Positions of two interacting identical solitons in one dispersion-managed channel vs. the propagation distance z . Curves: prediction of the variational approximation based on the ansatz (191)–(192) with parameters optimized as described in the text; symbols: direct numerical simulations for various values of the DM strength S .

which is extremely close to the shape found numerically, and simultaneously provides for a very accurate description of the interaction, as illustrated by fig. 27. The figure compares the evolution of the temporal positions of two interacting identical DM solitons, as predicted by the present version of VA and as obtained from direct simulations of eq. (164).

§ 6. Solitons in dual-core optical fibers

6.1. Solitons in a basic model of the dual-core fiber

A dual-core fiber (DCF), alias *directional coupler*, is a system of two parallel identical or different fibers with a gap between them on the order of the wavelength, so that light can linearly couple from one core into the other. DCF is a basis for design of optical switches (Trillo, Wabnitz, Wright and Stegeman [1988], Friberg, Weiner, Silberberg, Sfez and Smith [1988]). It can also be used for efficient compression of solitons by passing them into a fiber with a smaller value of the dispersion coefficient: as demonstrated by Hatami-Hanza, Chu, Malomed and Peng [1997], the highest-quality compression is achieved when two fibers with different dispersion coefficients are connected not by splicing, but rather when they form an *asymmetric* coupler.

Nonlinear DCFs are a promising medium for the observation of new types of optical solitons, for the description of which VA is a natural technique, as it was

first shown by Paré and Fłotjańczyk [1990] and Maimistov [1991] (see also an independent work by Chu, Malomed and Peng [1993]). The applicability of VA to the DCF model and its limitations were discussed by Ankiewicz, Akhmediev, Peng and Chu [1993]; however, the version of VA considered in that work was not flexible enough. Results obtained by means of VA for solitons in DCF are presented in this section, following the work by Malomed, Skinner, Chu and Peng [1996].

DCF is described by a system of linearly coupled NLS equations,

$$iu_z + \frac{1}{2}u_{\tau\tau} + |u|^2u + Kv = 0, \quad (200)$$

$$iv_z + \frac{1}{2}v_{\tau\tau} + |v|^2v + Ku = 0, \quad (201)$$

where K is the coupling constant accounting for the light exchange between the two cores. These equations admit the usual variational representation, the linear coupling being accounted for by additional terms in the Lagrangian density, $\Delta\mathcal{L} = K(U^*V + UV^*)$. An ansatz for a soliton with a component in each core can be taken as

$$u = A \cos \theta \operatorname{sech}\left(\frac{\tau}{a}\right) \exp[i(\phi + \psi) + ib\tau^2], \quad (202)$$

$$v = A \sin \theta \operatorname{sech}\left(\frac{\tau}{a}\right) \exp[i(\phi - \psi) + ib\tau^2]. \quad (203)$$

New parameters, in comparison with the sech ansatz (13) for the single-component soliton, are the angle θ which measures the distribution of energy between the two cores, and the relative phase ψ between them.

Note that the ansatz (202)–(203) assumes that the centers of the two components of the soliton are stuck together. This implies that the linear coupling between the two cores is strong, which corresponds to a real physical situation. However, one may also consider a case when the linear coupling is a small perturbation, so that a two-component soliton is a weakly bound state of two individual NLS solitons belonging to the two cores, as it was done by Abdullaev, Abrarov and Darmanyan [1989] and Kivshar and Malomed [1989b], using straightforward perturbation theory (see also a paper by Cohen [1995], where the Hamiltonian formalism was used to analyze the stability of bound states of solitons in weakly coupled fibers).

Switching of a soliton between the two cores was considered, on the basis of a full system of variational equations for the ansatz (202)–(203), by Uzunov, Muschall, Gölles, Kivshar, Malomed and Lederer [1995] (independently, a less sophisticated version of VA was used by Doty, Haus, Oh and Fork

[1995] to analyze interactions of solitons in DCF; accurate numerical results for the interaction were reported by Peng, Malomed and Chu [1998]). The corresponding ODEs were solved numerically, and the results were compared against direct numerical solutions of eqs. (200) and (201), showing very good accordance over a broad parametric region. It was demonstrated by Smyth and Worthy [1997] that the description of the switching dynamics in DCF can be improved further if the radiation component of the wave field is incorporated into the ansatz, similarly to what was done by Kath and Smyth [1995] in the model of the single-core fiber.

Here, consideration is focused on static solitons, which can be found from the variational equations generated by the ansatz (202)–(203), in which all parameters except the phase ϕ are assumed constant:

$$\sin(2\theta) \sin(2\psi) = 0, \quad (204)$$

$$\frac{E}{3a} \cos(2\theta) - K \cot(2\theta) \cos(2\psi) = 0, \quad (205)$$

$$\frac{1}{a} = E \left[1 - \frac{1}{2} \sin^2(2\theta) \right], \quad (206)$$

$$\frac{d\phi}{dz} = \frac{1}{6a^2} + \frac{2E}{3a} \left[1 - \frac{1}{2} \sin^2(2\theta) \right] + \kappa \sin(2\theta) \cos(2\psi),$$

where E is the net energy of the soliton, $E \equiv \frac{1}{2} \int_{-\infty}^{+\infty} (|U|^2 + |V|^2) d\tau = A^2 a$.

Equation (204) requires either $\sin(2\theta) = 0$ or $\sin(2\psi) = 0$. According to the ansatz (202)–(203), the former solution implies that all the energy resides in a single core, which contradicts eqs. (200) and (201), hence this solution is extraneous. The latter solution, $\sin(2\psi) = 0$, implies that $\cos(2\psi) = \pm 1$. According to the numerical findings of Soto-Crespo and Akhmediev [1993], the solutions corresponding to $\cos(2\psi) = -1$, i.e., with a phase shift π between the two components, are almost everywhere unstable. Therefore, only the case $\cos(2\psi) = +1$, corresponding to solitons with in-phase components, is considered below. Then, the width a is eliminated by means of eq. (206), and the remaining equation (206) for the energy-distribution angle θ takes the form

$$\cos(2\theta) \left\{ \frac{E^2}{3K} \sin(2\theta) \left[1 - \frac{1}{2} \sin^2(2\theta) \right] - 1 \right\} = 0. \quad (207)$$

A simple analysis reveals that, in the interval $0 < E^2 < E_1^2$, where

$$E_1^2 = \frac{9}{4} \sqrt{6K} \approx 5.511K, \quad (208)$$

the only solution to eq. (207) is the *symmetric* one, with $\theta = \frac{1}{4}\pi$, which implies equal energies in both components according to eqs. (202) and (203). When

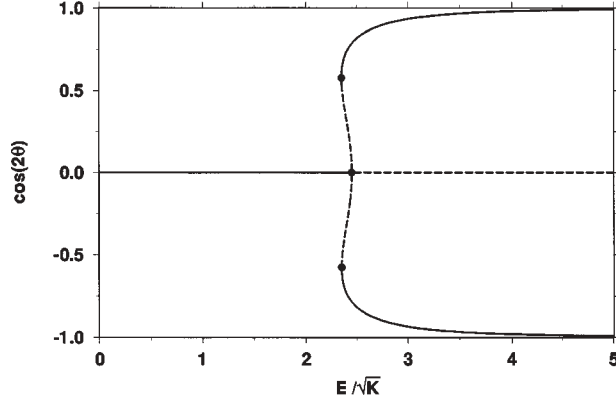


Fig. 28. Bifurcations between symmetric and asymmetric solitons in a dual-core nonlinear optical fiber. The solid and dashed branches correspond to stable and unstable solitons, respectively, and the thick dots indicate the bifurcation points.

the soliton's energy attains the value E_1 , *asymmetric* solutions emerge with $\cos(2\theta) = \pm 1/\sqrt{3}$. When E^2 attains a slightly larger value,

$$E_2^2 = 6K, \quad (209)$$

a *backward (subcritical) bifurcation* occurs, which makes the symmetric solution with $\theta = \frac{1}{4}\pi$ unstable.

The corresponding bifurcation diagram is displayed in fig. 28. Note that the quantity $\cos(2\theta)$, which is used as the vertical coordinate in the diagram, measures the asymmetry of the soliton because, as follows from eqs. (202) and (203),

$$\cos(2\theta) \equiv \frac{E^{(1)} - E^{(2)}}{E^{(1)} + E^{(2)}}, \quad (210)$$

where $E^{(j)}$ is the energy in the j th core. Even without detailed stability analysis, one can easily distinguish between stable and unstable branches in the diagram, using elementary theorems of bifurcation theory (see a book by Iooss and Joseph [1980]).

Thus, VA predicts backward bifurcation at the soliton energy $E_2 = \sqrt{6K} \approx 2.45\sqrt{K}$, whereas the known exact value is $4\sqrt{\frac{1}{3}K} \approx 2.31\sqrt{K}$ (Wright, Stegeman and Wabnitz [1989]), which illustrates the accuracy of VA. The bifurcation diagram produced by VA agrees with the numerical results (Akhmediev and Ankiewicz [1993], Soto-Crespo and Akhmediev [1993]) in showing that the region of bistability extends over a very narrow range of energies.

6.2. Fibers with a variable separation between the cores

An interesting dynamical generalization of the static problem outlined above is the consideration of bifurcations of solitons in a model of DCF with a *periodically modulated* coupling constant, i.e., $K = K_0 + K_1 \cos(kz)$ in eqs. (200) and (201). The periodic modulation may uncover hidden intrinsic resonances in the two-component DCF soliton, as was demonstrated, also by means of VA, in the work of Chu, Malomed, Peng and Skinner [1994]. A final result of the analysis is the prediction of a bifurcation from a two-component soliton whose energy oscillates *symmetrically* between the two cores to a pair of mutually symmetric solitons with *broken symmetry* of the oscillations (fig. 29).

A dual-core configuration of practical importance is a *fused coupler*, in which two far-separated fibers are bent so that they converge, reach a minimum separation at which light can couple between them, and then diverge again. The accordingly modulated coupling coefficient is, for instance, $K(z) = K_0 \operatorname{sech}(\kappa z)$. In this case, a natural dynamical problem is to consider how the energy of a soliton launched into one core is split between the cores after the passage of the coupling region. The variational technique can be applied to this problem in a straightforward way and, as demonstrated by Skinner, Peng, Malomed and Chu [1995], it produces results which are very close to those obtained from direct simulations of the NLS equations coupled by the linear terms with the variable coefficient $K(z)$.

Note that the limiting case of the fused coupler is when the coupling may be assumed to be concentrated at a single point, $K(z) = K_0 \delta(z)$. In this limit, the

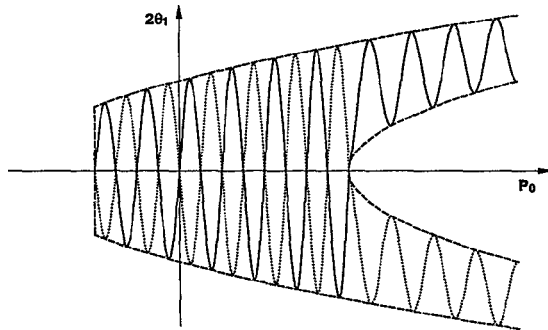


Fig. 29. Schematic representation of the symmetry-breaking bifurcation of a soliton whose energy oscillates between the two cores in a dual-core fiber with the coupling constant periodically modulated along the propagation distance. Here, $\theta_1 \equiv \theta - \frac{1}{4}\pi$ is the asymmetry parameter (see eqs. 202 and 203), and the rest of the notation is as in the paper by Chu, Malomed, Peng and Skinner [1994]. The solid and dashed lines represent two asymmetric solitons existing past the bifurcation point; the unstable symmetric solution remaining beyond the bifurcation (cf. fig. 28) is not shown.

problem of the soliton passage through the fused coupler admits an exact solution, as shown by Chu, Kivshar, Malomed, Peng and Quiroga-Teixeiro [1995].

Another source of z -dependence of the coupling constant K in the DCF model may be small fluctuations of the separation between the cores, as K is very sensitive to the exact value of the separation. However, it was demonstrated by Mostofi, Malomed and Chu [1998] that the solitons in DCF are not critically sensitive to fluctuations of K , except for an extremely narrow vicinity of the bifurcation point.

6.3. Gap solitons in asymmetric dual-core fibers

Asymmetric DCFs, consisting of two different cores, can be fabricated easily, and the properties of solitons in these DCFs may be quite different from those in the symmetric DCF. A general model for an asymmetric DCF is (cf. eqs. 200, 201)

$$iu_z + qu + \frac{1}{2}u_{\tau\tau} + |u|^2u + v = 0, \quad (211)$$

$$iv_z - \delta \cdot (qv + \frac{1}{2}v_{\tau\tau}) + |v|^2v + u = 0, \quad (212)$$

where the real parameter δ accounts for the difference in dispersion coefficients in the cores, and the real q defines the phase-velocity mismatch between them; possible group-velocity terms, $\sim iu_\tau$ and iv_τ , can be eliminated from the equations.

The influence of the asymmetry between the cores on soliton bifurcations was considered in the above-mentioned paper by Malomed, Skinner, Chu and Peng [1996], and in more detail by Kaup, Lakoba and Malomed [1997]. In the latter work, an analytical approach based on VA showed good agreement with direct numerical results. A noteworthy feature of bifurcations in the asymmetric model is the possibility of hysteresis in a broad region (in the symmetric model, hysteresis is only possible in the narrow bistable region between the two bifurcation points, see fig. 28).

The most interesting version of the asymmetric model is that with $\delta > 0$ in eq. (212), i.e., with *opposite* signs of the dispersion in the two cores, which was studied by means of VA and direct numerical methods by Kaup and Malomed [1998]. To understand the fundamental properties of solitons in this model, it is first of all necessary to analyze its linear spectrum. Substituting $u, v \sim \exp(ikz - i\omega\tau)$ into the linearized equations (211) and (212) yields the dispersion relation

$$k = \frac{1}{4}(\delta - 1)(\omega^2 - 2q) \pm \sqrt{\frac{1}{16}(\delta + 1)^2(\omega^2 - 2q)^2 + 1}. \quad (213)$$

Solitons may exist at values of the propagation constant k that belong to a *gap* in the spectrum (213), i.e., where both values of ω^2 corresponding to a given k

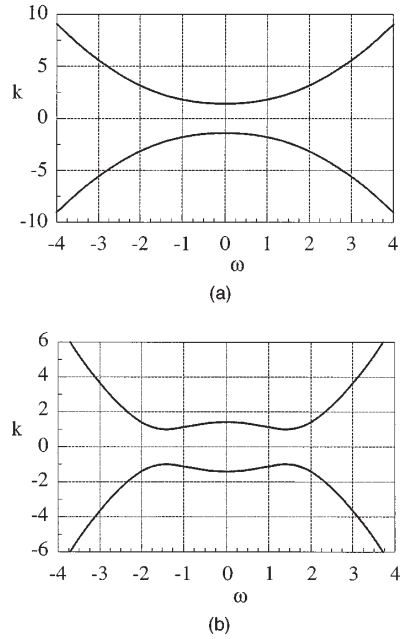


Fig. 30. Typical dispersion curves given by eq. (213) for a dual-core fiber with opposite dispersions in the cores, described by eqs. (211) and (212) with $\delta = 1$: (a) $q = -1$; (b) $q = +1$.

are nonphysical (negative or complex). Moreover, if these values are complex, soliton tails decay with oscillations, rather than monotonically. In particular, it follows from eq. (213) that, in the subgap $0 \leq k^2 < 4\delta/(1+\delta)^2$, only solitons with oscillating decaying tails may exist. The existence of this type of soliton is an essential result (similar solitons were also found by Malomed [1995] in a model with equal dispersions in both cores, $\delta = -1$, and a group-velocity mismatch between them, which is a special case not comprised in eqs. 211 and 212; as shown in that work, the solitons may form bound states, interacting through the oscillating tails). In the case of opposite dispersions in the two cores ($\delta > 0$), the spectrum always contains a finite gap; typical results for negative and positive values of the mismatch q are shown in fig. 30.

Once the gap has been found, stationary *gap solitons* residing in it are sought for as $u(z, \tau) = U(\tau) \exp(ikz)$, $v(z, \tau) = V(\tau) \exp(ikz)$ with real U and V that obey ODEs

$$(q-k)U + \frac{1}{2}U'' + U^3 + V = 0, \quad -(\delta q + k)V - \frac{1}{2}\delta V'' + V^3 + U = 0, \quad (214)$$

the prime standing for $d/d\tau$. Approximate solutions to eqs. (214) were constructed by means of VA, using the Gaussian ansatz

$$U = A \exp\left(-\frac{\tau^2}{2a^2}\right), \quad V = B \exp\left(-\frac{\tau^2}{2b^2}\right). \quad (215)$$

The amplitudes A and B can be eliminated from the resulting system of variational algebraic equations, leading to the following equations for the widths a and b :

$$\begin{aligned} & [3 - 4(k - q)a^2] [3\delta + 4(k + \delta q)b^2] \\ & = 32(ab)^3 (b^2 - 3a^2) (3b^2 - a^2) (a^2 + b^2)^{-3}, \end{aligned} \quad (216)$$

$$\begin{aligned} & \frac{[3 - 4(k - q)a^2] (3a^2 - b^2)^2}{[3\delta + 4(k + \delta q)b^2] (3b^2 - a^2)^2} \\ & = \frac{a^3 [\delta \cdot (3a^2 + b^2) + 4(k + \delta q)b^2 (b^2 - a^2)]}{b^3 [(3b^2 + a^2) + 4(k - q)a^2 (b^2 - a^2)]}. \end{aligned} \quad (217)$$

Equations (216) and (217) were solved numerically to find a and b as functions of the control parameters, δ and q , and the propagation constant k .

To present the results in a physically meaningful form, one should define, as usual, the energies of the two components of the soliton,

$$E_u \equiv \int_{-\infty}^{+\infty} |U(\tau)|^2 dt = \sqrt{\pi} A^2 a, \quad E_v \equiv \int_{-\infty}^{+\infty} |V(\tau)|^2 dt = \sqrt{\pi} B^2 b, \quad (218)$$

and the net energy $E \equiv E_u + E_v$. The dependence $E(k)$ is particularly important as, according to the condition put forward by Vakhitov and Kolokolov [1973] (VK), a necessary condition for the stability of the soliton is $dk/dE > 0$. Detailed results presented in the above-mentioned paper by Kaup and Malomed [1998] show that the gap solitons exist indeed in some part of the available gap, and, in most cases, they are stable according to the VK criterion; however, another part of the gap remains *empty* (there are intervals of the propagation constant k inside the gap, in which no soliton can be found).

A noteworthy property of the gap solitons is that (slightly) more than half of their net energy *always* resides in the normal-dispersion component v (i.e., $E_v/E > \frac{1}{2}$, see eq. 218), despite the obvious fact that the normal-dispersion core cannot, by itself, support any (bright) soliton. Accordingly, a typical soliton

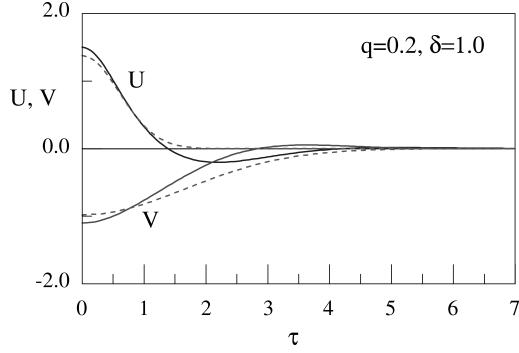


Fig. 31. Numerically found (solid lines) gap-soliton solution to eq. (214) with oscillating decaying tails, in the case $\delta = 1$, $q = 0.2$, and $E = 2.734$, displayed along with its variational counterpart (dashed curves).

predicted by VA (see fig. 31) has a narrower component with a larger amplitude in the anomalous core, and a broader component with a smaller amplitude in the normal one.

As can be seen from fig. 31, VA in general correctly approximates the soliton's core, but the simple ansatz (215) does not take into account the fact that, as explained above, the soliton tails decay with oscillations. The contribution of the tails is also amenable for a conspicuous difference of the energy share E_v/E in the normal-dispersion core against the value predicted by VA for the same net energy E : for example, in the case shown in fig. 31, the predicted value is $E_v/E = 0.585$, while the numerically found one is $E_v/E = 0.516$ (but still larger than $\frac{1}{2}$, as stressed above).

6.4. Two polarizations in the dual-core fiber

A physically interesting extended model of DCF, that was developed by Lakoba, Kaup and Malomed [1997], takes into account the fact that light may have two polarizations in each core. The model (a bimodal dual-core fiber) is based on a system of four equations,

$$\begin{aligned}
 i(u_1)_z + \frac{1}{2}(u_1)_{\tau\tau} + (|u_1|^2 + \frac{2}{3}|v_1|^2) u_1 + u_2 &= 0, \\
 i(v_1)_z + \frac{1}{2}(v_1)_{\tau\tau} + (|v_1|^2 + \frac{2}{3}|u_1|^2) v_1 + v_2 &= 0, \\
 i(u_2)_z + \frac{1}{2}(u_2)_{\tau\tau} + (|u_2|^2 + \frac{2}{3}|v_2|^2) u_2 + u_1 &= 0, \\
 i(v_2)_z + \frac{1}{2}(v_2)_{\tau\tau} + (|v_2|^2 + \frac{2}{3}|u_2|^2) v_2 + v_1 &= 0,
 \end{aligned} \tag{219}$$

where u and v refer to two linear polarizations (in the case of circular polarizations, the XPM coefficient $\frac{2}{3}$ should be replaced by 2), the subscripts 1 and 2 label the cores, and the coupling coefficient between them is $K \equiv 1$.

Four-component soliton solutions to eqs. (219) can be sought for by means of VA based on the Gaussian ansatz,

$$\begin{aligned} u_{1,2}(z, \tau) &= A_{1,2} \exp(ipz - \frac{1}{2}a^2 \tau^2), \\ v_{1,2}(z, \tau) &= B_{1,2} \exp(iqz - \frac{1}{2}b^2 \tau^2), \end{aligned} \quad (220)$$

with arbitrary real propagation constants p and q . In the general case, the corresponding variational equations for the ansatz parameters A_n, B_n and a, b , which are sought for as functions of p and q , are cumbersome. The equations admit both symmetric solutions, with $A_1^2 = A_2^2$ and $B_1^2 = B_2^2$, and asymmetric ones, which are generated by symmetry-breaking bifurcations, similar to the model of DCF with a single polarization considered above.

The existence regions of all the solutions in the (p, q) plane, obtained from numerical solution of the algebraic variational equations, are displayed in fig. 32 for the most important case when the signs of the amplitudes $A_{1,2}$ and $B_{1,2}$ inside each polarization coincide (other cases can also be considered, but they yield unstable solutions only). Outside the hatched area, there are only solutions with a single polarization (i.e., with either $v_{1,2} = 0$ or $u_{1,2} = 0$), which amount to solutions considered in § 6.1; in particular, at the dashed-dotted borders of the hatched area, asymmetric four-component solitons (designated by the symbol AS1 in fig. 32) change over to the two-component asymmetric solitons of the single-component DCF model. Symmetric solitons exist inside the sector bordered by the solid lines. The bifurcation which gives rise to the asymmetric solitons AS1 and destabilizes the symmetric solitons occurs along the short dashed curve in the lower left part of the hatched area.

There is an extra asymmetric soliton (denoted by AS2 in fig. 32) inside the area confined by the dashed curve. Thus, the total number of soliton solutions changes, as one crosses the bifurcation curves in fig. 32 from left to right, from 1 to 3 to 5. However, the soliton AS2 is generated from the symmetric soliton by an additional symmetry-breaking bifurcation which takes place *after* the symmetric soliton has already been destabilized by the bifurcation which gives rise to the asymmetric soliton AS1, therefore the soliton AS2 is always unstable, while the primary asymmetric soliton AS1 is, most plausibly, always stable. Further details about the stability of different solitons in this model can be found in a paper by Lakoba and Kaup [1997].

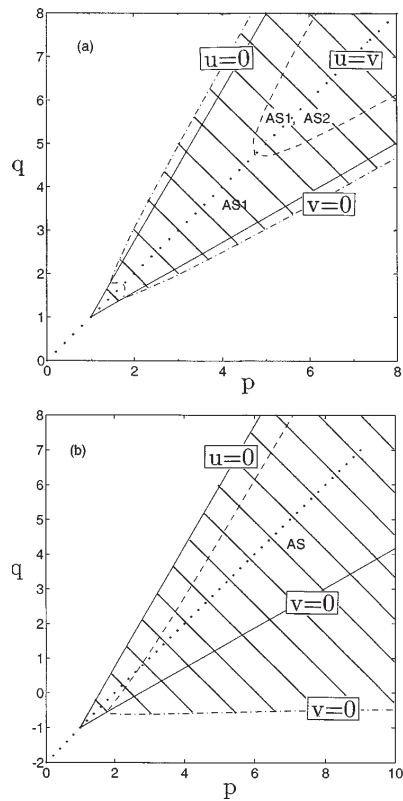


Fig. 32. Regions of existence of the symmetric and two types of asymmetric (stable, AS1, and unstable, AS2) solitons in the plane (p, q) in the bimodal dual-core-fiber model (219). The symbols $u = 0$, $v = 0$, and $u = v$ refer to particular solutions with a single polarization and equal polarizations.

§ 7. Bragg-grating (gap) solitons

7.1. Instability of gap solitons

In the systems described by the single or coupled NLS equations, the second-derivative terms account for the intrinsic material dispersion of the fiber or waveguide. Contrary to this, strong artificial dispersion can be induced by a Bragg grating (BG), i.e., a periodic modulation of the refractive index written along the fiber, the modulation period being half the wavelength of the light

signal. The model for a nonlinear optical fiber equipped with BG is based on the coupled equations (see the review by de Sterke and Sipe [1994])

$$iu_t + iu_x + (\sigma|u|^2 + |v|^2)u + v = 0, \quad (221)$$

$$iv_t - iv_x + (|u|^2 + \sigma|v|^2)v + u = 0, \quad (222)$$

where u and v are the amplitudes of the right- and left-traveling waves, the linear coupling terms take into account resonant reflection of light on BG, and the cubic terms account for the usual SPM and XPM nonlinearities. In this context, the SPM coefficient takes the value $\sigma = \frac{1}{2}$, while in the case $\sigma = 0$ eqs. (221) and (222) constitute a *massive Thirring model*, which is exactly integrable by means of IST. The limiting case $\sigma \rightarrow \infty$, when eqs. (221) and (222) take the form

$$iu_t + iu_x + |u|^2u + v = 0, \quad iv_t - iv_x + |v|^2v + u = 0, \quad (223)$$

has a different application to nonlinear optics: after making the replacements $t \rightarrow z$ and $x \rightarrow \tau/c$, eqs. (223) describe a dual-core fiber with a group-velocity mismatch $2c$ between the cores, while their intrinsic dispersion is neglected, cf. eqs. (211) and (212) (Malomed and Tasgal [1994]).

Although the system of equations (221)–(222) with $\sigma \neq 0$ is not integrable, it has a family of exact soliton solutions found by Aceves and Wabnitz [1989] and Christodoulides and Joseph [1989]. In particular, the expression for zero-velocity solitons is

$$\begin{aligned} u &= (1 + \sigma)^{-1/2}(\sin Q) \operatorname{sech}(x \sin Q - \frac{1}{2}iQ) \cdot \exp(-it \cos Q), \\ v &= -(1 + \sigma)^{-1/2}(\sin Q) \operatorname{sech}(x \sin Q + \frac{1}{2}iQ) \cdot \exp(-it \cos Q), \end{aligned} \quad (224)$$

where the parameter Q , which takes values $0 < Q < \pi$, determines the soliton's width and amplitude. These solitons are frequently called *gap solitons* (GSs), as they exist inside the gap, $\omega^2 < 1$, in the linear spectrum, $\omega^2 = 1 + k^2$, of the system (221)–(222). The exact zero-velocity GS solution to eqs. (223) is obtained from eqs. (224) by setting $\sigma = 0$.

A problem that may be considered by means of VA is internal vibrations of perturbed GSs. The analysis, developed by Malomed and Tasgal [1994], has produced an unexpected prediction – an intrinsic instability of a part of the family of GS solutions (224). At the time this result was published, it seemed to be an artifact generated by VA, and it was even regarded as a major failure of the variational technique, stimulating a sophisticated analysis of situations when VA may generate false soliton instabilities (Kaup and Lakoba [1996]; it was

concluded that a spurious instability is possible, roughly speaking, in models in which the quadratic part of the Hamiltonian is not positive definite, which is the case for eqs. (221), (222), but not for the single or coupled NLS equations). Indeed, in the case $\sigma = 0$, the solitons of the integrable massive Thirring model have no instability. However, rigorous results of direct investigation of the soliton stability in the general model (221)–(222) with $\sigma \neq 0$, based on numerical solution of the corresponding linearized equations, which were later reported by Barashenkov, Pelinovsky and Zemlyanaya [1998] and De Rossi, Conti and Trillo [1998], have confirmed that a part of the GS family (224) is indeed unstable if $\sigma \neq 0$. In fact, the border between stable and unstable solitons in the cases $\sigma = \frac{1}{2}$ and $\sigma = \infty$, which are relevant to nonlinear optics (see above), is close to that predicted by Malomed and Tasgal [1994] on the basis of VA, see details below.

The variational ansatz for perturbed GS follows the pattern of the exact solution (224):

$$\begin{aligned}
 u &= \eta_u(1 + \sigma)^{-1/2} [\sin(Q + q)] \\
 &\quad \times \operatorname{sech} \left[(x + \zeta) \sin(Q + q) - \frac{1}{2}(Q + q) \right] \\
 &\quad \times \exp \left[-i \left(a_u + b_u(x + \zeta) + \frac{1}{2}c_u \sin\left(\frac{1}{2}Q\right) \cdot (x + \zeta)^2 \right) \right], \\
 v &= -\eta_v(1 + \sigma)^{-1/2} [\sin(Q - q)] \\
 &\quad \times \operatorname{sech} \left[(x - \zeta) \sin(Q - q) + \frac{1}{2}(Q - q) \right] \\
 &\quad \times \exp \left[-i \left(a_v + b_v(x - \zeta) + \frac{1}{2}c_v \sin\left(\frac{1}{2}Q\right) \cdot (x - \zeta)^2 \right) \right],
 \end{aligned} \tag{225}$$

where η_u , η_v , Q , q , a_u , a_v , b_u , b_v , c_u , c_v and ζ are variational parameters that may be functions of t . This ansatz lets one vary independently the central position, width, amplitude, phase, carrier frequency, and chirp of the u - and v -components.

Equations (221) and (222) can be derived from the Lagrangian $L = \int_{-\infty}^{+\infty} \mathcal{L} dx$ with the density

$$\begin{aligned}
 \mathcal{L} &= \frac{i}{2} [u^*(\partial_t + \partial_x)u - u(\partial_t + \partial_x)u^* + v^*(\partial_t - \partial_x)v - v(\partial_t - \partial_x)v^*] \\
 &\quad + \frac{1}{2}\sigma (|u|^4 + |v|^4) + |u|^2|v|^2 + u^*v + uv^*
 \end{aligned} \tag{226}$$

[for the model (223), one should set $\sigma = 1$ and drop the XPM term $|u|^2|v|^2$ in eq. (226)]. Substituting eqs. (225) into the Lagrangian, performing the integration, and varying with respect to the free parameters yield a cumbersome system of dynamical equations which have a fixed point (FP) corresponding to

the unperturbed soliton (224): $\eta_u = \eta_v = 1$, $Q = \text{const.} \equiv Q_0$, $a_u = a_v = t \cos Q$, $b_u = b_v = c_u = c_v = q = \zeta = 0$.

Linearization of the general variational equations about FP leads to a sixth-order system of equations for small internal vibrations of GS, which give rise to the corresponding eigenfrequencies. They take a simple form in the case $Q^2 \ll 1$, when GS (224) has a small amplitude and large width, its shape being close to that of the usual NLS soliton:

$$\omega_q = \pm \sqrt{\frac{16(3 + \pi^2)}{45} - \left[\frac{80 + 192(1 + \sigma)^{-1}}{675} \pi^4 + \frac{124}{45} \pi^2 + 4 \right] \left(\frac{Q}{\pi} \right)^2} \quad (227)$$

$$\approx \pm [2.14 - (1.01 + 0.66(1 + \sigma)^{-1})Q^2],$$

$$\omega_{Q+} = \pm \sqrt{\left(\frac{2\pi}{3} \right)^2 + \left[4 - \frac{48(1 + \sigma)^{-1} + 20}{135} \pi^2 \right] Q^2} \quad (228)$$

$$\approx \pm \{2.09 + [0.61 - 0.84(1 + \sigma)^{-1}] Q^2\},$$

$$\omega_{Q-} = \pm \frac{6Q^2}{\pi^2} \sqrt{1 + \left[\frac{4(1 + \sigma)^{-1} + 1}{5} \pi^2 - 12 \right] \left(\frac{Q}{\pi} \right)^2} \quad (229)$$

$$\approx \pm 0.61 Q^2 \{1 - [0.51 - 0.40(1 + \sigma)^{-1}] Q^2\}$$

(note that ω_{Q-}^2 is much smaller than ω_q^2 and ω_{Q+}^2 , as $Q^2 \ll 1$). The eigenmode corresponding to ω_q is dominated by the oscillations of the dynamical parameters q/Q , $(\eta_u^2 - \eta_v^2)$ and $(a_u - a_v)$ in the ansatz (225), while the oscillation amplitudes of other variables are smaller by a factor $\sim Q$. The ω_{Q+} and ω_{Q-} eigenmodes are dominated by oscillations of the variables ζ and $(a_u + a_v)$, but in different ratios.

With increasing Q , the shape of GS becomes essentially different from that of the NLS soliton, and it becomes unstable at some critical value Q_{cr} . In fact, each of the three eigenfrequencies becomes unstable at some critical value of Q , as illustrated by fig. 33, which displays the eigenfrequencies vs. Q/π in the limit case corresponding to eqs. (223), i.e., $\sigma \rightarrow \infty$ (recall it is a model for a group-velocity-mismatched dual-core fiber). In this case, the smallest Q_{cr} is generated by the eigenfrequency ω_q , which becomes imaginary, giving rise to a monotonic (nonoscillatory) instability at $Q \approx 0.4\pi$ (see fig. 33a). This instability is indeed spurious, as it has no counterpart in the numerically exact results which were later reported for the same case by Barashenkov, Pelinovsky and Zemlyanaya [1998]. However, two other eigenfrequencies found by means of VA become *complex* (rather than imaginary) at $Q \approx 0.53\pi$, giving rise to oscillatory instabilities. The onset of this instability, which is oscillatory too,

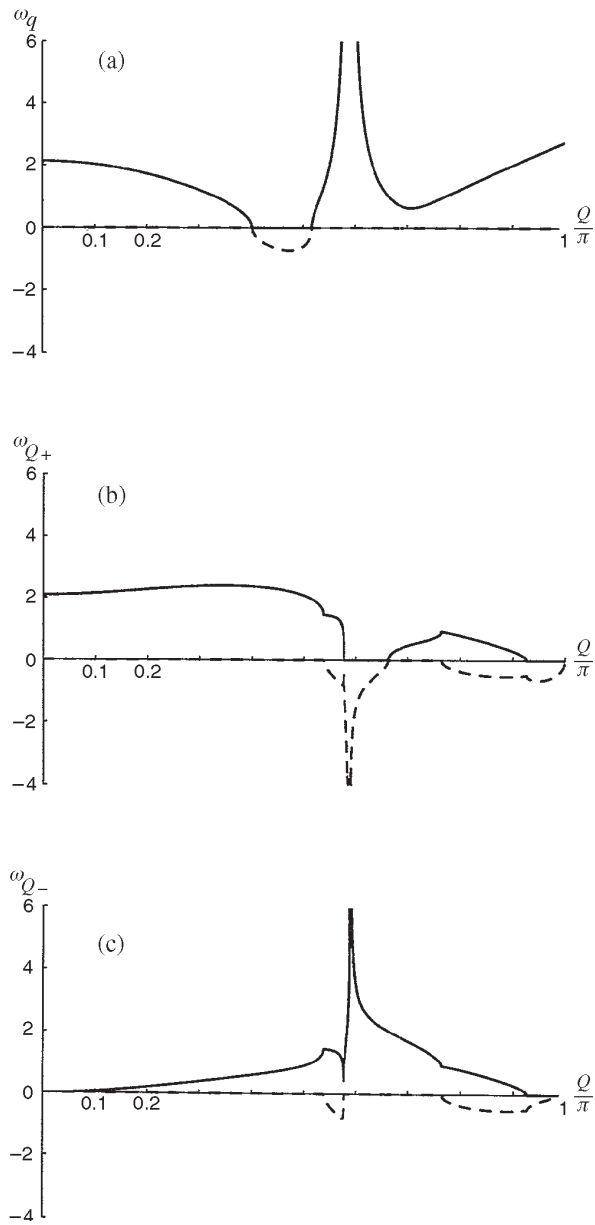


Fig. 33. Eigenfrequencies of internal vibrations of the gap soliton in the model (223) vs. the intrinsic soliton parameter Q (see eq. 224), as produced by VA. The real part of the eigenfrequencies is shown by the solid curve above the Q axis, and the absolute value of the dashed branches below the Q axis gives the instability growth rate $|\text{Im } \omega|$, if any.

was discovered by Barashenkov, Pelinovsky and Zemlyanaya [1998] at virtually the same point, $Q \approx 0.53\pi$. Moreover, it is seen in figs. 33b,c that a secondary oscillatory instability sets in at a still larger value of Q , which also complies with the numerically exact results.

Lastly, as concerns the spurious nonoscillatory instability generated by the eigenfrequency ω_q (fig. 33a), this artifact can probably be explained by the theory developed by Kaup and Lakoba [1996]; note that the maximum growth rate of the spurious instability is 6 times as small as that of the genuine instability, cf. figs. 33a and 33b, hence the spurious instability is not so important in practical terms.

7.2. Solitons in linearly coupled waveguides with Bragg gratings

A natural generalization of the model for an optical fiber equipped with a Bragg grating (BG) is a system of two parallel-coupled cores with the grating written on both of them. As shown by Mak, Chu and Malomed [1998], this model gives rise to generalized gap solitons (GSs) with interesting dynamical properties. The model can be cast into the following normalized form [cf. eqs. (221)–(222) for the single-core BG fiber and (200)–(201) for the dual-core fiber without BG]:

$$iu_{1t} + iu_{1x} + \left(\frac{1}{2}|u_1|^2 + |v_1|^2\right)u_1 + v_1 + \lambda u_2 = 0, \quad (230)$$

$$iv_{1t} - iv_{1x} + \left(\frac{1}{2}|v_1|^2 + |u_1|^2\right)v_1 + u_1 + \lambda v_2 = 0, \quad (231)$$

$$iu_{2t} + iu_{2x} + \left(\frac{1}{2}|u_2|^2 + |v_2|^2\right)u_2 + v_2 + \lambda u_1 = 0, \quad (232)$$

$$iv_{2t} - iv_{2x} + \left(\frac{1}{2}|v_2|^2 + |u_2|^2\right)v_2 + u_2 + \lambda v_1 = 0, \quad (233)$$

where the usual ratio 1 : 2 between the SPM and XPM coefficients is implied, the BG-induced coefficient of the conversion between left- ($u_{1,2}$) and right- ($v_{1,2}$) traveling waves is normalized to be 1, and λ is the coefficient of the linear coupling between the two cores. The same model can be realized as describing stationary field distributions in two parallel-coupled planar waveguides with BGs in the form of a system of parallel scores, in which case t and x play the roles of the propagation distance and transverse coordinate, the diffraction in the waveguides being neglected.

Zero-velocity solitons are sought for as

$$u_{1,2} = \exp(-i\omega t) U_{1,2}(x), \quad v_{1,2} = \exp(-i\omega t) V_{1,2}(x), \quad (234)$$

where the reduction $V_{1,2} = -U_{1,2}^*$ may be imposed [in fact, the exact GS solutions (224) in the single-core model are subject to the same reduction].

Substituting this into eqs. (230)–(233) leads to coupled ODE's (with the prime standing for d/dx),

$$\omega U_1 + iU_1' + \frac{3}{2}|uU_1|^2 U_1 - U_1^* + \lambda U_2 = 0, \quad (235)$$

$$\omega U_2 + iU_2' + \frac{3}{2}|U_2|^2 U_2 - U_2^* + \lambda U_1 = 0. \quad (236)$$

A possible existence range for solitons in the (λ, ω) plane can be found from the linear dispersion relation for eqs. (230)–(233). Looking for a linearized solution in the form $u_{1,2}, v_{1,2} \sim \exp(ikx - i\omega t)$, one obtains

$$\omega^2 = \lambda^2 + 1 + k^2 \pm 2\lambda\sqrt{1+k^2}. \quad (237)$$

As was mentioned in the preceding subsection, the solitons can only exist in the gap of the linear spectrum, i.e., at values of ω which cannot be obtained from eq. (237) at any real value of k . At $\lambda = 0$, when the two waveguides decouple, the gap is widest, $-1 < \omega < 1$. At $|\lambda| = 1$, the gap closes up, i.e., no soliton may exist at $|\lambda| > 1$. To summarize, the soliton existence region is a part of the rectangle $|\lambda| < 1, |\omega| < 1$.

The stationary equations (235) and (236) can be derived from the Lagrangian with the density

$$\begin{aligned} \mathcal{L} = & \omega(U_1 U_1^* + U_2 U_2^*) + \frac{i}{2} [U_1' U_1^* - (U_1^*)' U_1 + U_2' U_2^* - (U_2^*)' U_2] \\ & + \frac{3}{4}(|U_1|^4 + |U_2|^4) - \frac{1}{2}(U_1^2 + U_1^{*2} + U_2^2 + U_2^{*2}) + \lambda(U_1 U_2^* + U_1^* U_2). \end{aligned}$$

Then, the following ansatz is adopted for the *complex* soliton solution sought for:

$$U_{1,2} = A_{1,2} \operatorname{sech}(\mu x) + iB_{1,2} \sinh(\mu x) \operatorname{sech}^2(\mu x), \quad (238)$$

with real $A_{1,2}, B_{1,2}$ and μ . The corresponding effective Lagrangian is

$$\begin{aligned} L \equiv & \int_{-\infty}^{+\infty} \mathcal{L} dx \\ = & \mu^{-1} [2\omega(A_1^2 + A_2^2) + \frac{2}{3}\omega(B_1^2 + B_2^2) - \frac{4}{3}\mu(A_1 B_1 + A_2 B_2) \\ & + (A_1^4 + A_2^4) - 1.2857(B_1^4 + B_2^4) + \frac{2}{5}(A_1^2 B_1^2 + A_2^2 B_2^2) \\ & - 2(A_1^2 + A_2^2) + \frac{2}{3}(B_1^2 + B_2^2) + 4\lambda A_1 A_2 + \frac{4}{3}\lambda B_1 B_2] \end{aligned} \quad (239)$$

(the numerical coefficient 1.2857 is given by some integral), which generates variational equations

$$3\lambda A_{2,1} - 3(1 - \omega)A_{1,2} + 3A_{1,2}^3 + \frac{3}{5}A_{1,2}B_{1,2}^2 - \mu B_{1,2} = 0, \quad (240)$$

$$\lambda B_{2,1} + \frac{3}{2}B_{1,2} - 3.857B_{1,2}^3 + \frac{3}{5}A_{1,2}^2 B_{1,2} - \mu A_{1,2} = 0, \quad (241)$$

$$\begin{aligned} 2\omega(A_1^2 + A_2^2) + \frac{2}{3}\omega(B_1^2 + B_2^2) + (A_1^4 + A_2^4) - 1.2857(B_1^4 + B_2^4) \\ + \frac{2}{5}(A_1^2 B_1^2 + A_2^2 B_2^2) - 2(A_1^2 + A_2^2) + \frac{2}{3}(B_1^2 + B_2^2) + 4\lambda A_1 A_2 + \frac{4}{3}\lambda B_1 B_2 = 0. \end{aligned} \quad (242)$$

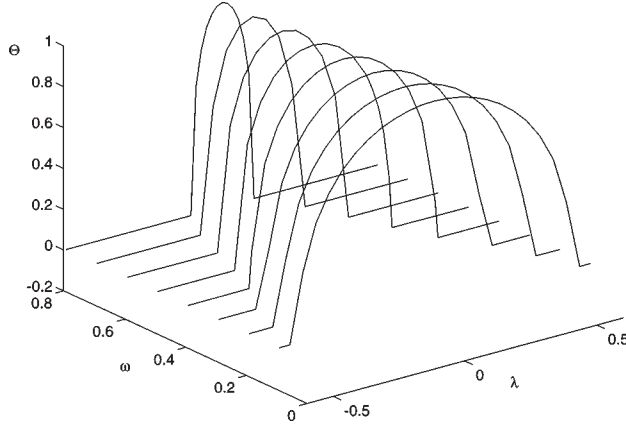


Fig. 34. Bifurcation diagram for zero-velocity solitons in the model of a dual-core nonlinear optical fiber with Bragg gratings written on both cores.

A general result, following both from numerical solution of eqs. (240)–(242) and from direct numerical solution of ODEs (235) and (236), is that a symmetric solution, with $A_1^2 = A_2^2$ and $B_1^2 = B_2^2$, exists at all values of ω and λ inside the above-mentioned spectral gap, and it is the only soliton solution if the coupling constant λ is large enough. However, below a critical value of λ (which depends on ω), the symmetric solution bifurcates, giving rise to three branches: one remains symmetric, while two new mutually symmetric branches represent nontrivial *asymmetric* solutions.

The bifurcation can be conveniently displayed in terms of an effective asymmetry parameter

$$\Theta \equiv \frac{U_{1m}^2 - U_{2m}^2}{U_{1m}^2 + U_{2m}^2}, \quad (243)$$

where U_{1m} and U_{2m} are the amplitudes (maxima of the absolute values) of the fields $U_{1,2}$ in the two cores. A complete three-dimensional plot of the bifurcation, i.e., Θ vs. ω and λ , is shown in fig. 34. At $\lambda = 0$, when eqs. (235) and (236) decouple, the numerical solution matches the exact single-core solution (224), while the other core is empty.

Generally, this symmetry-breaking bifurcation is similar to that shown in fig. 28 for the dual-core nonlinear fiber without BG. However, unlike the (slightly) subcritical bifurcation in fig. 28, both VA and direct numerical solutions show that the present bifurcation is *supercritical* (alias a forward bifurcation).

The bifurcation diagram in fig. 34 was drawn using direct numerical results obtained from eqs. (235)–(236), but its variational counterpart is very close

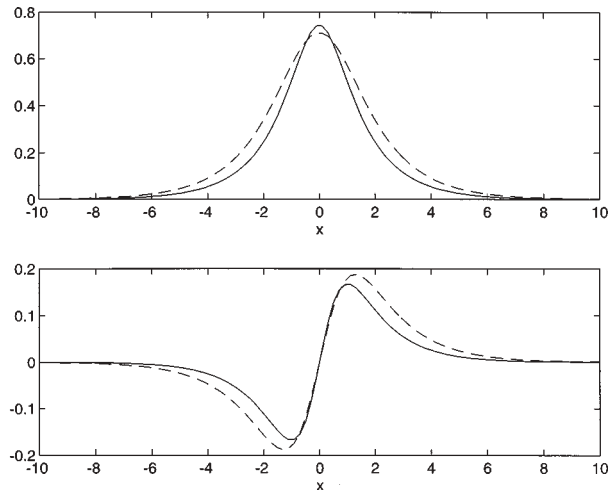


Fig. 35. Shapes of the larger component U_1 of the asymmetric soliton in the dual-core Bragg-grating fiber at $\omega = 0.5$ and $\lambda = 0.2$. The upper and lower panels show $\text{Re } U_1(x)$ and $\text{Im } U_1(x)$. In each panel, the solid and dashed lines represent the numerical and variational results.

to it: the relative discrepancy between the VA-predicted and numerically exact values of λ at which the bifurcation takes place for fixed ω is $\sim 5\%$. To illustrate the accuracy of VA, fig. 35 presents, for a typical case, a comparison between the shapes of the asymmetric soliton predicted by VA and obtained from direct numerical integration.

A direct numerical test of the stability of symmetric and asymmetric solitons in the present model has yielded results exactly conforming to what should be expected on the basis of the general bifurcation theory (see a book by Iooss and Joseph [1980]): all the asymmetric solitons are stable whenever they exist, while all the symmetric solitons, whenever they coexist with the asymmetric ones, are unstable. However, beyond the bifurcation points, where the asymmetric solitons do not exist, all the symmetric ones are stable.

§ 8. Stable beams in a layered focusing–defocusing Kerr medium

It is well known that the standard NLS equation governing the spatial evolution of signals in bulk nonlinear optical media cannot support stable soliton-like cylindrical beams: if the nonlinearity is self-defocusing (SDF), any beam spreads out, while in the case of a self-focusing (SF) nonlinearity, a stationary-beam solution with a *critical value* of its power does exist (Chiao, Garmire and Townes

[1964]; as a matter of fact, this was the first soliton considered in nonlinear optics), but it is unstable because of the possibility of wave collapse (see review by Bergé [1998]). Recently, Bergé, Mezentsev, Juul Rasmussen, Christiansen and Gaididei [2000] have demonstrated, by means of direct simulations, that the beam can be partly stabilized if the nonlinearity coefficient is subjected to weak spatial modulation along the propagation direction, so that the beam power (which is virtually constant, as radiative losses turn out to be negligible) effectively oscillates about the modulated critical value, sometimes being slightly larger and sometimes slightly smaller than it. As a result, it was observed that the beam could survive over a large propagation distance, although eventually it might be destroyed by the instability.

Here, a model is considered in which the nonlinearity is subjected to a more radical modulation, so that SDF and SF layers alternate periodically. The model is based on the NLS equation

$$iu_z + \frac{1}{2}\nabla_{\perp}^2 u + \gamma(z)|u|^2 u = 0, \quad (244)$$

where the diffraction operator ∇_{\perp}^2 acts on the transverse coordinates x and y , and the nonlinearity coefficient γ assumes positive and negative values γ_{\pm} inside alternating layers with widths L_{\pm} . While particular realizations of such a layered medium are not discussed here in detail, it is relevant to note that it has been demonstrated experimentally by Liu, Qian and Wise [1999a] that narrow layers with a large negative value of the effective Kerr coefficient can be created, using the cascading mechanism based on the quadratic nonlinearity. A novel result, obtained recently by Towers and Malomed [2002] by means of both VA and direct simulations, is that this type of nonlinear medium gives rise to *completely stable* beams, which is the subject of the present section.

Axisymmetric spatial solitons are sought for in the form

$$u(z, r, \theta) = \exp(iS\theta) U(z, r), \quad (245)$$

where r and θ are the polar coordinates in the transverse plane, the integer S is vorticity (“spin”), and the function $U(z, r)$ obeys the PDE

$$iU_z + \frac{1}{2} \left(U_{rr} + \frac{1}{r} U_r - \frac{S^2}{r^2} U \right) + \gamma(z)|U|^2 U = 0. \quad (246)$$

To apply VA to eq. (246), a natural ansatz is adopted,

$$U = A(z) r^S \exp [ib(z)r^2 + i\phi(z)] \operatorname{sech} \left(\frac{r}{W(z)} \right), \quad (247)$$

where b and W are the soliton’s chirp and width. Skipping details of straightforward calculations, the following set of variational equations for the parameters

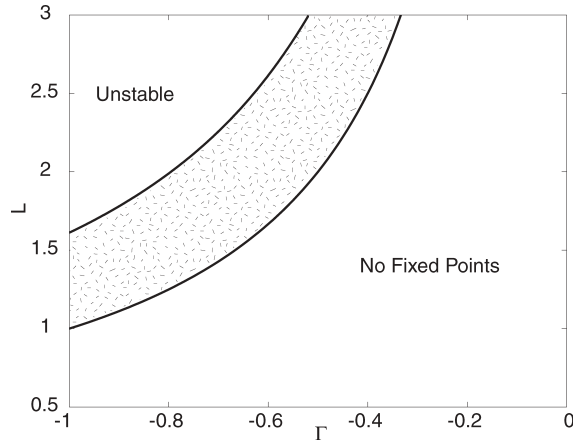


Fig. 36. Parameter space of the variational model describing the cylindrical zero-vorticity beam in a layered focusing–defocusing medium. The fixed point is stable in the speckled area.

of the ansatz (247) can be derived. First, due to the conservation of energy E (actually, E is the power of the beam), there is a dynamical invariant

$$A^2 W(z)^{2(S+1)} = \text{const.} \equiv E, \quad (248)$$

which makes it possible to eliminate the amplitude A in favor of the width W . After that, there remains a second-order equation for $W(z)$,

$$\frac{d^2 W}{dz^2} = \left[\frac{2I_2}{I_1} - \frac{2I_4}{I_1} \gamma(z) \right] W^{-3}, \quad (249)$$

the chirp being expressed in terms of $W(z)$ as $b(z) = (2W)^{-1} dW/dz$, cf. similar equations (32) and (31) for the usual 1D soliton. The constants $I_{1,2,4}$ are integrals resulting from VA; for $S = 0$ (zero-spin beam), $I_{1,2,4} \approx (1.352, 0.398, 0.295)$.

For the piece-wise constant function $\gamma(x)$ defined above, eq. (249) can be integrated inside each interval where γ is constant. The result is

$$\left(\frac{dV}{dz} \right)^2 + \Gamma = HV, \quad (250)$$

where $V \equiv W^2$, $\Gamma \equiv 8[I_2/I_1 - (I_4/I_1)\gamma]$, $H \equiv 8h$, and h [which is the Hamiltonian of eq. (249) with $\gamma = \text{const.}$] is an arbitrary integration constant.

Within the interval $0 < z < L_+$, the parameter Γ keeps a constant given value Γ_+ , then it assumes another constant value Γ_- in the interval

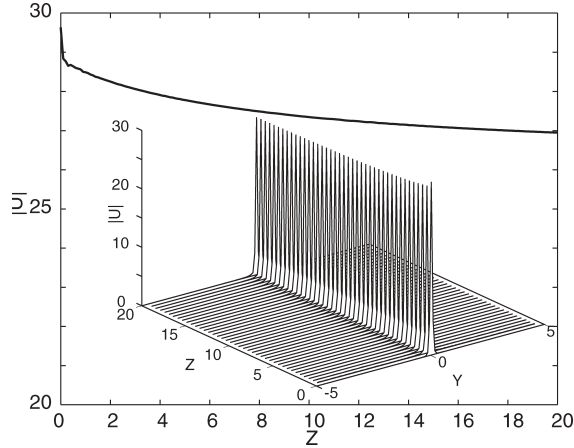


Fig. 37. Numerically simulated evolution initiated by the configuration (247) with $S = 0$, $L = 1$, and $\Gamma = -1.3$. The upper and lower plots show the evolution of the beam's peak amplitude and cross-section, respectively, vs. the propagation distance.

$L_+ < z < L_+ + L_-$, and this configuration repeats itself periodically. The formulas can be additionally rescaled to set $L_- \equiv 1$ and $\Gamma_- \equiv 1$, then there remain two irreducible control parameters, $L_+ \equiv L$ and $\Gamma_+ \equiv \Gamma$ (note that the definition of Γ implies that, once $\Gamma_- = 1$ is set, then $\Gamma \equiv \Gamma_+$ may only be < 1 , including negative values). Across each junction point, the values of V and dV/dz are related according to the physical conditions that the width and chirp of the pulse, as functions of z , must be continuous. As immediately follows from the above equations, this simply means that both V and dV/dz are continuous across the jump.

Starting with arbitrary initial values V_0 and V'_0 of $V(z)$ and dV/dz at $z = 0$, one can derive a *map* that yields the values \tilde{V}_0 and \tilde{V}'_0 of the same variables at the end of the period, $z = L_+ + L_- \equiv 1 + L$. Straightforward integration of eq. (250) in the segments L_\pm , with regard to the continuity of V and dV/dz at the junction points, makes it possible to derive the map in an explicit although rather cumbersome form. Nevertheless, a *fixed point* (FP) of the map, that corresponds to the quasi-stationary propagation of the beam, is given by simple expressions:

$$V_0 = \pm \frac{L(\Gamma - 1)}{4\sqrt{L+1}\sqrt{-1-L\Gamma}}, \quad V'_0 = \mp \frac{\sqrt{-1-L\Gamma}}{\sqrt{L+1}}, \quad (251)$$

which make sense only for negative values $\Gamma < -1/L$.

To investigate the stability of FP, one should find eigenvalues λ of the Jacobian of the map, $\partial(\tilde{V}_0, \tilde{V}'_0)/\partial(V_0, V'_0)$. The FP is stable if both eigenvalues satisfy the condition $|\lambda| \leq 1$. The results of this analysis are summarized in fig. 36. No

FP exists beneath the curve $L = -1/\Gamma$. Above this curve, FP is stable inside a speckled band. Outside the band, FP is unstable.

To test the VA-based analytical results against direct simulations, the underlying equation (244) was solved numerically, using the ansatz (247), whose parameters were taken at FP (251), as the initial configuration. A typical result is shown in fig. 37: after a short relaxation period, the initial beam reshapes into a nearly stationary stable one, which propagates with small residual oscillations. This seems to be the first example of a *stable* cylindrical beam in a medium with a Kerr nonlinearity. Simulations of the beams with nonzero vorticity S , see eq. (245), show that, unlike the $S = 0$ beam, they are all unstable.

§ 9. Conclusion

The aim of this review was to demonstrate that a combination of the variational approximation with direct numerical simulations is the most natural and efficient approach to many problems in nonlinear optics and other areas of physics which are based on nonlinear PDEs. Although the technique has already been applied to a large number of systems, its potential is far from being exhausted. The outburst of activity in the field of dispersion management has been responsible for the recent renaissance of variational methods. Another fast developing topic which calls for the development of these methods at a higher level is the study of spatiotemporal pulses in multidimensional optical media. Beyond the limits of nonlinear optics, the variational approximation has recently often been used in studies of Bose–Einstein condensates. Thus, variational methods remain a powerful and universal tool in the arsenal of modern-day nonlinear science.

Acronyms adopted in the text

1D	one-dimensional
2D	two-dimensional
BDW	Bloch domain wall
BG	Bragg grating
c.c.	complex conjugate (in equations)
CQ	cubic–quintic (equation)
CW	continuous wave
DCF	dual-core fiber

DDF	dispersion-decreasing fiber
DM	dispersion management
DS	dark soliton
FP	fixed point (of dynamical equations or map)
FWHM	full width at half-maximum (of a solitary pulse)
GL	Ginzburg–Landau (equation)
GS	gap soliton
IST	inverse scattering transform
KdV	Korteweg–de Vries (equation)
NLS	nonlinear Schrödinger (equation, or soliton)
ODE	ordinary differential equation
PAD	path-average dispersion (in a dispersion-managed fiber-optic link)
PDE	partial differential equation
rhs	right-hand side (of an equation)
SDF	self-defocusing (nonlinearity)
SF	self-focusing (nonlinearity)
SPM	self-phase modulation
TOD	third-order dispersion
VA	variational approximation
VK	Vakhitov–Kolokolov (stability criterion for solitons)
WDM	wavelength-division multiplexing
XPM	cross-phase modulation
ZDP	zero-dispersion point
ZS	Zakharov–Shabat (equations)

Acknowledgements

Outstanding contributions to the fields comprised by the review were made by D. Anderson, D.J. Kaup and M. Lisak. This review is, to a large extent, a result of my collaboration with them. It is also my pleasure to appreciate valuable collaborations and/or discussions with other colleagues working in the areas comprised by this review: F.Kh. Abdullaev, V.V. Afanasjev, J. Atai, Y. Band, I.V. Barashenkov, A. Berntson, A.V. Buryak, J.G. Caputo, A.R. Champneys,

P.L. Chu, S.R. Clarke, P.D. Drummond, C. Etrich, D.J. Frantzeskakis, B.V. Gisin, R. Grimshaw, K. Hizanidis, P. Kevrekidis, Yu.S. Kivshar, G. Kurizki, F. Lederer, T.I. Lakoba, W.C.K. Mak, D. Mazilu, D. Mihalache, A.I. Maimistov, U. Peschel, M. Quiroga-Teixeiro, G.D. Peng, A. Shipulin, I. Skinner, N.F. Smyth, M. Weinstein, F. Wise and J. Yang. Important contributions to results included into the review were made by my younger collaborators: L.-C. Crasovan, R.S. Tasgal, A. Desyatnikov, I. Towers and M. Wald. Special thanks are due to J. Peřina, who suggested writing this review for *Progress in Optics*. Lastly, I appreciate valuable aid in the preparation of this article for printing from Jeroen Soutberg, of ISYS Prepress Services.

References

- Abdullaev, F.Kh., R.M. Abrarov and S.A. Darmany, 1989, *Opt. Lett.* **14**, 131.
 Abdullaev, F.Kh., and B.B. Baizakov, 2000, *Opt. Lett.* **25**, 93.
 Abdullaev, F.Kh., J. Bronski and G.C. Papanicolaou, 1999, *Physica D* **135**, 369.
 Abdullaev, F.Kh., and J.G. Caputo, 1998, *Phys. Rev. E* **58**, 6637.
 Abdullaev, F.Kh., J.G. Caputo and N. Flytzanis, 1994, *Phys. Rev. E* **50**, 1552.
 Ablowitz, M.J., and G. Biondini, 1998, *Opt. Lett.* **23**, 1668.
 Ablowitz, M.J., G. Biondini, S. Chakravarty and R.L. Horne, 1998, *Opt. Commun.* **150**, 305.
 Ablowitz, M.J., D.J. Kaup and A.C. Newell, 1974, *J. Math. Phys.* **15**, 1852.
 Ablowitz, M.J., D.J. Kaup, A.C. Newell and H. Segur, 1973, *Phys. Rev. Lett.* **30**, 1262.
 Ablowitz, M.J., D.J. Kaup, A.C. Newell and H. Segur, 1974, *Stud. Appl. Math.* **53**, 249.
 Ablowitz, M.J., and H. Segur, 1981, *Solitons and Inverse Scattering Transform* (SIAM, Philadelphia, PA).
 Aceves, A.B., and S. Wabnitz, 1989, *Phys. Lett. A* **141**, 116.
 Afanasjev, V.V., and N. Akhmediev, 1996, *Phys. Rev. E* **53**, 6471.
 Afanasjev, V.V., E.M. Dianov and V.N. Serkin, 1989, *IEEE J. Quantum Electron.* **QE-25**, 2656.
 Afanasjev, V.V., B.A. Malomed and P.L. Chu, 1997, *Phys. Rev. E* **56**, 6020.
 Afanasjev, V.V., B.A. Malomed, P.L. Chu and M.K. Islam, 1998, *Opt. Commun.* **147**, 317.
 Agrawal, G.P., 1995, *Nonlinear Fiber Optics*, 2nd Ed. (Academic Press, San Diego, CA).
 Agrawal, G.P., 1997, *Nonlinear Optical Communication Networks* (Wiley, New York).
 Aitchison, J.S., A.M. Weiner, Y. Silberberg, D.E. Leaird, M.K. Oliver, J.L. Jackel and P.W.E. Smith, 1991, *Opt. Lett.* **16**, 15.
 Aitchison, J.S., A.M. Weiner, Y. Silberberg, M.K. Oliver, J.L. Jackel, D.E. Leaird, E.M. Vogel and P.W.E. Smith, 1990, *Opt. Lett.* **15**, 471.
 Akhmediev, N., and A. Ankiewicz, 1993, *Phys. Rev. Lett.* **70**, 2395.
 Akhmediev, N., and J.M. Soto-Crespo, 1994, *Phys. Rev. E* **49**, 4519.
 Anderson, D., 1983, *Phys. Rev. A* **27**, 3135.
 Anderson, D., M. Desaix, M. Karlsson, M. Lisak and M.L. Quiroga-Teixeiro, 1993, *J. Opt. Soc. Am. B* **10**, 1185.
 Anderson, D., Y.S. Kivshar and M. Lisak, 1991, *Phys. Scripta* **43**, 273.
 Anderson, D., and M. Lisak, 1986a, *Opt. Lett.* **11**, 174.
 Anderson, D., and M. Lisak, 1986b, *Phys. Scripta* **33**, 193.
 Anderson, D., M. Lisak, B.A. Malomed and M. Quiroga-Teixeiro, 1994, *J. Opt. Soc. Am. B* **11**, 2380.

- Anderson, D., M. Lisak and T. Reichel, 1988a, *J. Opt. Soc. Am. B* **5**, 207.
- Anderson, D., M. Lisak and T. Reichel, 1988b, *Phys. Rev. A* **27**, 3135.
- Ankiewicz, A., N. Akhmediev, G.D. Peng and P.L. Chu, 1993, *Opt. Commun.* **103**, 410.
- Barashenkov, I.V., 1996, *Phys. Rev. Lett.* **77**, 1193.
- Barashenkov, I.V., M.M. Bogdan and V.I. Korobov, 1991, *Europhys. Lett.* **15**, 113.
- Barashenkov, I.V., A.D. Gocheva, V.G. Makhankov and I.V. Puzynin, 1989, *Physica D* **34**, 240.
- Barashenkov, I.V., and E.Yu. Panova, 1993, *Physica D* **69**, 114.
- Barashenkov, I.V., D.E. Pelinovsky and E.V. Zemlyanaya, 1998, *Phys. Rev. Lett.* **80**, 5117.
- Barashenkov, I.V., Yu.S. Smirnov and N.V. Alexeeva, 1998, *Phys. Rev. E* **57**, 2350.
- Barashenkov, I.V., and E.V. Zemlyanaya, 1999, *Phys. Rev. Lett.* **83**, 2568.
- Bélanger, P.-A., and C. Paré, 1999, *J. Lightwave Technol.* **17**, 495.
- Bergé, L., 1998, *Phys. Rep.* **303**, 259.
- Bergé, L., V.K. Mezentsev, J. Juul Rasmussen, P.L. Christiansen and Yu.B. Gaididei, 2000, *Opt. Lett.* **25**, 1037.
- Berntson, A., D. Anderson, M. Lisak, M.L. Quiroga-Teixeiro and M. Karlsson, 1996, *Opt. Commun.* **130**, 153.
- Berntson, A., N.J. Doran, W. Forsysiak and J.H.B. Nijhof, 1998, *Opt. Lett.* **23**, 900.
- Bertilsson, K., T. Aakjer, M. Quiroga-Teixeiro, P.A. Andrekson and P.-O. Hedekvist, 1995, *Opt. Fiber Technol.* **1**, 117.
- Blanchard, P., and E. Brünig, 1992, *Variational Methods in Mathematical Physics* (Springer, Berlin).
- Boffeto, G., and A.R. Osborne, 1992, *J. Comp. Phys.* **102**, 252.
- Bondeson, M., M. Lisak and D. Anderson, 1979, *Phys. Scripta* **20**, 479.
- Bullough, R.K., A.P. Fordy and S.V. Manakov, 1982, *Phys. Lett. A* **91**, 98.
- Caglioti, E., S. Trillo, S. Wabnitz, B. Crossignani and P. DiPorto, 1990, *J. Opt. Soc. Am. B* **7**, 374.
- Chernikov, S.V., E.M. Dianov, D.J. Richardson and D.N. Payne, 1993, *Opt. Lett.* **18**, 476.
- Chiao, R.Y., E. Garmire and C.H. Townes, 1964, *Phys. Rev. Lett.* **13**, 479.
- Christodoulides, D.N., and R.I. Joseph, 1989, *Phys. Rev. Lett.* **62**, 1746.
- Chu, P.L., Y.S. Kivshar, B.A. Malomed, G.D. Peng and M.L. Quiroga-Teixeiro, 1995, *J. Opt. Soc. Am. B* **12**, 898.
- Chu, P.L., B.A. Malomed and G.D. Peng, 1993, *J. Opt. Soc. Am. B* **10**, 1379.
- Chu, P.L., B.A. Malomed and G.D. Peng, 1996, *J. Opt. Soc. Am. B* **13**, 1794.
- Chu, P.L., B.A. Malomed, G.D. Peng and I.M. Skinner, 1994, *Phys. Rev. E* **49**, 5763.
- Clarke, S.R., R.H.J. Grimshaw and B.A. Malomed, 2000, *Phys. Rev. E* **61**, 5794.
- Cohen, G., 1995, *Phys. Rev. E* **52**, 5562.
- Cooper, F., H. Shepard, C. Lucheroni and P. Sodano, 1993, *Physica D* **68**, 344.
- Coulet, P., J. Lega and Y. Pomeau, 1991, *Europhys. Lett.* **15**, 221.
- De Angelis, C., 1994, *IEEE J. Quantum Electron.* **QE-30**, 818.
- De Rossi, A., C. Conti and S. Trillo, 1998, *Phys. Rev. Lett.* **81**, 85.
- de Sterke, C.M., and J.E. Sipe, 1994, in: *Progress in Optics*, Vol. 33, ed. E. Wolf (North-Holland, Amsterdam) ch. 3.
- Desaix, M., D. Anderson and M. Lisak, 1990, *Opt. Lett.* **15**, 18.
- Desaix, M., D. Anderson and M. Lisak, 1991, *J. Opt. Soc. Am. B* **8**, 2082.
- Desaix, M., D. Anderson and M. Lisak, 1994, *Phys. Rev. E* **50**, 2253.
- Desaix, M., D. Anderson, M. Lisak and M.L. Quiroga-Teixeiro, 1996, *Phys. Lett. A* **212**, 332.
- Desyatnikov, A., A.I. Maimistov and B.A. Malomed, 2000, *Phys. Rev. E* **61**, 3107.
- Dimitrevski, K., E. Reimhult, E. Svensson, A. Öhgren, D. Anderson, A. Berntson, M. Lisak and M. Quiroga-Teixeiro, 1998, *Phys. Lett. A* **248**, 369.
- Dodd, R.J., 1996, *J. Res. Natl. Inst. Stand. Technol.* **101**, 545.
- Doty, S.L., J.W. Haus, Y. Oh and R.L. Fork, 1995, *Phys. Rev. E* **51**, 709.

- Eisenberg, H.S., Y. Silberberg, R. Morandotti, A.R. Boyd and J.S. Aitchison, 1998, *Phys. Rev. Lett.* **81**, 3383.
- Etrich, C., F. Lederer, B.A. Malomed, T. Peschel and U. Peschel, 2000, in: *Progress in Optics*, Vol. 41, ed. E. Wolf (Elsevier, Amsterdam) ch. 7.
- Friberg, S.A., A.M. Weiner, Y. Silberberg, B.G. Sfez and P.S. Smith, 1988, *Opt. Lett.* **13**, 904.
- Friedland, L., 1998, *Phys. Rev. E* **58**, 3865.
- Gabitov, I., E.G. Shapiro and S.K. Turitsyn, 1997, *Phys. Rev. E* **55**, 3624.
- Gabitov, I., and S.K. Turitsyn, 1996, *Opt. Lett.* **21**, 327.
- Georges, T., 1998, *J. Opt. Soc. Am. B* **15**, 1553.
- Gerjuoy, E., A.R.P. Rau and L. Spruch, 1983, *Rev. Mod. Phys.* **55**, 725.
- Gordon, J.P., 1983, *Opt. Lett.* **8**, 596.
- Gorshkov, K.A., and L.A. Ostrovsky, 1981, *Physica D* **3**, 428.
- Gorshkov, K.A., L.A. Ostrovsky and E.N. Pelinovsky, 1974, *Proc. IEEE* **82**, 1511.
- Grimshaw, R., J. He and B.A. Malomed, 1996, *Phys. Scripta* **53**, 385.
- Grünbaum, F.A., 1989, *Inverse Problems* **5**, 287.
- Haelterman, M., A.P. Sheppard and A.W. Snyder, 1993, *Opt. Commun.* **103**, 145.
- Hasegawa, A., and Y. Kodama, 1995, *Solitons in Optical Communications* (Oxford University Press, Oxford).
- Hatami-Hanza, H., P.L. Chu, B.A. Malomed and G.D. Peng, 1997, *Opt. Commun.* **134**, 59.
- Hizanidis, K., N. Efremidis, B.A. Malomed, H.E. Nistazakis and D.J. Frantzeskakis, 1998, in: *Trends in Optical Soliton Transmission Systems*, ed. A. Hasegawa (Kluwer Academic Publishers, Dordrecht) p. 117.
- Hmurcik, L.V., and D.J. Kaup, 1979, *J. Opt. Soc. Am.* **69**, 597.
- Iannone, E., F. Matera, A. Mecozzi and M. Settembre, 1998, *Nonlinear Optical Communication Networks* (Wiley, New York).
- Iooss, G., and D.D. Joseph, 1980, *Elementary Stability and Bifurcation Theory* (Springer, New York).
- Karpman, V.I., 1979, *Phys. Scripta* **20**, 462.
- Karpman, V.I., and V.V. Solov'ev, 1981, *Physica D* **3**, 487.
- Kath, W.L., and N.F. Smyth, 1995, *Phys. Rev. E* **51**, 1484.
- Kaup, D.J., 1976, *SIAM J. Appl. Math.* **31**, 121.
- Kaup, D.J., 1977, *Phys. Rev. A* **16**, 704.
- Kaup, D.J., 1991, *Phys. Rev. E* **44**, 4582.
- Kaup, D.J., J. El-Reedy and B.A. Malomed, 1994, *Phys. Rev. E* **50**, 1635.
- Kaup, D.J., and T.I. Lakoba, 1996, *J. Math. Phys.* **37**, 3442.
- Kaup, D.J., T.I. Lakoba and B.A. Malomed, 1997, *J. Opt. Soc. Am. B* **14**, 1199.
- Kaup, D.J., and B.A. Malomed, 1995, *Physica D* **87**, 101.
- Kaup, D.J., and B.A. Malomed, 1998, *J. Opt. Soc. Am. B* **15**, 2838.
- Kaup, D.J., B.A. Malomed and R.S. Tasgal, 1993, *Phys. Rev. E* **48**, 3049.
- Kaup, D.J., B.A. Malomed and J. Yang, 1999, *J. Opt. Soc. Am. B* **16**, 1628.
- Kaup, D.J., and A.C. Newell, 1978, *Proc. R. Soc. London A* **361**, 413.
- Kaup, D.J., and L.R. Scacca, 1980, *J. Opt. Soc. Am.* **70**, 224.
- Kivshar, Y.S., and D.K. Campbell, 1993, *Phys. Rev. E* **48**, 3077.
- Kivshar, Y.S., and W. Królikowski, 1995, *Opt. Commun.* **114**, 353.
- Kivshar, Y.S., and B. Luther-Davies, 1998, *Phys. Rep.* **298**, 81.
- Kivshar, Y.S., and B.A. Malomed, 1989a, *Rev. Mod. Phys.* **61**, 763.
- Kivshar, Y.S., and B.A. Malomed, 1989b, *Opt. Lett.* **14**, 1365.
- Kivshar, Y.S., and X. Yang, 1994, *Phys. Rev. E* **49**, 1657.
- Knox, F.M., W. Forsyiaik and N.J. Doran, 1995, *J. Lightwave Technol.* **13**, 1955.

- Krökel, D., N.J. Halas, G. Giuliani and D. Grischkowsky, 1988, *Phys. Rev. Lett.* **60**, 29.
- Kuehl, H.H., 1988, *J. Opt. Soc. Am. B* **5**, 709.
- Kumar, A., S.N. Sarkar and A.K. Ghatak, 1986, *Opt. Lett.* **11**, 321.
- Kumar, S., M. Wald, F. Lederer and A. Hasegawa, 1998, *Opt. Lett.* **23**, 1019.
- Kutz, J.N., P. Holmes, S.G. Evangelides and J.G. Gordon, 1998, *J. Opt. Soc. Am. B* **15**, 87.
- Kuznetsov, E.A., A.V. Mikhailov and I.A. Shimokhin, 1995, *Physica D* **87**, 201.
- Lakoba, T.I., and D.J. Kaup, 1997, *Phys. Rev. E* **56**, 4791.
- Lakoba, T.I., D.J. Kaup and B.A. Malomed, 1997, *Phys. Rev. E* **55**, 6107.
- Lakoba, T.I., J. Yang, D.J. Kaup and B.A. Malomed, 1998, *Opt. Commun.* **149**, 366.
- Landau, L.D., and E.M. Lifshitz, 1975, *Mechanics* (Pergamon Press, New York).
- Landau, L.D., and E.M. Lifshitz, 1977, *Quantum Mechanics* (Pergamon Press, New York).
- Lewis, Z.W., 1985, *Phys. Lett. A* **112**.
- Lin, C., H. Kogelnik and L.G. Cohen, 1980, *Opt. Lett.* **5**, 476.
- Lisak, M., A. Höök and D. Anderson, 1990, *J. Opt. Soc. Am. B* **7**, 810.
- Liu, X., K. Beckwitt and F. Wise, 2000, *Phys. Rev. E* **62**, 1328.
- Liu, X., L.J. Qian and F.W. Wise, 1999a, *Opt. Lett.* **24**, 1777.
- Liu, X., L.J. Qian and F.W. Wise, 1999b, *Phys. Rev. Lett.* **82**, 4631.
- Maimistov, A.I., 1991, *Kvant. Elektron.* **18**, 758 [*Sov. J. Quantum Electron.* **21**, 687].
- Maimistov, A.I., 1993, *Zh. Eksp. Teor. Fiz.* **104**, 3620 [*Sov. Phys. JETP* **77**, 727].
- Maimistov, A.I., and Yu.M. Sklyarov, 1987, *Kvant. Elektron.* **14**, 796 [*Sov. J. Quantum Electron.* **17**, 500].
- Mak, W.C.K., P.L. Chu and B.A. Malomed, 1998, *J. Opt. Soc. Am. B* **15**, 1685.
- Malomed, B.A., 1987, *Physica D* **23**, 155.
- Malomed, B.A., 1991a, *Phys. Rev. A* **43**, 410.
- Malomed, B.A., 1991b, *Phys. Rev. A* **44**, 6954.
- Malomed, B.A., 1993, *Phys. Scripta* **47**, 797.
- Malomed, B.A., 1994a, *Phys. Rev. E* **50**, 1565.
- Malomed, B.A., 1994b, *Opt. Lett.* **19**, 341.
- Malomed, B.A., 1995, *Phys. Rev. E* **51**, R864.
- Malomed, B.A., 1996, *J. Opt. Soc. Am. B* **33**, 677.
- Malomed, B.A., 1997, *Opt. Commun.* **136**, 313.
- Malomed, B.A., 1998a, *Opt. Commun.* **147**, 157.
- Malomed, B.A., 1998b, *Opt. Lett.* **23**, 1250.
- Malomed, B.A., 1998c, *Phys. Rev. E* **58**, 7928.
- Malomed, B.A., 2000, in: *Nonlinear Science at the Dawn of the 21st Century*, eds P.L. Christiansen, M.P. Sorensen and A.C. Scott (Springer, Berlin) p. 247.
- Malomed, B.A., D. Anderson, M. Lisak, M.L. Quiroga-Teixeiro and L. Stenflo, 1997, *Phys. Rev. E* **55**, 962.
- Malomed, B.A., and A. Berntson, 2002, *J. Opt. Soc. Am. B* **18**, 1243.
- Malomed, B.A., P. Drummond, H. He, A. Berntson, D. Anderson and M. Lisak, 1997, *Phys. Rev. E* **56**, 4725.
- Malomed, B.A., A.I. Maimistov and A. Desyatnikov, 1999, *Phys. Lett. A* **254**, 179.
- Malomed, B.A., and A.A. Nepomnyashchy, 1990, *Phys. Rev. A* **42**, 6238.
- Malomed, B.A., and A.A. Nepomnyashchy, 1994, *Europhys. Lett.* **27**, 649.
- Malomed, B.A., D.F. Parker and N.F. Smyth, 1993, *Phys. Rev. E* **48**, 1418.
- Malomed, B.A., and A. Shipulin, 1999, *Opt. Commun.* **162**, 140.
- Malomed, B.A., I. Skinner, P.L. Chu and G.D. Peng, 1996, *Phys. Rev. E* **53**, 4084.
- Malomed, B.A., and N.F. Smyth, 1994, *Phys. Rev. E* **50**, 1535.
- Malomed, B.A., and R.S. Tasgal, 1994, *Phys. Rev. E* **49**, 5787.

- Malomed, B.A., and R.S. Tasgal, 1998, Phys. Rev. E **58**, 2564.
- Malomed, B.A., Z.H. Wang, P.L. Chu and G.D. Peng, 1999, J. Opt. Soc. Am. B **16**, 1197.
- Malomed, B.A., and M.I. Weinstein, 1996, Phys. Lett. A **220**, 91.
- Manakov, S.V., 1973a, Zh. Eksp. Teor. Fiz. **65**, 505 [1974, Sov. Phys. JETP **38**, 248].
- Manakov, S.V., 1973b, Zh. Eksp. Teor. Fiz. **65**, 1392 [1974, Sov. Phys. JETP **38**, 693].
- Maneuf, S., and F. Reynaud, 1988, Opt. Commun. **65**, 325.
- Matsumoto, M., 1997, Opt. Lett. **22**, 1238.
- Matsumoto, M., 1998, IEEE Photon. Technol. Lett. **10**, 373.
- Menyuk, C.R., 1987, IEEE J. Quantum Electron. **QE-23**, 174.
- Michaelis, D., U. Peschel and F. Lederer, 1997, Phys. Rev. A **56**, 3366.
- Michinel, H., 1995, Pure Appl. Opt. **4**, 701.
- Mitschke, F.M., and L.F. Mollenauer, 1987, Opt. Lett. **12**, 407
- Mollenauer, L.F., R.H. Stolen and J.P. Gordon, 1980, Phys. Rev. Lett. **45**, 1095.
- Mostofi, A., B.A. Malomed and P.L. Chu, 1998, Opt. Commun. **145**, 274.
- Muraki, D., and W.L. Kath, 1989, Phys. Lett. A **139**, 379.
- Muraki, D., and W.L. Kath, 1991, Physica D **48**, 53.
- Nakazawa, M., and H. Kubota, 1995, Electron. Lett. **31**, 216.
- Newell, A.C., 1985, Solitons in Mathematics and Physics (SIAM, Philadelphia, PA).
- Newell, A.C., and J.V. Moloney, 1992, Nonlinear Optics (Addison-Wesley, Reading, MA).
- Niculae, A.N., W. Forysiak, A.J. Gloag, J.H.B. Nijhof and N.J. Doran, 1998, Opt. Lett. **23**, 1354
- Paré, C., and P.-A. Bélanger, 2000, Opt. Lett. **25**, 881.
- Paré, C., and M. Florjańczyk, 1990, Phys. Rev. A **41**, 6287.
- Paré, C., V. Roy, F. Lesage, P. Mathieu and P.-A. Bélanger, 1999, Phys. Rev. E **60**, 4836.
- Pelinovsky, D.E., 2000, Phys. Rev. E **62**, 4283.
- Peng, G.D., B.A. Malomed and P.L. Chu, 1998, Phys. Scripta **58**, 149.
- Pérez-García, V.M., V.V. Konotop and J.J. García-Ripoll, 2000, Phys. Rev. E **62**, 4300.
- Pérez-García, V.M., H. Michinel, J.I. Cirac, M. Lewenstein and P. Zoller, 1997, Phys. Rev. A **56**, 1424.
- Petviashvili, V.I., and A.M. Sergeev, 1984, Dokl. Akad. Nauk SSSR **276**, 1380 [Sov. Phys. Dokl. **26**, 493].
- Pushkarov, D.I., and S. Tanev, 1996, Opt. Commun. **124**, 354.
- Pushkarov, Kh.I., D.I. Pushkarov and I.M. Tomov, 1979, Opt. Quantum Electron. **11**, 471.
- Quiroga-Teixeiro, M., D. Anderson, P.A. Andrekson, A. Berntson and M. Lisak, 1996, J. Opt. Soc. Am. B **13**, 687.
- Quiroga-Teixeiro, M., D. Anderson, A. Berntson and M. Lisak, 1995, J. Opt. Soc. Am. B **12**, 1110.
- Quiroga-Teixeiro, M., and H. Michinel, 1997, J. Opt. Soc. Am. B **14**, 2004.
- Reynaud, F., and A. Barthelemy, 1990, Europhys. Lett. **12**, 401.
- Romagnoli, M., S. Trillo and S. Wabnitz, 1992, Opt. Quantum Electron. **24**, S1237.
- Satsuma, J., and N. Yajima, 1974, Progr. Theor. Phys. (Suppl.) **55**, 284.
- Shalaby, M., and A. Barthelemy, 1991, Opt. Lett. **16**, 1472.
- Shipulin, A., G. Onishchukov and B.A. Malomed, 1997, J. Opt. Soc. Am. B **14**, 3393.
- Skinner, I.M., G.D. Peng, B.A. Malomed and P.L. Chu, 1995, Opt. Commun. **113**, 493.
- Smith, N.J., F.M. Knox, N.J. Doran, K.J. Blow and I. Bennion, 1996, Electron. Lett. **32**, 54.
- Smyth, N.F., 2000, Opt. Commun. **175**, 469.
- Smyth, N.F., and A.L. Worthy, 1997, J. Opt. Soc. Am. B **14**, 2610.
- Soto-Crespo, J.M., and N. Akhmediev, 1993, Phys. Rev. E **48**, 4710.
- Suzuki, M., I. Morita, N. Edagawa, S. Yamamoto, H. Taga and S. Akiba, 1995, Electron. Lett. **31**, 2027.
- Turner, L., D. Mazilu and D. Mihalache, 1996, Phys. Rev. Lett. **77**, 2455.

- Towers, I., and B.A. Malomed, 2002, *J. Opt. Soc. Am. B* **19**, 537.
- Tran, H.T., R.A. Sammut and W. Samir, 1994, *Opt. Commun.* **113**, 292.
- Trillo, S., S. Wabnitz, W.C. Banyai, N. Finlayson, C.T. Seaton, G.I. Stegeman and R.H. Stolen, 1989, *IEEE J. Quantum Electron.* **QE-25**, 104.
- Trillo, S., S. Wabnitz, E.M. Wright and G.I. Stegeman, 1988, *Opt. Lett.* **13**, 672.
- Trillo, S., S. Wabnitz, E.M. Wright and G.I. Stegeman, 1989, *Opt. Commun.* **70**, 166.
- Turitsyn, S.K., 1997, *Phys. Rev. E* **56**, R3784.
- Turitsyn, S.K., A.B. Aceves, C.K.R.T. Jones, V. Zharnitsky and V.K. Mezentsev, 1999, *Phys. Rev. E* **59**, 3843.
- Turitsyn, S.K., I. Gabitov, E.W. Laedke, V.K. Mezentsev, S.L. Musher, E.G. Shapiro, T. Schäfer and K.H. Spatschek, 1998, *Opt. Commun.* **151**, 117.
- Turitsyn, S.K., T. Schaefer and V.K. Mezentsev, 1998, *Phys. Rev. E* **58**, R5264.
- Ueda, T., and W.L. Kath, 1990, *Phys. Rev. A* **42**, 563.
- Ueda, T., and W.L. Kath, 1992, *Physica D* **55**, 166.
- Uzunov, I.M., R. Muschall, M. Gölles, Yu.S. Kivshar, B.A. Malomed and F. Lederer, 1995, *Phys. Rev. E* **51**, 2527.
- Vakhitov, M.G., and A.A. Kolokolov, 1973, *Radiophys. Quantum Electron.* **16**, 783.
- Wai, P.K.A., H.H. Chen and Y.C. Lee, 1990, *Phys. Rev. A* **41**, 426.
- Wai, P.K.A., C.R. Menyuk, H.H. Chen and Y.C. Lee, 1987, *Opt. Lett.* **12**, 628.
- Wald, M., B.A. Malomed and F. Lederer, 1999, *Opt. Commun.* **172**, 31.
- Wang, L., and C.C. Yang, 1990, *Opt. Lett.* **15**, 474.
- Whitham, G.B., 1974, *Linear and Nonlinear Waves* (Wiley, New York).
- Wright, E.M., B.I. Lawrence, W. Torruellas and G. Stegeman, 1996, *Opt. Lett.* **20**, 2481.
- Wright, E.M., G.I. Stegeman and S. Wabnitz, 1989, *Phys. Rev. A* **40**, 4455.
- Yang, J., 1997a, *Stud. Appl. Math.* **98**, 61.
- Yang, J., 1997b, *Physica D* **108**, 92.
- Yang, T.S., and W.L. Kath, 2001, *Physica D* **149**, 80.
- Yu, T., E.A. Golovchenko, A.N. Pilipetskii and C.R. Menyuk, 1997, *Opt. Lett.* **22**, 793.
- Zakharov, V.E., S.V. Manakov, S.P. Novikov and L.P. Pitaevskii, 1980, *Solitons* (Nauka, Moscow).
English translation: 1984 (Consultants Bureau, New York).
- Zakharov, V.E., and A.B. Shabat, 1971, *Zh. Eksp. Teor. Fiz.* **61**, 118 [1972, *Sov. Phys. JETP* **34**, 62].
- Zaks, M.A., A.A. Nepomnyashchy and B.A. Malomed, 1996, *Phys. Scripta T* **67**, 143.